**Palacký University Olomouc**

**Faculty of Science**

**Department of Cell Biology and Genetics**

**and**

**Institute of Experimental Botany AS CR**

**Centre of Plant Structural and Functional Genomics**

**Olomouc**

**Alžběta Němečková**

# Spatial and temporal characterization of DNA replication in plants

**Ph.D. Thesis**

**Supervisor: Mgr Eva Hřibová, PhD.**

**Olomouc 2020**

**Acknowledgements**

I would like to express my deepest gratitude to my supervisor, Mgr. Eva Hřibová, Ph.D., for professional guidance, invaluable advices, inspirational ideas and help. Further, I would like to thank to prof. Ing. Jaroslav Doležel, DrSc., the head of the laboratory, for the opportunity to work in the Centre of Plant Structural and Functional Genomics. Last but not least, I would like to thank my family for all their love and support during my whole studies.

**Declaration**

I hereby declare that I have written the Ph.D. thesis independently under the supervision of Mgr. Eva Hřibová, Ph.D. using the information sources listed in the References.

……..

This work was supported by the Czech Science Foundation (Grant award 17-14048S).

## BIBLIOGRAPHICAL IDENTIFICATION

**Author's name:** Alžběta Němečková

**Title:** Spatial and temporal characterization of DNA replication in plants

**Type of thesis:** Ph.D. thesis

**Department:** Department of Cell Biology and Genetics

**Supervisor:** Mgr. Eva Hřibová, Ph.D.

**The Year of Presentation:** 2020

**Abstract:**

DNA replication is a fundamental process necessary for the growth and development of all living organisms. Genetic information is replicated during the S phase of the cell cycle. The whole process is under strict control to ensure that replication takes place only once per the cell cycle. DNA replication has been intensively studied in yeast and animals. Unfortunately, information about the replication process in plants is still limited.

The present thesis is focused on replication in seven economically important crop species belong to the *Poaceae* family, which differ in many characteristics such as genome size, repetitive DNA sequences content, and their genome organization, number, and morphology of chromosomes, and chromosome orientation in interphase nuclei. Previous studies were based on the use of 5-Bromo-2'-deoxyuridine (BrdU) to visualize the genome region which undergoes DNA replication. This thymidine analog incorporates into the newly synthesized DNA strand during replication. Its visualization is time-consuming and requires DNA denaturation and specific antibodies that bind to BrdU. In the framework of this thesis, usage 5-Ethynyl-2'-deoxyuridine (EdU) was optimized. EdU is also incorporated into the newly synthesized DNA strand and visualized using fluorochrome(s) without the denaturation step. Fluorochrome labeling made it possible to distinguished nuclei that pass the cell cycle. EdU labeling followed by

flow cytometry analysis then enables to study course of the DNA replication process, and in combination with flow sorting of nuclei representing different phases of the cell cycle played this approach a key role in the present study. Cell nuclei representing G1, G2, and early, middle, and late S phase were used for three-dimensional fluorescent *in situ* hybridization (3D FISH), which allowed visualization of telomeric replicating regions together with specific immunolabeling (3D) of centromere regions with the aim to study their replication timing. At the same time, 3D analysis of the spatial arrangement of specific DNA regions (centromere, telomere) at different stages of the plant cell cycle was analyzed.

Detailed analysis of chromatin structure is influenced by the denaturation step during visualization of DNA sequences localized using a standard FISH approach, which can alter the native structure of the chromatin. Within the framework of this thesis, we focused on an alternative, recently described CRISPR-Cas9 method, which enables fluorescent visualization of specific DNA sequences without denaturation. The method, called RGEN-ISL (Ishi *et al*., 2019), has been successfully optimized for maize Knob repeat, and a new approach allowing the simultaneous and specific visualization of proteins, DNA repeat, and sites of DNA replication *in situ* has been developed.

**Keywords:** DNA replication, EdU, S phase, three-dimensional fluorescent *in situ* hybridization (3D-FISH), Rabl configuration, immunostaining, CRISPR/Cas9

**Number of Pages/Appendices:** 95/V

**Language:** English

## BIBLIOGRAFICKÉ IDENTIFIKACE


**Jméno:** Alžběta Němečková


**Název práce:** Studium replikace DNA v průběhu buněčného cyklu rostlin

**Typ práce:** Disertační práce


**Katedra:** Katedra buněčné biologie a genetiky

**Školitel:** Mgr. Eva Hřibová, Ph.D.


**Rok obhajoby:** 2020


**Abstrakt:**

Replikace DNA je proces nezbytný pro růst a vývoj všech živých organismů. Genetická informace je replikována v průběhu S fáze buněčného cyklu. Celý proces probíhá pod přísnou kontrolou, aby k replikaci došlo pouze jednou v průběhu buněčného cyklu. Dosud byl proces replikace DNA intenzivně studován u kvasinek a živočišných buněk, u rostlin byl tento proces podrobně popsán teprve nedávno, a to u dvou druhů s velmi malým a středně velkým genomem – *Arabidopsis thaliana* a *Zea mays*. Informace o průběhu replikace rostlin, především těch s velkým genomem, jsou tak stále předmětem studia.

Předkládaná disertační práce je zaměřena na studium DNA replikace u sedmi vybraných rostlin, které se řadí do čeledi lipnicovité (*Poaceae)*, a které se liší v mnoha vlastnostech, ať už se jedná o velikost genomu, množství repetitivních sekvencí DNA a jejich organizaci v genomu, počet a morfologie chromozómů či uspořádání chromozomů v interfázním jádře. Dřívější práce využívaly pro studium replikace 5-Bromo-2'-deoxyuridine (BrdU). Tento analog tymidinu, inkorporující se v průběhu replikace do nově vznikajícího vlákna DNA, je možné vizualizovat použitím specifických protilátek, které se na BrdU navazují. Vizualizace BrdU však vyžaduje denaturační krok, který negativně ovlivňuje strukturu chromatinu. V průběhu doktorské práce byl pro analýzu průběhu replikace využití tymidinový analog 5-Ethynyl-2'-deoxyuridine (EdU), který se stejně jako BrdU inkorporuje do nově vznikajícího vlákna DNA, a je vizualizován fluorochromy bez použití

denaturace. Následná analýza pomocí průtokové cytometrie umožňuje studovat průběh DNA replikace a identifikovat buněčná jádra procházející různými fázemi buněčného cyklu. Možnost oddělit jednotlivé fáze buněčného cyklu byla klíčovou a za pomocí průtokového cytometru byly získány jednotlivé frakce buněčného cyklu: G1, G2, počáteční, střední a konečná fáze S fáze. Získaná jádra byla použita pro třídimenzionální fluorescenční *in situ* hybridizaci (3D FISH), která umožnila vizualizovat telomerické oblasti DNA podléhající replikaci, společně s cetromerickými oblastmi vizualizovanými pomocí imunolokalizace v trojrozměrném prostoru buněčného jádra. Použití konfokální mikroskopie a umožnilo, na základě překryvů centromer a telomer s replikujícím se chromatinem (značený pomocí EdU), vyhodnotit časový průběh replikace. Výsledkem této komplexní studie je popis časového průběhu replikace centromerických a telomerických oblastí. 3D analýza zároveň umožnila studovat prostorové uspořádání chromozómových oblastí (centromera-telomera) v různých fázích buněčného cyklu rostlin.

Detailní analýza struktury chromatinu naráží na problém denaturace, která je nezbytným krokem v průběhu vizualizace specifických oblastí pomocí standardní FISH metody, čímž může dojít ke změně přirozené struktury chromatinu. Dalším dílčím cílem dizertační práce proto byla optimalizace alternativní, nedávno popsané metody CRISPR-Cas9, která mimo jiné umožňuje i fluorescenční vizualizaci specifických sekvencí DNA a to bez použití denaturačního kroku. Metoda, s názvem RGEN_ISL (Ishi *et al*., 2019), byla s úspěchem optimalizována na kukuřici se sondami specifickými pro Knob oblast a byl vypracován nový přístup nedenaturující kombinace barvení, který umožňuje studovat specifickou sekvenci DNA, průběh její replikace a také epigenetické modifikace *in situ*.

**Klíčová slova**: replikace DNA, EdU, S faze, třidimenzionální fluorescenční *in situ* hybridizace, Rablova konfigurace, immunolokalizace, CRISPR/Cas9

**Počet stran/příloh:** 95/V

**Jazyk:** Anglický

**CONTENT**

# 1 INTRODUCTION

DNA replication is one of the fundamental processes of every living organism. The nuclear genome replicates during the S phase of the cell cycle under strict rules, which ensures that the replication occurs only once per cell cycle. DNA replication must be coordinated with other processes in chromatin such as transcription and remodeling to safeguard accurate duplication of both genetics and epigenetics features.

The core machinery of DNA replication preserves within bacteria, archaea, and eukaryotes (reviewed in O'Donnel *et al*., 2013). DNA replication process has been explored extensively in bacteria circular chromosomes, which has one replication origin (oriC). Bacterial replication protein DnaA binds to oriC, which is unwound and serves for the assembly of the replisome (Gowrishankar 2015; McHenry 2011). Two replication forks assemble and move in the opposite direction around the chromosome from the replication origin. Replication terminates in the terminus region surrounded by Ter sequences binding Tus protein, which mediates direction-specific arrest of progression (Neylon *et al*., 2005; Kaplan *et* Bastia, 2009).

Most of the genomes of eukaryotes are larger than those of prokaryotes and consists of multiple linear DNA molecules, called chromosomes. To assure completion of DNA replication in the time, the process initiates from hundreds to thousands of origins of replication (ORs). Compared to bacteria, eukaryotic ORs are not specified by specific DNA sequences (except *Saccharomyces cerevisiae*) but rather by specific chromatin organization (Bell *et al*., 2010; Rhind *et* Gilbert 2013). In mammals, the ORs very often correspond to transcriptionally active genome regions or other features that allow access to the origin - binding proteins, such as AT-rich sequences and dinucleotide repeats, asymmetrical purine-pyrimidine sequences, or matrix attachment region (MAR) sequences (reviewed in Masai *et al*., 2010).

In contrast to numerous studies on DNA replication in yeasts, *Drosophila*, mouse, and human, little is known about DNA replication dynamics in plants, especially at the molecular level. DNA replication at chromosome level was analyzed in more detail only recently in a few plant species with small genomes, such as *Arabidopsis* and rice, which contain a relatively small proportion of repetitive DNA (Dresselhaus *et al*., 2006; Shultz *et al*. 2007; Lee *et al*., 2010;

Concia *et al*., 2018). In addition to studies focusing on small genome species, the spatial pattern of DNA replication in maize, a plant with the more complex genome (1C ~ 2 655 Mb) containing highly fused heterochromatin blocks, including specific satellite DNA that forms large clusters on chromosomes, was studied (Bass *et al*., 2014; 2015; Wear *et al*., 2017).

Studies of replication dynamics are usually based on the use of thymidine analogs that incorporate into the DNA during the synthesis of a new DNA strand. These approaches have been used for decades with the aim of identification of replication origins; analysis of DNA replication dynamics across different groups of prokaryotic and eukaryotic organisms; study of regulating mechanisms and proteins; and DNA modifications included in the replication process. To clarify these tasks, cytogenetics analysis and the application of next generation sequencing (NGS) followed by the bioinformatic analysis were used.

Replication processes analyzed at the microscopic level provided first information on the disposition of DNA replication dynamics in interphase nuclei or on condensed mitotic chromosomes in time and space (Bass *et al.,* 1997). Cytogenetic analysis of DNA replication dynamics led to the creation of two (2D) and three dimensional (3D) models of replication processing through the whole S phase in human, mammals as well as different plant species including *Arabidopsis*, barley, and maize (Jasencakova *et al*., 2001; Li *et al*., 2001; Gilbert *et al*., 2010a; Brant *et* Aves 2011; Pope *et* Gilbert 2013; Bass *et al.,* 2014; Bass *et al*., 2015; Dvořáčková *et al*., 2018). In these cytogenetic studies, fluorescently labeled thymidine analogs incorporate into nascent DNA and in combination with fluorescent *in situ* hybridization (FISH) resulted in the identification of differences in replication profile during the S phase in different organisms (Hayashi *et al*., 2013; Bass *et al*., 2014; Bass *et al*., 2015; Dvořáčková *et al*., 2018).

Recently, the application of next generation sequencing technologies followed by the bioinformatic analysis was applied to study replication dynamics and provides a new and complex insight into this process (Hansen *et al*. 2010; Wear *et al*., 2017; Zynda *et al*., 2017; Concia *et al*., 2018). Thymidine analogs incorporated into the newly synthesized DNA strand were used for immunoprecipitation followed by ChiP-seq or Repli-seq studies. While ChiP-seq analyses create a specific map of replication origins in the human genome (Dellino *et al*., 2013; Miotto *et al.*, 2016; Sugimoto *et al*., 2018), the Repli-seq approach enabled to analyze temporally order

of replicating DNA at a genome-scale level using massively parallel sequencing (Hansen *et al*. 2010; Wear *et al*., 2017; Zynda *et al*., 2017; Concia *et al*., 2018).

# 2 LITERATURE OVERVIEW

## 2.1 CHROMATIN ORGANISATION IN THE CELL

Long, negatively charged DNA is wrapped around a protein complex known as a histone octamer and consist of two copies of four histone proteins H2A, H2B, H3, and H4 (Figure 1) (Kornberg *et* Lorch 1999; Olins *et* Olins 2003). These complexes form a small structural component of chromatin - nucleosomes (Olins *et* Olins 2003; reviewed in Maeshima *et al*., 2014), which are linked to the next one by 10 - 60 bp DNA linker (Figure 1). DNA in the length of 147 base pairs is wrapped in a left-handed super helicase and turned around the histone octamer (Figure 1). Composite fiber is known as a 10 nm long nucleosome fiber (Olins *et al*.,1974; Maeshima *et al.,* 2014). By application of transmission electron microscopy, Woodcock *et* al. (1984) described that isolated nucleosome fibers formed 30 nm chromatin fibers. Further studies proposed different higher-order structures, which included solenoid, a two-start helix (zig-zag) (van Holde *et* Zlatanova, 2007); hierarchical helical folding model; and radial loop model (reviewed in Maeshima *et al*., 2014).

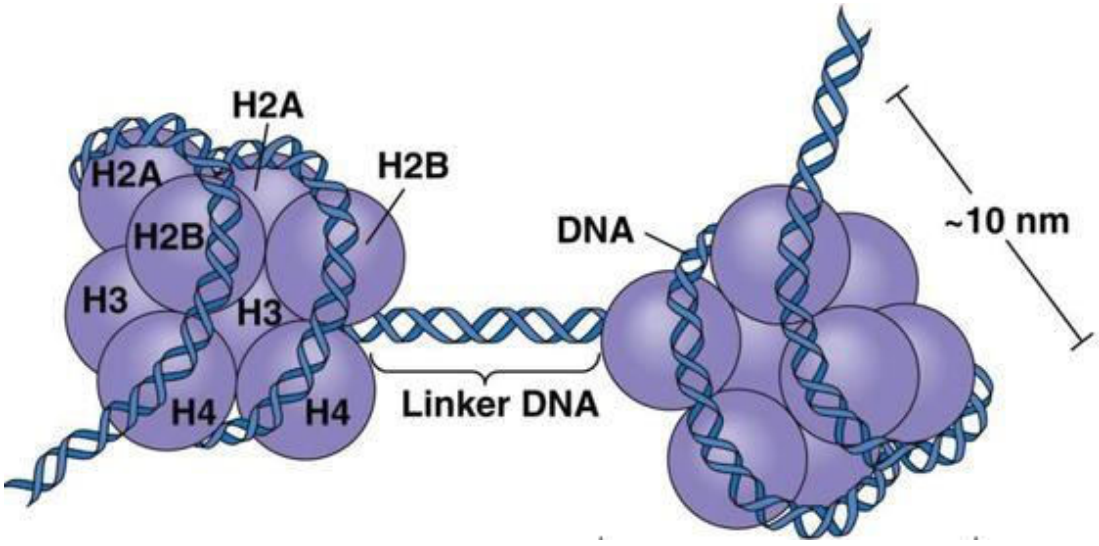


**Figure 1**: Schematic structure of the nucleosome (Caputi *et al*., 2017)

The proposed structure of the 30 nm chromatin fiber is controversial due to the differences observed *in vitro* and *in vivo* conditions (reviewed in Maeshima *et al*., 2019; Prieto *et* Maeshima, 2019). Studies based on cryo-electron microscopy showed that 30 nm chromatin fibers are not present *in vivo* (pioneering work by McDowall *et*

*al*., 1986). This approach used frozen-hydrated cells that were sectioned and observed directly without fixation or chemical treatment. Later, high-resolution information of the cell of yeast and mammalian organisms did not reveal the presence of any higher structures or even 30 nm chromatin fibers (McDowall *et al*., 1986; Dubochet *et al*., 1988; Eltsov *et al*., 2008; Chen *et al*., 2016; Cai *et al*., 2018; Maeshima *et al*., 2019).

Consequently, Dubochet *et al*. (1988) proposed that the basic structure of the chromosome appears to be a liquid-like compact aggregation of 11 nm nucleosome fibers, but not 30 nm chromatin fibers (Dubochet *et al*. 1988). The absence of 30-nm chromatin fibers in mitotic chromosomes *in situ* was also confirmed later by electron cryotomography (Chen *et al*., 2016; Cai *et al*., 2018,), by electron spectroscopic imaging (ESI) in pluripotent mouse cells (Sanborn *et al*., 2015) and also by analysis of X-ray scattering on human interfacial nuclei and mitotic chromosomes (Joti *et al*., 2012; Nishino *et al*., 2012; reviewed in Maeshima *et al*., 2019).

Even more, high-resolution fluorescence-lifetime imaging microscopy (FLIM-FRET) of mammalian HeLa cells and ESI tomography of mouse embryonic fibroblast cells showed the occurrence of 10-nm fibers in condensed heterochromatin domains which create chromocenters in interphase cells, but 30-nm fibers were not detected (Fussner *et al*., 2012; Visvanathan *et al*., 2013).

### 2.1.1 Chromatin structure in the cell - *in vivo* observations

Chromatin is a negatively charged polymer consisting of DNA, and various associated proteins. Observation focused on charged DNA showed that the electrostatic state of the chromatin surrounding environment (cations like $Mg^{2+}$, $Na^{+}$) can influence the organization of the chromatin (Figure 2) (reviewed in Maeshima *et al*., 2019). Based on this knowledge, experiments simulated *in vivo* conditions were provided to describe chromatin structure. The general view of chromatin structure has shifted in the recent 40 years from a static structure to dynamic and highly variable, locally similar to a fluid-like structure (reviewed in Maeshima *et al*., 2019; Maeshima *et al*., 2020). The discrepancies in fiber structures revealed by *in vitro* studies that assumed a 30 nm structure (Woodcock *et al*., 1984; Gilbert *et al*., 2004; Schalch *et al*., 2005; Robinson *et al*., 2006; Song *et al*., 2014) were most likely

caused by experimental low salt buffer conditions in which nucleosome fibers gently repelled due to the insufficient negative charge (Figure 2).

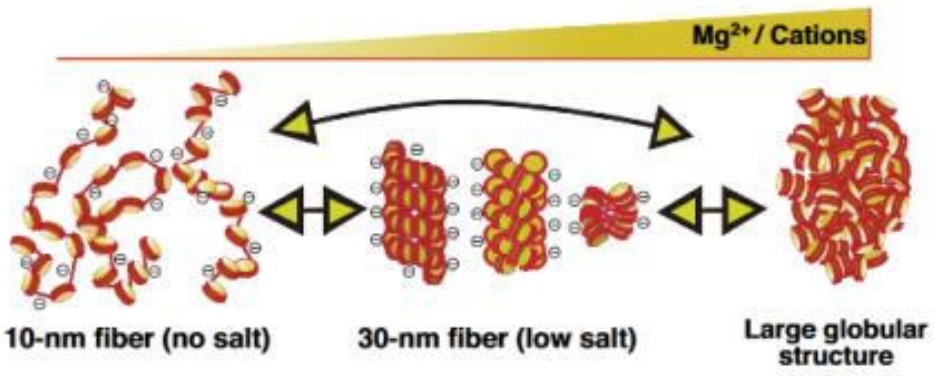


**Figure 2**: Chromatin structure based on buffer conditions (Prieto and Maeshima 2019)

And accordingly, each nucleosome tended to bind selectively to the close neighbor on the DNA strand, and this binding led to the formation of stable 30 nm fiber (reviewed in Maeshima *et al*., 2019). Recently, small-angle X-ray scattering (SAXS) found no evidence of 30 nm fibers of chromatin in interphase nuclei and human mitotic chromosomes (Nishino *et al*., 2012). Studies focused on nucleosome-nucleosome interactions observed using SAXS reflected bulk packaging of 10 nm fibers in a highly disordered state. This structure called 'polymer melt' structure means that nucleosome fibers may move continuously and rearrange at the local level (Maeshima *et al*., 2014; Hansen *et al*., 2018).

*In vivo* studies showed, that 30 nm structure is quite common absent, and the chromatin is composed of irregular 10 nm-fibers (Prieto *et* Maeshima 2019). However, 30 nm fibers also exist *in vivo* in particularly rare cases, e.g. in regions of interchromatin space (Cremer *et* Cremer, 2019) or uncertain terminally differentiated cells which are transcriptionally silent, such as chicken erythrocytes (Langmore *et* Schutt, 1980; Scheffer *et al*., 2011), starfish sperm (Scheffer *et al*., 2011), and mouse photoreceptor cells (Kizilyaprak *et al*., 2010). The shift from a static solid-like regular substance to a structure with dynamic behavior including fluid 10-nm fibers similar to a polymer melt allowed to explain a biological process such as transcription, replication, and DNA repair (reviewed in Prieto *et* Maeshima, 2019).

### 2.1.2 Large scale chromatin organization: chromatin domains

Chromatin 10-nm fiber structure is not randomly packed within the nucleus and adopts various higher-order structures (Sexton *et* Cavalli, 2015). Hi-C analysis of budding yeasts revealed that chromatin is essentially open and forms clusters of only a few nucleosomes (Hsieh *et al*., 2015). Similarly, the budding yeast chromatin analyzed *in vivo* in three-dimensional space (using electron cryotomography) revealed open configuration instead of compact structures with an absence of chromatin domains in interphase and mitosis (Chen *et al*., 2016; Cai *et al*., 2018). The large-scale chromatin higher organization included chromonema, a fiber with a diameter of 100-200 nm, which was observed by electron microscopy during the process of chromosome decondensation during the G1 phase of the cell cycle in synchronized ovary cells of Chinese hamster (Belmont and Bruce, 1994).

Another stable unit of chromosome structure made up of replicon clusters with an average diameter of about 110-150 nm and was observed in human HeLa cells and rat kidney cells by pulls labeling of replication domains analyzed by high-resolution microscopy (Jackson *et* Pombo, 1998; Xiang *et al*., 2018). The same structures were previously revealed using three-dimensional structured illumination microscopy (3D-SIM) (Markaki *et al*., 2010). Mammalian live-cell imaging by super-resolution photoactivated localization microscopy (PALM) observation and single-molecule tracking revealed nucleosome clusters/domains with a diameter of about 200 nm (Nozaki *et al*., 2017).

Higher chromatin organization in mammalian and insect cells inspected using genomic approaches such as chromosome conformation capture (3C) and Hi-C methods (Dekker and Heard 2015), revealed numerous chromatin domains known as topologically associating domains (TADs) (Dixon *et al*., 2012; Sexton *et al.,* 2012; Dixon *et al*., 2016) and additional loop domains formed by cohesins (Rao *et al*., 2014; Rao *et al*., 2017). The TAD-like domains were revealed also by high-resolution Stochastic optical reconstruction microscopy (STORM) based on chromatin tracking in combination with chromatin painting (Bintu *et al*., 2018).

In plants, using the Hi-C analysis, TADs were founded in rice, foxtail millet, sorghum, tomato, cotton, and maize. Surprisingly, in *Arabidopsis thaliana* and *A. lyrata* TADs can be hardly found in chromosome arm, despite appearing to be a

prevalent structural feature of genome packing in many other species (reviewed in Doğan *et* Liu, 2018).

Recently, super-resolution live-cell imaging (Nozaki *et al*., 2017), similar to chromosome conformation capture studies, revealed how large-scales substructures of chromatin are created (Ghirlando *et* Felsenfeld 2016). Local nucleosome-nucleosome interactions by histone tails were reported as a crucial mechanism for substructures compaction. Long disordered tails were suggested as multivalent liquid-like glues for chromatin (reviewed in Maeshima *et al*., 2019). Other suggestions were proposed based on transcriptional repressor CTCF (known as 3D structure regulation factor) (Ghirlando *et* Felsenfeld 2016) or based on super-resolution chromatin tracking in mammalian single cells (Bintu *et al*., 2018) when cohesin complexes played a role as a holder of nucleosome fibers which generated loops during chromatin domain formation (reviewed in Maeshima *et al*., 2019).

Two major factors contribute to TADs formation in animals. The formation is caused by the action of loop extrusion by cohesion and action by CTCF proteins. The second-factor which plays a role in formation is the spatial chromatin compartmentalization in accordance with the epigenomic landscape and transcriptional activity (reviewed in Doğan *et* Liu, 2018). In the case of plants, the presence of TADs seems to be related to its genome size (reviewed in Doğan *et* Liu, 2018). The absence of TADs in the small genome of *Arabidopsis* (more than three times smaller than rice) is explained due to the absence of CTCF proteins (reviewed in Doğan *et* Liu, 2018). But it should be pointed out, that the chromatin region of *Arabidopsis* was referred to as a TAD if it has a comparable size such as in animal cases (reviewed in Doğan *et* Liu, 2018).

### 2.1.3 Chromosome organization

The most compact structure of chromatin is necessary for effective cell division and subsequent transmission of genetic information to daughter cells. In this stage, chromatin is highly condensed and forms a unique chromosome structure. Different models were proposed to describe a process of this higher chromatin structure condensation (reviewed in Beseda *et al*., 2020): a model of hierarchical helical folding (Figure 3A) (Finch *et* Klug, 1976; Woodcock *et al*., 1984), radial loop model (Figure 3B) (Paulson *et* Laemmli, 1977), dynamic matrix model (Figure 3C)

(Wanner *et* Formanek 2000), chromatin network model (Figure 3D) (Poirier *et* Marko 2002), constitutive/nested loop model (Figure 3E) (Gibcus *et al*., 2018), and stacked layer loop model (Figure 3F) (Daban 2015).

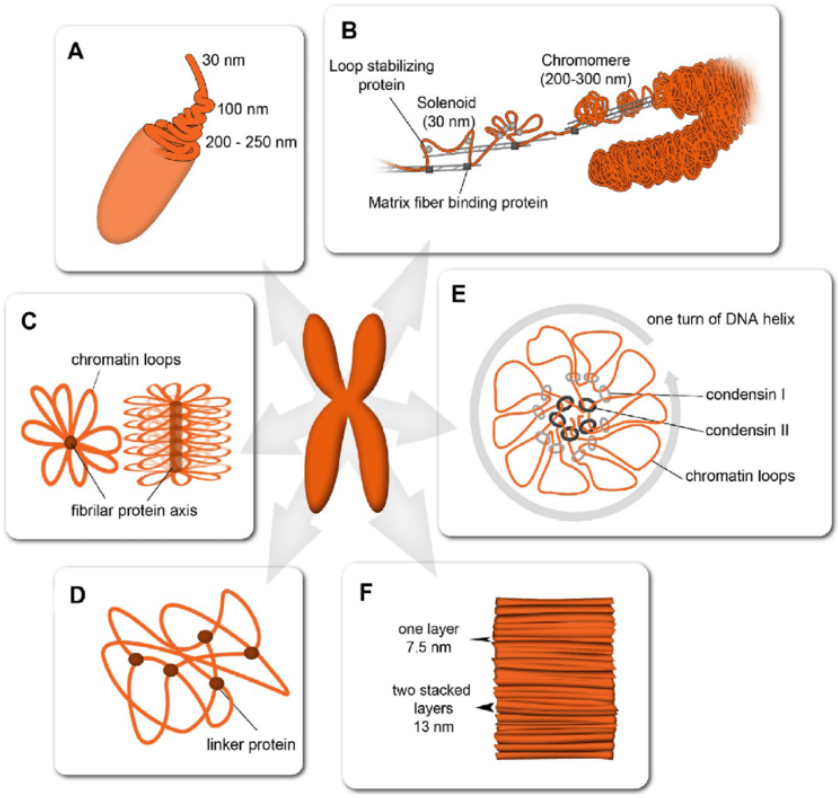


**Figure 3**: Models of chromosome organization. A: Hierarchical helical folding, B: Dynamic matrix model, C: Radial loop model, D: Chromatin network model, E: constitutive/nested loop model, F: Stacked layer loop model (Beseda *et al*., 2020)

Pioneering works focused on chromosome folding (reviewed in Beseda *et al*., 2020) begun with the use of electron and light microscopy of human and *Drosophila* chromosomes. The studies assumed classical hierarchical helical folding of chromatin, in which 10 nm fiber coiling in 30 nm fiber and then 100-nm and 200-250 nm fiber form (Figure 3A) (Finch *et* Klug, 1976; Woodcock *et al*., 1984). This model was proposed based on *in vitro* conditions of vertebrate and plant chromosomes (Manton 1950; Ohnuki 1968; Rattner *et* Lin, 1985). The idea about the classical hierarchical folding model of mitotic chromosomes was disturbed using modern 3C, 5C, and Hi-C methods, which principle is the fixation of chromatin by the formaldehyde and it's cross-linking (Dekker *et al*., 2002; Lieberman-Aiden *et al*.,

2009). Formaldehyde fixation preserves the protein-mediated contacts of adjacent chromatin regions. Following the sequencing of contact regions and subsequent polymer simulations disrupted the classical hierarchical model of chromosomes. This approach used in human study revealed much lower interaction distance than in a hierarchical model and described the linearly-organized longitudinally compressed array of constitutive chromatin loops (Figure 3E) (Naumova *et al*., 2013).

The dynamic matrix model (Figure 3B) was proposed for barley mitotic chromosomes analyzed by electron microscopy (Wanner *et* Formanek, 2000). According to this model, solenoid chromatin structures associate with proteinaceous parallel matrix fibers, which formed loops. Solenoid subsequently condensed into 200-300 nm knobby fiber (Hozier *et al*., 1977) celled chromosomes and suggestively stabilized by cross-linker protein (reviewed in Beseda *et al*., 2020).

The radial loop model (Figure 3C) in which chromosomes consisted of scaffolds or cores, which were surrounded by a loop of DNA (10-30 nm long, 30-90 kb), was proposed in the study of HeLa cells, where histone-depleted chromosomes were observed by electron microscopy (Paulson *et* Laemmli, 1977). This radial model was more consistent with Hi-C data than the hierarchical model (Naumova *et al*., 2013). Recently, fluorescent labeling and subsequent tree dimensional-structured illumination microscopy (3D-SIM) of human chromosomes revealed that chromosome scaffolds were made by discontinuously arranged protein complexes, which formed double helix instead of continuous fiber (Paulson *et* Laemmli 1977; Poonperm *et al*., 2015).

The chromatin network model (Figure 3D) presented in the study of amphibian mitotic chromosomes (using microchemical force measurement during nuclease digestion) suggested chromatin as an only component of the chromosome, and any “scaffolds” were not observed (Poirier *et* Marko, 2002). Later studies suggested linker proteins as a component which were involved in chromosome condensation (Ono *et al*., 2003; Maeshima 2003; Sun *et al*., 2018; Hirano 2016; Piskadlo 2017).

The stacked-layer loop model consisting of stacked layers of planar chromatin perpendicular to the chromosome axis are corresponding with classical cytogenetic banding approaches (Daban 2015), and can also explain long-distance interaction frequencies obtained from Hi-C data (reviewed in Beseda *et al*., 2020). Experiments based on micrococcal nuclease digestion of nuclei showed that

chromatin fragments self-assembled into plate-like structures. The proximity of multi-layered structures differed in metaphase chromosomes, where stacked and more compact structures appeared. In comparison, in the interphase nuclei, more open chromatin structures were observed (Chicano *et* Daban, 2019).

The nested loop model (Figure 3E) was described after Hi-C data analyses of chicken DT40 cells after depletion of condensin I, condensin II, or both (Gibcus *et al*., 2018). This model supported the role of the complex of condensin I and condensin II in a mitotic chromosome condensation process (Gibcus *et al*., 2018).

## 2.2 Chromosome organization (arrangement) in interphase nuclei

As mentioned above, chromatin was found very dynamic and appeared in different levels of compaction, which were essential for the DNA-dependent process that occurred during the cell cycle. The eukaryotic genome consists of chromosomes that occupy specific regions, so-called chromosome territories (CTs) in interphase nuclei (Figure 4) (Cremer *et* Cremer, 2001). CTs can be visualized using chromosome painting in which a fluorescent probe covered whole chromosomes (Lysak *et al*., 2001; Mandáková *et* Lysak 2008; Han *et al*., 2015; Šimoníková *et al*., 2019; Jiang 2019). CTs were found in animal nuclei and plants as well, but specific differences were discovered (Fransz *et al*., 2002; Cremer *et* Cremer, 2010). The evolutionary conversed radial arrangement is known in mammals, where gene-rich chromosome regions preferentially located in the nuclear interior (Tanabe *et al*., 2002; Cremer *et* Cremer 2010). On the contrary, the radial arrangement was not revealed in insect nuclei (McKee 2004). In the plants with large metacentric chromosomes, clusters of centromeres and telomeres were arranged on the opposite poles in the interphase nuclei (Schubert *et* Show 2011).

Beside chromosome territories, interphase chromatin can be distinguished based on its condensation into heterochromatin or euchromatin compartments. In the last decades, chromosome organization in interphase nuclei was revealed by Hi-C methods (Dekker *et al*., 2002; Lieberman-Aiden *et al*., 2009), which allowed to investigate chromosome contact and revealed general rules for chromosome folding. Based on chromatin interactions, different compartments such as “A” and “B” compartments (Figure 4) (Lieberman-Aiden *et al*., 2009; Rao *et al*., 2014), functional units of chromosome ‘loops’ known as topologically associated domains (TADs)

(Figure 4) (Dixon *et al*., 2012) and lamina-associated domains (LADs) were defined (Figure 4) (Cremer *et* Cremer 2010; Szabo *et al*., 2019).

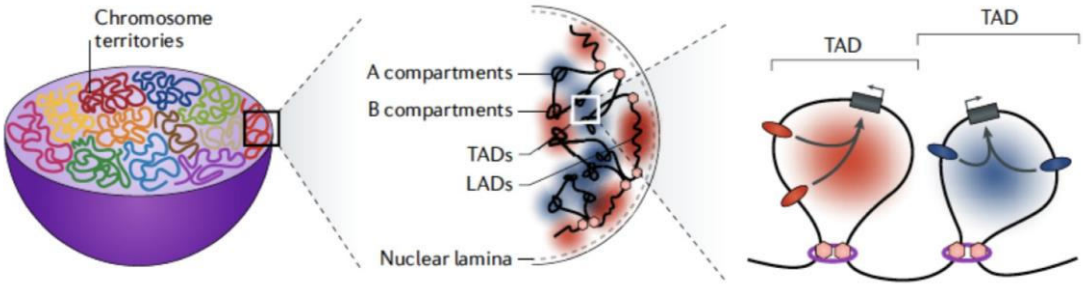


**Figure 4**: Chromatin organization in interphase nuclei (Spielmann *et al*., 2018).

### 2.2.1 Chromosome arrangement

Chromosome arrangement in interphase nuclei was firstly observed in salamander nuclei and published by Carl Rabl in 1885. In this study, a model where centromeres and telomeres were localized on opposite nuclear poles was proposed. This arrangement was later assigned to the organization of chromosomes in mitotic anaphase as a remnant of relic cell poles, and further observed by fluorescent *in situ* hybridization in human, animal, and plant cells (for example, Heslop-Harrison 1991; Rawlins *et al*., 1991; Werner *et al*., 1992). The above mentioned centromere - telomere orientation was later named after its discoverer (who also proposed the existence of chromosome territories), as Rabl orientation (Figure 5A). The interphase arrangement of chromosomes was initially studied on human fibroblast metaphase spreads. Human larger chromosomes were located near the periphery compared to smaller ones (Ockey 1969; Hoo *et* Cramer, 1971). Later studies on different human cell types showed the radial position of chromosome territories with the association to the nuclear lamina, associated with gene density. Radial arrangement correlated with gene density, where gene-rich chromosome arms were located preferentially in the nuclear interior (Bolzer *et al*., 2005; Grasser *et al*., 2008; Jowhar *et al*., 2018; reviewed in Crosetto *et* Bienco, 2020). Similar observations were confirmed in primates, mouse, chicken, turkey, and duck cells (Mayer *et al*., 2005; Mora *et al*., 2006; Skinner *et al*., 2009).

In contrast, knowledge about the interphase chromatin organization of plants is still limited. A focus on plant interphase arrangement revealed two chromosomes

arrangement types: 1) Rabl orientation was described for the plant with the large genomes; and 2) Rosette-like organization which remained a pattern of centromere - telomere orientation in mammalian cells (Weierich *et al*., 2003). The Rosette-like structure (Figure 5B) was described in *Arabidopsis* cells, where the tendency of positioning centromeres closer to the nuclear lamina and telomeres closer to the nucleus center was proposed by Fransz *et al*. (2002). Centromeres consisted of heterochromatic regions, chromocenters, were located in the nuclear periphery, whereas telomeres were congregated around nucleolus (Figure 5B) (Fransz *et al*., 2002; Pecinka *et al*., 2004; Tiang *et al*., 2012; Schubert *et al*., 2014).

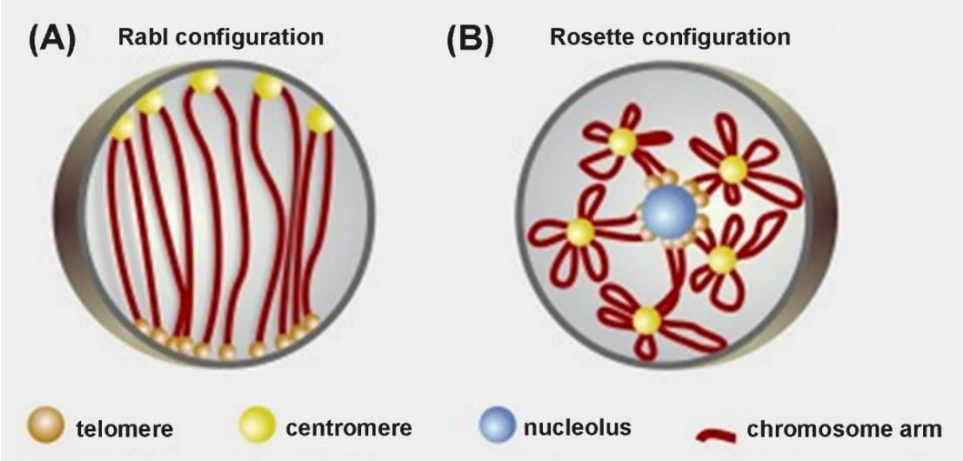


**Figure 5**: Chromosome arrangement interphase nuclei (according to Grob and Grossniklaus, 2017)

Plants with large genomes such as barley, rye, and oat displayed different centromere - telomere orientation. Centromeres and telomeres are positioned on the opposite poles in interphase nuclei. However, many exceptions can be found in the plant kingdom. Most somatic cells of plants with smaller and moderate genomes like rice, maize, and sorghum lack of Rabl configuration (Dong *et* Jiang, 1998; Armstrong *et al*., 2001; Fransz *et al*., 2002; Schubert *et* Shaw 2011; Tiang *et al*., 2012; Idziak *et al*., 2015). On the other hand, premeiotic anther cells or xylem-vessel precursor cells of rice seem to be organized in Rabl (Prieto *et al*., 2004; Santos *et* Show, 2004). Furthermore, plants with larger genomes such as onion, garden pea, potato, and filed bean did not show Rabl configuration (Rawlins *et al*., 1991; Fussell 1992; Harrison *et* Heslop-Harrison 1995; Kamm *et al*., 1995). Some cytogenetic studies also suggested differences of inner nuclei organization, with larger

chromosomes located on the nuclear periphery and smaller chromosomes near to the center (Sun *et al.* 2000; Koláčková *et al*., 2019; Perničková *et al*., 2019), similar to mammalian nuclei. Another hypothetical factor that could play a role in the interphase arrangement in eukaryotic cells could be connected with nuclear shape, surrounding cell types and the geometry of tissues (reviewed in Crosetto *et* Bienko, 2020). It was shown, that the shape and size of each nucleus were determined by the cytoskeleton. Despite chromosome repositioning after experimental perturbations on human cultured fibroblasts were observed, the connection between nuclear shape and chromatin arrangement remains to be investigated (reviewed in Crosetto *et* Bienko, 2020).

### 2.2.2 Heterochromatin and euchromatin compartments

Interphase chromatin is historically classified based on the level of condensation as heterochromatin and euchromatin. This classification was described based on cytogenetic methods and microscopic observation (Heitz 1928). Euchromatin regions are less compact, and correspond to actively transcribed genes or potentially active genes. Heterochromatin domains are more compact, composed of nucleosomes condensed in 30 nm fiber, and consisted of transcriptionally inactive and highly conserved regions (reviewed in Janssen *et al*., 2018). Heterochromatin regions are traditionally divided into constitutive and facultative heterochromatin (Kosak *et* Groudine, 2004). Constitutive heterochromatin is usually gene-poor and mainly formed by repetitive sequences like centromeric or pericentromeric repeats (Kosak *et* Groudine, 2004). Facultative heterochromatin is more dynamic than constitutive, and can change in response to cellular signals and contains genetic information that is transcribed (reviewed in Grewal *et* Jia, 2007).

### 2.2.3 Topologically associated domain (TADs)

As mentioned before, a detailed focus on chromosome organization in interphase provided by Hi-C analysis in mammals revealed topologically associating domains (TADs) (Figure 4) (reviewed in Pombo *et* Dillon, 2015). The structural organization of TADs in the genome is maintained across different cell types and it was shown that is partially conserved. Mammalian TADs were found to be highly conserved between different cell types and tissues, and even between different

species (Dixon *et al*., 2012). In *D. melanogaster*, smaller TAD domains were proposed and their size perhaps reflected a smaller genome of the fruit fly compared to mammals, and closer packaging of the genes (Szabo *et al*., 2019)

To this date, TADs have not been identified in *S. cerevisiae* (reviewed in Pombo *et* Dillon, 2015). In plants, TADs genome distribution was described in rice where their formation seemed to be linked to gene densities. It was shown that protein-coding gene density was much lower inside TADs borders than in regions outside of TADs (Liu *et al*., 2017). This may be connected with chromatin properties, that histone modifications and gene expression might correlate with TADs formation (Dong *et al*., 2017). No synteny between plant species (sorghum, maize) was observed, and any conserved features, such as in mammalian cells, were not supposed (Dong *et al*., 2017).

### 2.2.4 Lamina Associated Domains (LADs)

Chromatin regions that are preferentially in contact with nuclear lamina at the inner membrane of the nucleus are so-called lamina associated domains (LADs), or B compartments (Meuleman *et al*., 2013) (Figure 4). LADs interaction was identified in metazoans by Guelen *et al*. (2008) and Pickersgill *et al*. (2006). LADs were visualized by microscopy or chromatin immunoprecipitation (ChIP) (Handoko *et al*., 2011). LADs were revealed in *D. melanogaster*, *Caenorhabditis elegans*, and mammalian cells (reviewed in Van Steensel *et* Belmont, 2017) as well as in *Arabidopsis* (Pontvianne *et al*., 2016; Hu *et al*., 2019;).

These domains are mostly constituted of transcriptionally silent genes or genes characterized by a low level of expression (reviewed in Van Steensel *et* Belmont, 2017) and corresponded to late replicating regions of the genome (Pope *et al*., 2014; Peric-Hupkes *et al*., 2010). LADs preferentially represented gene-poor regions less than 1 Mb large, and rich for chromatin modification such as H3K9me2 and H3K27me3, which are typical for heterochromatin (Guelen *et al*., 2008; Wen *et al*., 2009; Harr *et al*., 2015). Based on the traditional classification of heterochromatin, LADs consisted of constitutive and facultative chromatin regions. In mouse and human studies, constitutive LADs were found to be rich in the A/T base pairs. Changes in the interactions with lamina during the cell differentiation

were found typical for facultative LADs, which were also found to be cell-specific (Peric-Hupkes *et al*., 2010; Meuleman *et al*., 2013; Dobrzynska *et al*., 2016).

Similar to LADs, nucleolus associated domains (NADs) were described (Németh *et al.* 2010; van Koningsbruggen *et al*., 2010). The NADs represented genome regions associated with the nuclear lamina at the nucleus periphery (Pontvianne *et al*., 2016). These domains were first described in HeLa carcinoma cells (Németh *et al*., 2010; van Koningsbruggen *et al*., 2010). Recent studies showed that NADs represented mainly, but not exclusively, specific heterochromatin regions associated with the nucleolus. Similarly, to LADs, histone constitutive heterochromatin modifications were described also in NADs (Matheson *et* Kaufman 2016; Van Steensel *et* Belmond 2017). NADs were identified in human and mouse cells, and also in *A. thaliana* (Németh *et al*., 2010, van Koningsbruggen *et al*., 2010; Pontvianne *et al*., 2016; Dillinger *et al*., 2017; Vertii *et al*., 2019)

## 2.3 Cell cycle in eukaryotes

The cell cycle is a series of processes leading to cell reproduction. This process is evolutionarily conserved from unicellular microorganisms to highly organized eukaryotes. The cell cycle process ensures growth, differentiation, and transmission of genetic information to the next generation. The cell cycle is generally divided into two main stages: interphase and mitotic phase (M). M phase includes mitosis and subsequent cytokinesis. During interphase, cells grow and accumulate nutrients, and DNA replication occurs in the synthetic (S) phase. The mentioned S and M phases are separated by two gap phases - G1 and G2 (Figure 6).

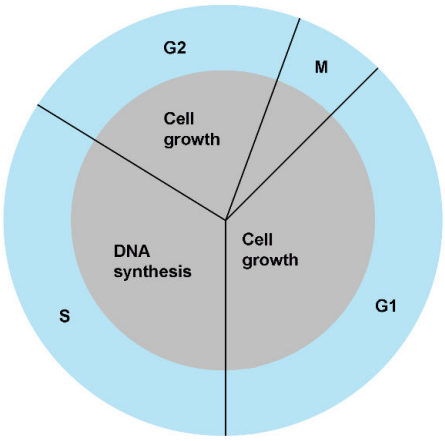


**Figure 6**: Scheme of the cell cycle

During interphase in the postmitotic G1 phase, the cells are prepared for replication by the intensive synthesis of the necessary component such as proteins, RNA, and nucleotides (Houtgraaf *et al*., 2006). At the end of the G1 phase, the cell is about double its original size, more organelles are produced, and the volume of cytoplasm increased. Subsequent replication of the nuclear genome is a fundamental process of the life that occurs in the synthetic phase (S phase). During the DNA replication, double-strand DNA separates, and individual strands are served as a template for the replication (firstly described by Watson *et* Crick, 1953). As a result, new DNA is composed of the original DNA strand as well as a newly synthesized strand (Burgers *et* Kunkel, 2017). After the replication phase, the cell prepares for division in the post-synthetic G2 phase, continues with growing, production of extra proteins, and preparation for mitosis occurs. After the mitotic phase, when chromosomes are organized into the genetically identical daughter cells, the cell cycle starts again (Houtgraaf *et al*., 2006). After the M phase, cells can stop in the G0 phase knows as the resting phase. These phases can occur for multiple reasons.

Primarily, cells enter the G0 phase due to environmental factors like nutrient deprivation. But for example, neuron cells are fully differentiated and reside in the terminal G0 phase not because of nutrient deficiency but because of genetic programming (Bernstein *et al*., 2008). Same as neuron cells, differentiated muscle, bone, and same renewable tissue cells can stay in the G0 phase. In the plant, no cycling cell was observed in maize roots (Clowes 1971; reviewed in Velappan *et al*., 2017).

The passage of the cell cycle is regulated by the checkpoints. Eukaryotes have two main points located on the interface G1/S and G2/M phases and inter-S phase checkpoint which prevents un-replicated DNA (Houtgraaf *et al*., 2006).

### 2.3.1 Alterations of the cell cycle

In many plant and animal cells, alterations of the cell cycle can occur. In addition to the mitotic cycle mentioned above, two main alternations are described: 1) endocycle (also known as endoreduplication) and 2) endomitosis (Figure 7).

During endocycle, cells undergo successive DNA replication, but the cell avoids mitosis entirely (Joubes *et* Chevalier, 2000). Endocycle usually occurs in specialized cells and contributes to the synthesis of a higher amount of proteins, or is

essential for reproduction like in mouse trophoblast (Gandarillas *et al*., 2018). In plants, for example, endoreduplication cells are present in seed endosperm, fruits, cotton fibers, or nitrogen-fixing roots (Sabelli *et* Larkins, 2009; Chevalier *et al*. 2011; Wilkins *et al*., 2000; Kondorosi *et* Kondorosi 2004). During tomato fruit development, nine rounds of endoreduplication can occur, which results in cells of the fruit's pericarp representing 512 C (Quinet *et al*., 2019). Compared to plants, endoreduplication in animal cells is not very common.

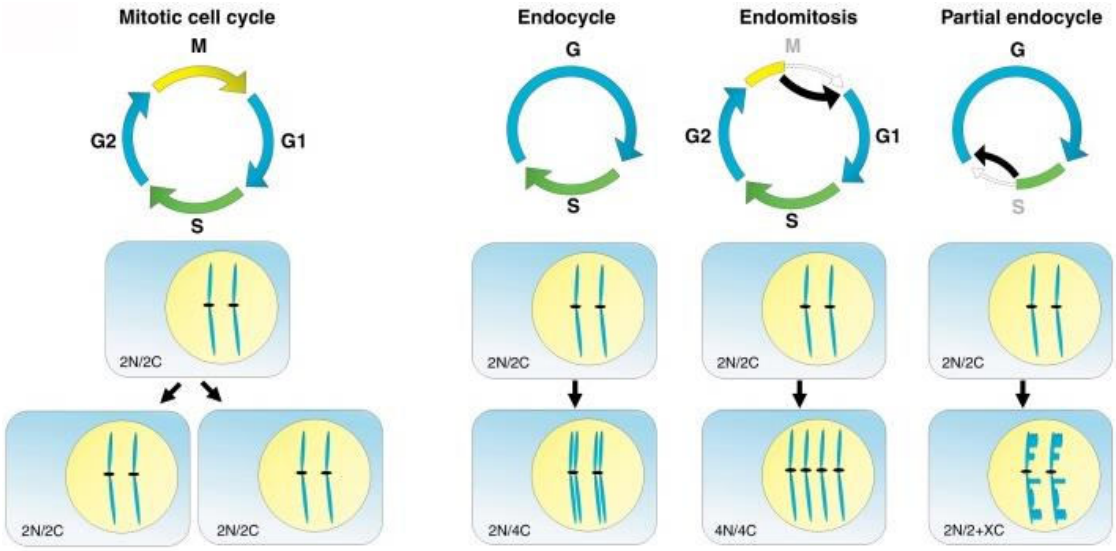


**Figure 7**: Cell cycle and its variants (Breuer *et al*., 2014).

During endomitosis (Figure 7), the cell division process is skipped, and the chromosome number is doubled in each cycle (Figure 7) (Joubes *et* Chevalier, 2000). This phenomenon was described in insect salivary gland cells and resulted in the formation of polytene chromosomes (Edgar *et al*., 2014).

A unique phenomenon, partial endoreplication was discovered in eukaryotes (Rosenbusch *et al*., 1998). This phenomenon was discovered based on DNA content measurement by flow cytometry in animals (Wang *et* Davis, 2014; Del Priore and Pigozzi, 2014) and in plants as well (Suda 2004; Suda *et al*., 2007). In animals, these processes are caused by DNA programmed elimination between germline and somatic cells (Wang *et* Davis, 2014). Whole chromosome elimination was described in Bengalese finch (Del Priore *et* Pigozzi, 2014). Another way of programmed elimination, chromatin diminution, which is connected with chromosome breaks and

following extrusion of chromatin proportions in the cytoplasm was described by Smith *et al*. (2009) and Bracht *et al*. (2013).

In the plants, progressively partial endoreduplication was described. During this process, the DNA content and the number of endoreplication cycles are in linear correlation. Endoreplicated cycles are then resulted based on DNA amount as 2C+P, 2C + 3P, 2C + 7 P, etc., where 2C is the DNA content of nuclear DNA, and P is the content of DNA which is partly replicated (Figure 7) (Suda 2004; Suda *et al*., 2007; Bory *et al*., 2008; Trávníček *et al*., 2011; Trávníček *et al*., 2015; Hřibová *et al*., 2016, Brown *et al.*, 2017). This unique phenomenon was revealed in orchid species and was found to be useful for their identification (Trávníček *et al*., 2011; Trávníček *et al*., 2015).

## 2.4 DNA replication

Replication of the nuclear genome is a fundamental process of the life that occurs in the synthetic phase (S phase) (Figure 6) of the cell cycle. This process is strictly controlled during the cell cycle to ensure complete DNA replication that is essential for growth and development. Errors that accompanied the replication process and consequent repair mechanisms result in a mutation at the DNA level can lead to genome instability (Gambus 2017). DNA replication process is highly conserved in all living organisms (reviewed in Oakley, 2019). Whole processes of replication started by initiation proteins, which binds to DNA and disrupts DNA helix structure in the region called replication origins (reviewed in Burgers *et* Kunkel, 2017). In bacteria and archaea, replication origins are defined by specific nucleotide sequences (reviewed in Costa *et al*., 2013). Higher eukaryotes consist of multiple origins of replication, which are not conserved at the nucleotide sequence level. In the beginning, DNA is unwinding into two parental strands, and new DNA strands are synthesized accordingly. During the elongation process, the DNA strand knows as the leading strand, is synthesized in 3' to 5' end direction according to the parental one by adding nucleotides by DNA polymerase. The second unwinds DNA strand, known as the lagging strand, is synthesized discontinuously from 5' to 3' direction by Okazaki fragments, which are synthesized and subsequently joined (reviewed in Burgers *et* Kunkel, 2017). DNA replication terminates when the replication fork meets each other (reviewed in Burgers *et* Kunkel, 2017).

### 2.4.1 DNA replication in bacteria and Archaea

Bacterial genome, which is usually one circle molecule (Casjens 1998) with a length of about several million base pairs, has only one replication origin (oriC) (Marczynski *et* Shapiro, 1993). Due to the one origin of replication, *E. coli* was used as a model organism for analysis of the initiation process of DNA replication (reviewed in Oakley 2019). In contrast to much larger eukaryotic genomes, which consisted of about 10 000 origins of replication, bacterial replication occurs in a relatively short time. Bacterial replication is initiated bidirectionally from OriC (Galli *et al*., 2019). The origin of replication is recognized by DnaA origin-binding protein, which binds ATP and A/T-rich regions (Figure 8). The protein complex responsible for dsDNA unwinding and RNA primers synthesizing is known as primosome (Figure 8). Primosome consists of helicase (DnaB) that unwinds the dsDNA, helicase loader (DnaC), and DnaG which synthesizes RNA primers (Figure 8). After DNA unwinding, a single strand "bubble" appears and replicative helicase can bind and a new DNA strand is synthesized (reviewed in O'Donnell *et al*., 2013). DNA replication terminates when replication forks reach the Ter region (region diametrically opposite to OriC) (reviewed in Oakley, 2019).

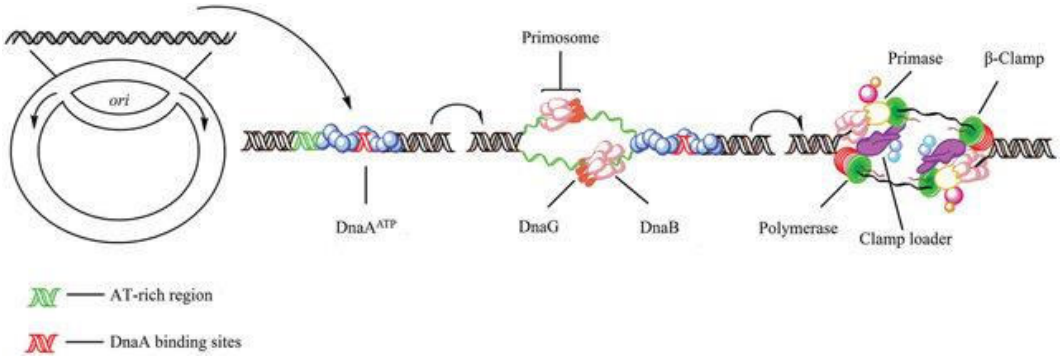


**Figure 8**: Replication process in bacteria (Song *et al*., 2015)

Archeae, similarly to eukaryotes, have more than one origin of replication (Figure 9) (reviewed in Costa *et al*., 2013). On the other hand, the same as bacteria, archaea have conserved sequence-specific sites for binding the initiator of replication (Robinson *et al.,* 2004; Robinson *et* Bell, 2007). Archaea DNA replication starts with a clearly defined AT-DNA rich structure. After DNA unwinding origin recognition proteins binds (reviewed in Ausiannikava *et* Allers, 2017). In Archaea,

controversially to bacteria, origins of replication are recognized by Orc1/Cdc6 proteins (Figure 9) (homologous to eukaryotic).

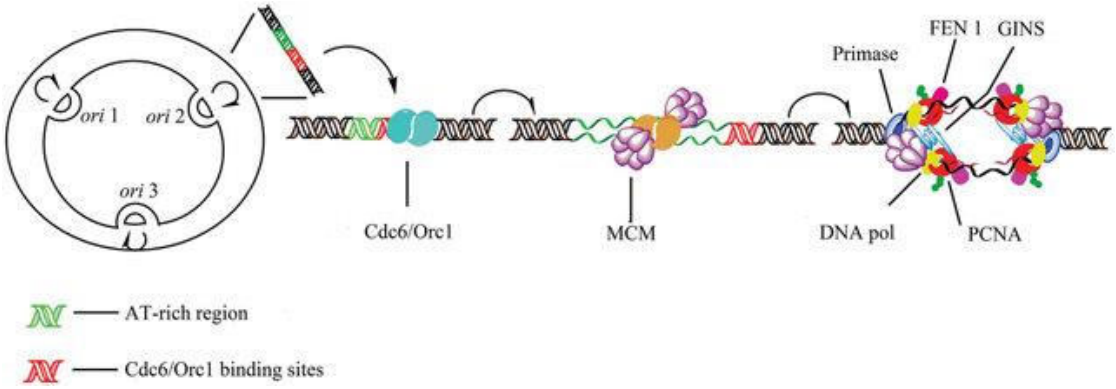


**Figure 9:** Replication process in Archaea (Song *et al*., 2015).

Replication of circular chromosome terminates when replication terminus binding protein (Tus) reaches the termination zone contains TER sites (reviewed in Dewar *et* Walter 2017).

### 2.4.2 DNA replication process in eukaryotes

Except for *Saccharomyces cerevisiae,* eukaryotic organisms containing multiple origins of replication which are not defined by specific DNA sequence were found. Multiple origins of replication are organized in clusters and activated at a specific time in the S phase (reviewed in O'Donnell *et al*., 2013). Origin recognition complex (ORC) in eukaryotes composed of six subunits (Orc1-6). The position of DNA replication initiation is genetically determined by elements to know as cis-acting sequences or replicator (Jacob *et al*., 1963). These cis-acting sequences act with trans active sequences knows as initiators. It was shown, that eukaryotes cis-acting sequences and DNA binding protein complex which is necessary for the proper formation of the pre-replication complex (pre-RC), are highly conserved (reviewed in Fragkos *et al*., 2015). Pre-RC is formed during the G1 phase, in the so-called origin licensing process (Masai *et al*., 2010; reviewed in Fragkos *et al*., 2015). During origin licensing, ORC binds to all replication origins, and the minichromosome maintenance protein complex (MCM) (Mcm2-7 proteins) is placed around dsDNA. With the help of Cdc1 and Cdc6 subunits, pre-RC is formed (Oehlmann *et al*., 2004). As a consequence of Mcm2-7 ring loading, the dsDNA is opened. Subsequently, cells enter the S phase, and Cdc45 and GINS factors bind to

the Mcm complex. As follows, CMG helicase which consists of Cdc45, Mcm2-7, and GINS is activated (Aparicio *et al*., 2006). After origins firing, initiator proteins must be degraded to ensure, that DNA synthesis occurs only once per cell cycle and re-replication is prevented. The complex, that carries out the replication of DNA is the so-called replisome (see Figure 10) consisting of already mentioned CMG helicase, DNA polymerase Pol α (primase), DNA polymerase ϵ and δ, PCNA clamps, replisome progression complex (RFC), and RPA (single-strand binding protein).

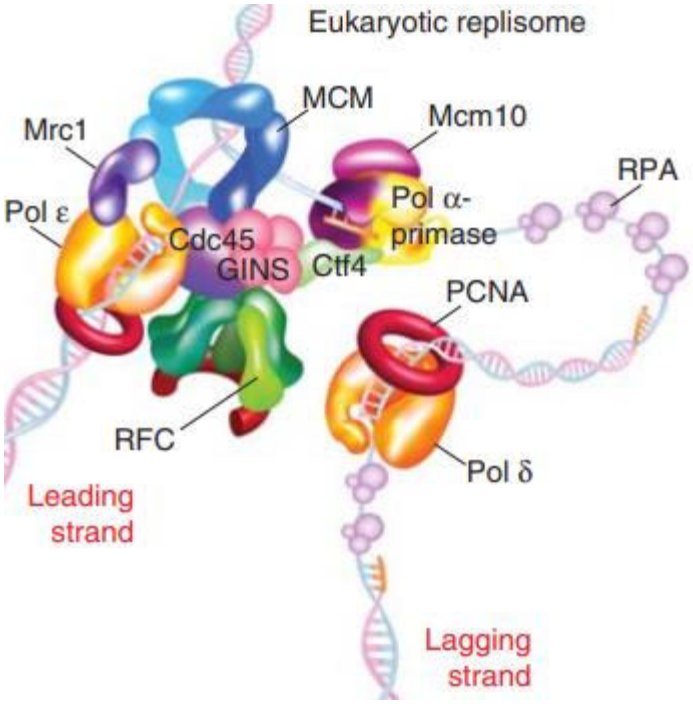


**Figure 10**: Organization of eukaryotic replisome mechanisms (O'Donnell *et al.,* 2013)

After initiation and DNA unwinding, single-strand DNA is stabilized by RPA protein (functional analog of bacterial SSB protein). Replication protein A (RPA) with polymerase α banded on single-strand DNA and make short RNA primers (Stillman 2008). At that moment, a unique DNA-RNA structure is established. DNA-RNA structure is served for the RFC complex. RFC is an ATP-dependent complex that binds on the ring-shaped DNA polymerase PCNA clamp. DNA polymerase clamp loads onto the double-strand DNA near the primer (Figure 11). After RFC-PCNA is established, polymerase ε and δ with higher processivity is bound to the DNA. At the replication fork, polymerase ε and δ are evolved in leading and also

lagging strand synteny (Choe and Moldovan, 2017). Both polymerases have exonuclease proofreading activity from 3' to 5' ends that allow removing incorrectly incorporated bases (Stillman 2008).

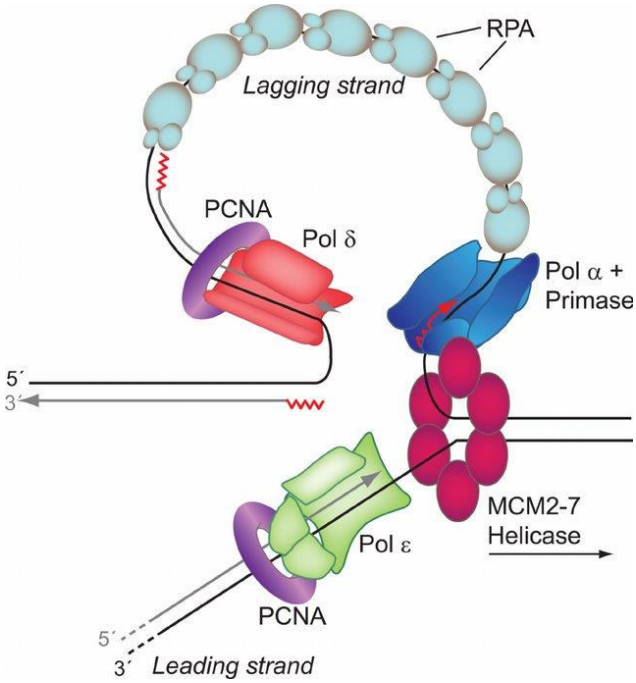


**Figure 11**: Replicative enzymes involved in eukaryotes replication process (McCulloch and Kunkel, 2008)

While the leading strand is continuously extended from 3' to 5' end from the primer by a Polymerase ε, the synthesis of the leading strand is complicated. In the lagging strand, Primase is displaced by Polymerase δ, PCNA/RFC dependent mechanisms, that initiates DNA synthesis discontinuously from 5' to 3' direction by Okazaki fragments. This process of synthesis of Okazaki fragments is completed in the maturation process, where polymerase removes 2-3 nucleotides of the RNA primer. This generated a short flap on the 5' end which is recognized by the FEN1 endonuclease. Displaced flap creates a substrate for subsequent ligation by DNA ligase 1 (Balakrishnan *et* Bambara, 2011).

The eukaryotic replication termination process is more complex than in prokaryotes. Based on high-resolution replication profiling and deep sequencing of Okazaki fragments on budding yeast (Hawkins *et al*., 2013; McGuffee *et al*., 2013) and also based on mapping of Okazaki fragment on human HeLa cells (Petryk *et al*., 2016), it was shown that termination of replication forks occurred midway between two adjacent replication origins (Gambus 2017). Although the majority of

termination events seems to be sequence non-specific, two groups of specific termination region were identified (Dalgaard *et al*., 2009; Bastia *et* Zaman 2014). The first group is known as replication fork barriers (RFBs). These sequence-specific barriers, which contain termination element were described in ribosomal DNA. Subsequently, these termination elements are bound by termination protein (Dewar *et* Walter, 2017). The second specific replication termination group was identified at telomeres (Martínez and Blasco, 2015)

### 2.4.3 Replication of the end of chromosomes

At the end of chromosomes, short DNA repeats usually rich for guanosines (e.g. TTAGG in vertebrates, TTGGGG in ciliates) are present to protect chromosome ends from fusion and degradation (reviewed by Gilson *et* Géli, 2007). Chromatin at the end of chromosomes is known for a various structure such as heterochromatin structure, T-loops, and G quadruplex and more hypothetical triple helicase, four-way junction, and D-loops which can be a source of difficulties for replication in replication fork (reviewed in Bryan, 2020).

Replication elongation takes place until the previous synthesized section of DNA is detected. At the end of the lagging strand, the attaching of RNA primer is impossible and without specific telomere replication mechanisms, linear chromosomes will be shortened by ∼20 nt per each replication round (Chai *et al*., 2006). Meanwhile, short RNA sequences are removing, which is caused by the absence of a 3' end for initiating synthesis and can lead to cellular senescence or apoptosis (Gilson *et* Géli, 2007; Armanios *et* Blackburn, 2012).

In fission yeast, telomere binding proteins were proved to have an essential role in coordinating replication forks. Telomeres length can be restored by telomerase enzyme activity, which was discovered in 1989 by Greider *et* Blackburn. Telomerase binds to the 3' end of the telomere sequence, along with an RNA template. Telomerase catalyzes the addition of bases and restores the telomere length. Finally, DNA polymerase extends and seals the DNA strands.

### 2.4.4 DNA replication errors

During the DNA replication, various events can contribute to replication stress, such as an impact of endogenous or exogenous factors which can result in slowing or stalling of the replication fork or fork asymmetry (Magdalou *et al*., 2014;

Zeman *et* Cimprich, 2014). In mammalian cells, replication stress is also connected with genetic disorders linked with the mutation of helicase (for example Werner and Bloom syndrome) (Brosh *et al*., 2001). Replication errors in plants can be also connected with helicase (MCM2-7) and strong regulation of licensing and initiating of replication (reviewed in Dorn *et* Puchta, 2019).

Generally, replication errors are caused by barriers that prevent the procedure of replisomes like a DNA-protein complex, unusual DNA structures, or transcription-replication collision (Mirkin *et* Mirkin, 2007). Two groups of genomic sequences are preferentially more sensitive to replication stress and are known as fragile sites (reviewed in Sinai *et* Kerem, 2018). Common fragile sites (CFSs) appear as breaks or constrictions on chromosomes and the second group of fragile sites appear rarely, only in small fractions, and can potentially form secondary structures (for example fragile site associated with human fragile X syndrome) (Sutherland 2003; Schwartz *et al*., 2006; reviewed in Sinai *et* Kerem 2018).

To avoid collisions between replication forks and transcription, organisms have evolved several mechanisms (reviewed in Achar *et* Foiani, 2017). In general, replication and transcription are two independent processes in which new DNA strand or RNA molecules are synthesized (reviewed in Sinai *et* Kerem, 2018).

### 2.4.5 Connection between replication and histone modification

The replication process is connected with some post-translational modifications. Specific modifications are necessary at replication origins, then during the synthesis new histones are incorporated into the nascent DNA and subsequently, post-replication modification is done (reviewed in Bar-Ziv *et al*., 2016; Li *et al*., 2008). Eukaryotic replication in the early S phase is connected with mono-, di- and tri-methylation of histone H3 lysine 4 – H3K4me1, H3K4me2, H3K4me3, and monomethylation H3K20me1, H3K36me3 and acetylation of H3K9, H3K27 (reviewed in Bar-Ziv *et al*., 2016). On the other hand, dimethylation of histone H3K9 is strongly connected with the eukaryotic late replication process. For a proper replication of some replication domain, another methylation – H4K20 is necessary, disruption of this modification may lead to further delays in late replicating regions (Brustel *et al*., 2017).

In plants, chromatin remodeling complex, histone chaperones, and histone modification enzymes were shown to be crucial for proper DNA replication (reviewed in de la Paz Sanchez *et al*., 2012) The analysis of *Arabidopsis* revealed that most of the epigenetic modifications occur on 5 ends of the gene bodies, and are associated with highly expressed genes (reviewed in de la Paz Sanchez *et al*., 2012).

Histone analysis of *A. thaliana* showed that replication origins are associated with H3K4me2, H3K4me3, and H3K5ac (Figure 12) and depleted of typical heterochromatin marks of plant H3K4me1 and H3K9me2. Depletion in CG methylation in early and mid-S phase was also indicated alongside with low CG methylation, a mark of more open chromatin connected with pre-RC complex assembly and origin activation. The same observations were done in *Drosophila* and mammalian cells (Costas *et al*., 2011; reviewed in de la Paz Sanchez *et al*., 2012;).

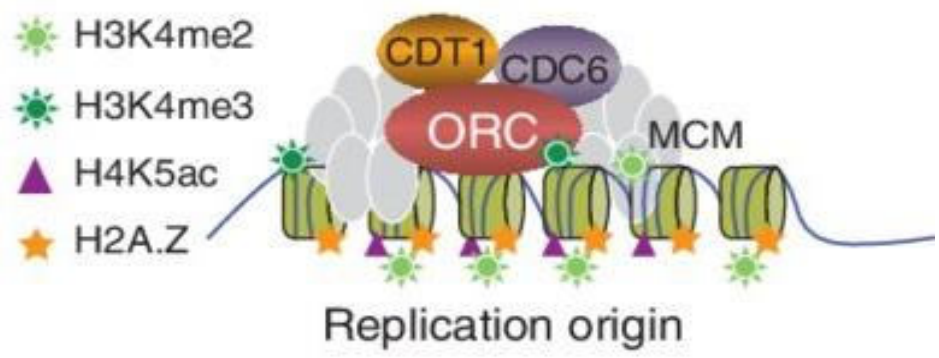


**Figure 12:** Epigenetic marks in the origin of replication (de la Paz Sanchez *et al*., 2012)

Except for H4K5ac, other histone acetylations are suggested for the activation of replication origins. In barley, it was found out, that histones H3K18ac, H4K16ac, and H3K56ac were connected with early replicons (Jasencakova *et al*., 2003). Similarly, in maize, a strong association with earlier replication region of H3K56ac in combination with H3K4me3 was described, using chromatin immunoprecipitation sequencing (ChiP-seq) (Wear *et al*., 2018).

### 2.4.6 Replication of mitochondrial and chloroplast DNA

Mitochondria and chloroplast are semi-autonomous organelles that are essential for plant respiration, ATP production, and photosynthesis. Both organelles contained their DNA that has to be replicated. Replication mechanisms of

mitochondrial DNA (mtDNA) are quite different from that of bacterial chromosomal replication as well as replication of the nucleolar DNA (Holt 2009; Holt *et* Reyes, 2012). Human mitochondrial DNA is very similar to vertebrates, where variability in non-coding DNA concentrated on the about kilobase region was found (Holt *et* Reyes, 2012). Replication of animal mitochondrial DNA initiates from one or two sites, and the leading strand is synthesized with concurrent incorporation of the RNA on the lagging strand. In parallel, the synthesis of the lagging strand initiates, and RNA from the lagging strand is replaced or converted to the DNA (Holt *et* Reyes, 2012). Unlike animals, plant mitochondrial DNA may dramatically vary in size, and its structure and replication process are much more complexed than those of animals. Apart from animals, plant mtDNA contains more genes and non-coding DNA (reviewed in Morley *et al*., 2019). The exact principle of plant mtDNA replication is still unclear. Regulation of plant mtDNA replication is similar to bacterial or eukaryotic nuclear genome regulations, including recombination-dependent replication, rolling circle similar to bacteriophage replication, and also classical bi-directional replication from origins of replication (reviewed in Morley *et* Nielsen, 2016). Rolling circle replication is suggested as a common replication model (Figure 13) (reviewed in Morley *et al*., 2019). Replication starts at the $O_H$ initiation point and proceeds unidirectionally to produce the nascent H strand. After that mtSSb protein binds as protection of strand. When the replisome passes the $O_L$ region, a loop is created and block the mtSSb binding (reviewed in Falkenberg 2018). In this place, the single-strand loop-region is ready for synthesis, and the POLRMT unit can initiate primer synthesis. The shift to L-strand DNA synthesis takes place after about 25 nt. At that time, Polymerase γ replaces the POLRMT unit at the 3′-end of the primer (reviewed in Falkenberg 2018). The synthesis of two strands proceeds continuously until double-strand DNA is formed (reviewed in Falkenberg 2018).

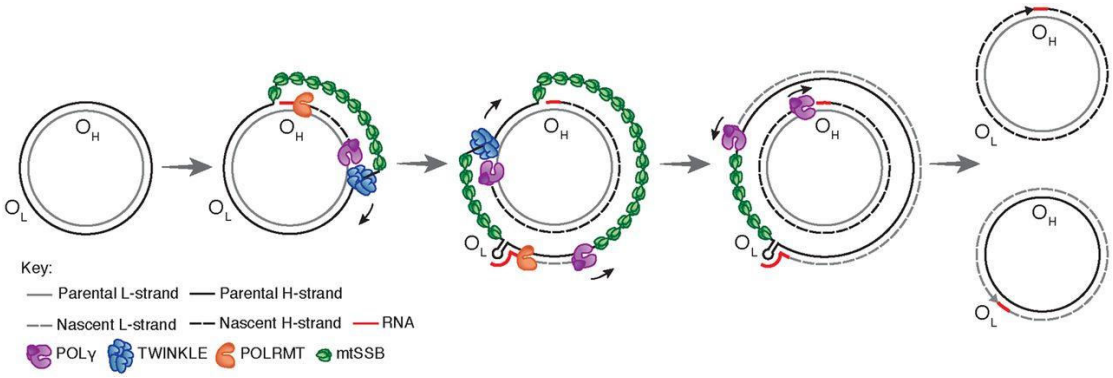


**Figure 13**: Replication of mitochondrial genome (Falkenberg 2018)

Chloroplast genomes (cpDNA) are primarily closed circles of DNA molecules (Palmer *et* Stein 1986; Sugiura 1995) with small variations, as a circular dimer. Genes are generally conserved in most protoplasts consist of rRNA, tRNA, and photosynthesis genes (Palmer 1985; Daniell *et al*., 2016). Chloroplasts replication is better known than mtDNA replication. Chloroplasts are replicated by a double displacement loop strategy. Replication begins on opposite strands of DNA by displacement loops. The process begins unidirectional toward loops until they join, loops fuse and creates a bidirectional replication bubble forming a theta structure. Replication continues bidirectional until daughter molecules are synthesized (reviewed in Morley *et al*., 2019).

### 2.4.7 Spatial and temporal organization of DNA replication

The timing of replication and its spatial organization has an important biological function. Replication of different segments of the genome in the different time ensures, that the number of replication forks does not exceed the ability of important factors for replication such as nucleotides and proteins necessary for the replication process (Mantiero *et al*., 2011). In eukaryotes such as human, mouse, and *Drosophila*, DNA replication is regulated by multi-megabase segments of chromosomes, referred to a constant timing region (CTR), that replicate by the coordinate activation of adjacent replicons at the characteristic time during the S phase (reviewed in Marchal *et al*., 2019). CTRs are delimited by large timing transition regions (TTRs) along which DNA synthesis progressively advances (reviewed in Marchal *et al*., 2019).

Spatial organization of chromatin influences replication timing which is established at the molecular level of domains independent of replication origins. Yeast studies demonstrated that late replication and positioning at the nuclear periphery in telomere locus is established at some point during the G1 phase (Raghuraman *et al* 1997; Heun *et al*., 2001). Factors regulating replication timing may disperse during mitosis and the anchorage of chromosome domains after mitosis could have an impact of the self-assembly of spatially separated compartments of specific protein composition replication (Gilbert *et al*., 2010b). Probably, these compartments would then set the threshold for initiation of replication, perhaps by regulating the accessibility of initiation of replication (Gilbert *et al*., 2010b).

Studies on mice showed different replication timing observed for example between two alleles, rRNA genes, or active and inactive chromosome X (Diaz-Perez *et al*., 2006). In animals, regulation of DNA replication of ribosomal genes, which are present in many copies, is controlled by chromatin remodeler complex NoRC (Strohner *et al*., 2001; Santoro *et al*., 2002). Each of the ribosomal genes can occur in two states. Whereas the first state is not associated with NORC and the level of methylation is low, early replication of active genes then occurs. The second stage is associated with NoRC and high methylation levels of silenced genes, which are replicated in the late S phase (Li *et al*., 2005).

In the terms of the cell cycle, replication forks from the early S phase are not necessarily terminated at the end of the S phase but in the early S phase (reviewed in Gambus 2017). As it was shown in human cells, forks with replicon size 31 kb were fired in the early S phase with an average speed of 1,5 kb per minute can reach the neighboring fork in 10 min and terminate also in the early S phase (Picard *et al*., 2014; Moreno *et al*., 2016; reviewed in Gambus *et al*., 2017). In the late S phase, termination occurred only within regions that were difficult to replicate, and usually, the replication process of these region started in the late S phase as well (Gilbert *et al*., 2010b; reviewed in Gambus 2017).

#### 2.4.7.1 Plant replication timing

Pioneering work describing replication timing in plants was done on ribosomal repeats 5,8S; 18S and 28S (Rivin *et al*., 1986), heterochromatin associated repeats like KNOB and TR1 in maize or centromere associated repeats (Peacock *et*

*al*., 1981; Ananiev *et al*., 1998) In maize, knob 180 and TR1 repeats, which consisted of heterochromatin block, were replicated almost entirely in the late S phase. Similarly, 45S rDNA in maize were found to be mostly replicated in the late S phase, with a smaller fraction of the transcriptionally active 45S rRNA genes replicated in the early and middle S phase, which corresponded with previously mentioned study on animals, that this is transcriptionally active copies (Wear *et al*., 2017). Similar progress of replication was also described in *Arabidopsis*, observed by Repli-seq analysis (Concia *et al*., 2018). A detailed study of 45S rDNA showed that inactive rDNA genes were replicated from the middle to the late S phase. In the very early S phase, a very low level of rDNA replication occurred. During the early to the middle S phase, rDNA units organized inside the nucleolus were replicated. During the middle S phase, replication of rDNA genes culminated, and replication of condensed inactive rDNA genes launched. In the final late S phase, replication of condensed rDNA loci terminated (as was shown in *Arabidopsis* by Dvořáčková *et al*., 2018). On the other hand, maize 5S rDNA replicated dominantly in the early S phase, and only a small fraction is replicated during the middle and late S phase. Surprisingly, the replication time of 5S rDNA in *Arabidopsis* was observed to replicate in the opposite order (Concia *et al*., 2018).

Centromeres contain a lot of repetitive sequences, including retrotransposons and tandem repeats (for example Zhang *et al*., 2005; Plohl *et al*., 2008; Wolfgruber *et al*., 2009). Their function is defined by the presence of centromere histone H3 (CENH3) (Gent *et al*., 2012). It was found that the centromere core of maize is replicated predominantly during the middle and middle-late S phase. Interestingly, a low amount of centromere replication activity was observed also during the early S phase (Wear *et al*., 2017). The same replication timing of centromeres was also discovered in *Arabidopsis thaliana* (Concia *et al*., 2018), although the arrangement in the interphase nuclei is different compared to maize. Replication of *Arabidopsis* centromere repeat Cent-C pass through the whole S phase, but most of the sequences are replicated in the late S phase (Concia *et al*., 2018).

Generally, it was shown that distal parts of plant chromosome arms were replicated earlier then proximal regions, and pericentromeric and centromeric regions were replicated in the late S phase (Wear *et al*., 2017; Concia *et al*., 2018). The analysis suggested that early and middle replicated segments were predominantly euchromatic, and late replicated regions were primarily heterochromatic.

## 2.5 Methods used for the analysis of DNA replication machinery

Methods for DNA replication analysis associated all procedures and approaches leading to a deeper knowledge about DNA replication machinery and spatiotemporal organization in the nucleus. Based on available approaches, mysteries about the DNA replication process are uncovering.

### 2.5.1 ChiP-seq approaches

Chromatin immunoprecipitation (ChiP) is a valuable method for the analysis of proteins or modified proteins and their interactions with genomic DNA (Carey *et al*., 2009). The first *in vivo* study based on immunoprecipitation was provided with RNA polymerase II and its association with genes in *E. coli* and *Drosophila* (Gilmour *et* Lis 1984; Gilmour *et* Lis 1985; Gilmour *et* Lis 1986). In a further study of Solomon *et al*. (1988), the fixation of chromatin structure by formaldehyde was used and allowed to extract DNA or RNA fragments cross-linked with proteins. Subsequent immunoprecipitation using specific antibodies, purification of DNA fragments associated with proteins was feasible (reviewed in Schepers *et* Papior, 2010). Purified DNA fragments were then analyzed by PCR and Southern blotting or using microarrays (ChIP-chip), and recently by next generation sequencing (ChiP-seq) (Johnson *et al*., 2007). Chromatin immunoprecipitation was used for the first time in connection with replication to analyze associations between the pre-replication complex (pre-RC) and chromatin in yeasts (Aparicio *et al*., 1997). Recently, ChiP-seq analyses were used in maize to explore the potential association of chromatin structure with replication time (Wear *et al*., 2017).

### 2.5.2 Isotype labeled nucleotides

In the first studies, radioactive modifications of thymidine were used to study the biosynthesis of DNA using *in vitro* as well as *in vivo* experiments. Modified thymidine - thymidine-C14 was used to analyze DNA replication in *Lactobacillus* (Downing *et* Schweigert, 1956), embryonic tissues of chicken (Friedkin *et al*., 1956) and rabbit bone marrow cells and isolated thymus nuclei (Friedkin *et* Wood, 1956). Semiconservative replication of eukaryotic chromosomes was demonstrated for the first time in the root meristem of faba bean using the incorporation of radioactive thymidine-H3 and subsequent autoradiography detection

(Taylor *et al*., 1957). Radioactive labeling was widely used during the following years and led to replication fork discovery in bacteria (Cairns 1962), human HeLa cells (Cairns 1966), and in Chinese hamster cells (Huberman and Riggs, 1966). Even more, different replication pattern in human leukocytes (Ribas-Mundo, 1966, reviewed in Ligasová *et* Koberna, 2018), and replication of lagging strand by Okazaki fragments in T4 phages and *E. coli* (Okazaki *et al*., 1968; Sugimoto *et al*., 1968; Okazaki *et* Okazaki 1969; Sugimoto *et al*., 1969) were also first shown using labeling by radioactive isotopes of nucleosides (reviewed in Ligasová *et* Koberna, 2018). Due to the lower resolution and time-consuming nature of this approach, an alternative system based on halogenated analogs of nucleotides was developed.

### 2.5.3 Halogenated analogs

Halogenated thymidine (bromine, fluorine, chlorine, iodine) replaced isotopically labeled nucleotides (reviewed in Ligasová *et* Koberna, 2018). First halogenated analogs 5-bromodeoxyuridine (BrdU) and 5-hydroxydeoxyuridin were synthesized before the development of isotopic detection (Beltz *et* Visser, 1955), unfortunately, the detection of non-isotopically labeled cell was a big challenge (Beltz *et* Visser, 1955). Progress in the use of non-isotopically labeled nucleosides was allowed by the discovery of specific antibodies in 1971 (Sawicki *et al*., 1971). Due to the effective incorporation of halogenated analogs into DNA and its potential toxicity, tests of lethal dosage were performed to find the optimal dose (Beltz *et* Visser 1955). Antibody specific to BrdU was first applied to analyze single-cell replication and sister strand chromatid exchange in hamster ovary cells culture using immunofluorescence (Gratzner *et al*., 1975). Immunofluorescence staining of BrdU (by Hoechst fluorophore) was later used also in cell cycle studies employed flow cytometry (Bohmer *et* Ellwart, 1981) to study replication dynamics. 5-chloro-2-deoxyuridine (CldU) and 5-iodo-2-deoxyuridine (IUdR) were used to analyze DNA fibers, and replication dynamics (replication fork speed, fork asymmetry) in mammalian cells (Techer *et al*., 2013). Even more, BrdU was used to describe mitochondrial DNA synthesis, as it was shown in intact mammalian cells (Davis *et* Clayton, 1996), and later in mouse and human neuroblastoma cells (Magnusson *et al*. 2003; Lentz *et al*. 2010). For antibody detection of BrdU, double-strand DNA had to be treated (denatured) by acid, heat, or hydroxide to make the DNA strand accessible

for antibodies. As a consequence of the denaturation, DNA lost its natural structure and cellular components (like antigens) were destructed, and depurination and deproteination occurred as well (reviewed in Ligasová *et* Koberna, 2018). Problems of disrupted DNA structure were overcome in 2008 when Salic and Mitchison used 5-ethynyl-2-deoxyuridine (EdU) and subsequent visualization by azide stain in cooper ions conditions in mammalian cells (Figure 14) (Salic *et* Mitchison, 2008).

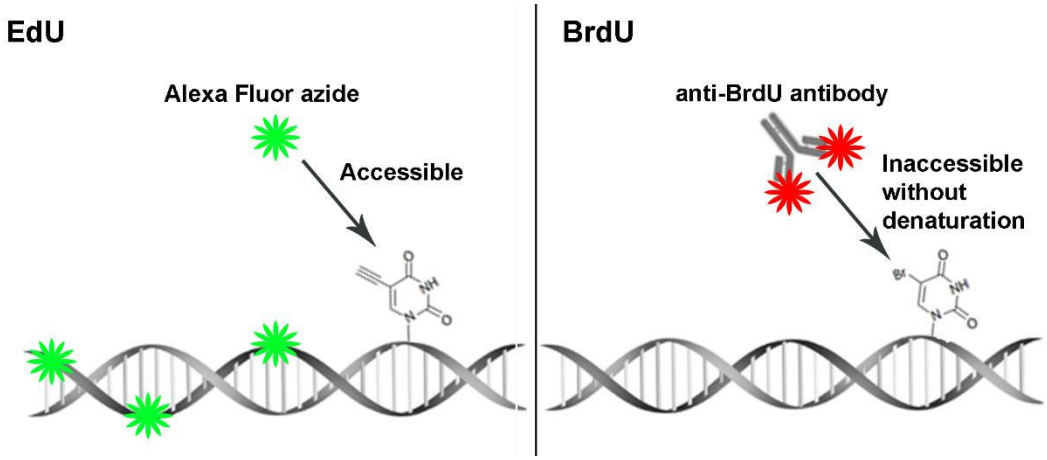


**Figure 14**: Principle of incorporation and visualization of halogenated analogs EdU and BrdU

The key feature of EdU success was caused by the terminal alkyne group and subsequent detection by cycloaddition. The terminal alkyne group of thymidine analog replaced the methyl group in thymidine. Thymidine analog is readily incorporated into cellular DNA during DNA replication. The terminal alkyne group is detected with fluorescent azides in Cu(I) catalyzed cycloaddition by forming a strong covalent bond (Salic *et* Mitchison, 2008). Due to the simplicity and fast visualization, EdU is nowadays used for a wide range of studies connected with DNA synthesis. On the other hand, high concentration and long-time incubation with EdU analog may cause toxicity and slowdown cell cycle, as it was shown in human and mouse cells (Kohlmeier *et al*., 2013). Another disadvantage of EdU use can reside in visualization by copper ions, which is not compatible with live-cell imaging (Baskin *et al*., 2007). Using EdU incorporation, new approaches to the analysis of DNA replication machinery became available. Such as protein (which are crosslinked by formaldehyde) analyses of replication forks (Sirbu *et al*., 2011), or genome-wide analysis of DNA replication using isolation of newly synthesized DNA

by antibody precipitation followed by NGS and *in silico* study - a method known as Repli-seq (Hansen *et al*., 2010; Wear *et al.,*2017; Concia *et al*., 2018).

### 2.5.4 Use of flow cytometry for analyses of DNA replication

Flow cytometry (FCM) is a technique allowing detection and measurements of the physical and chemical characteristics of a population of cells or other sub-cellular particles (Picot *et al*., 2012). This technique was initially developed in human research and further modified for use in plant science (Carrano *et al*. 1979; Doležel *et al*., 1991). Flow cytometers can analyze thousands of particles per second. FCM allows the rapid determination of nuclear DNA content (ploidy analysis) and analysis of the cell cycle progression by use of specific conditions. In plants, FCM is widely used to analyze the suspension of protoplasts, chromosomes, and nuclei.

Fluorescent-activated cell sorting (FASC) instruments are able to analyze particles (protoplasts, chromosomes, or intact nuclei) in liquid suspension (Figure 15) (Doležel *et al*., 2014). Based on differences of fluorescence intensity, particles are identified and sorted into tubes or on microscopic slides (Doležel *et al*., 2014). The ability of specific particle sorting is also useful for the analysis of DNA replication.

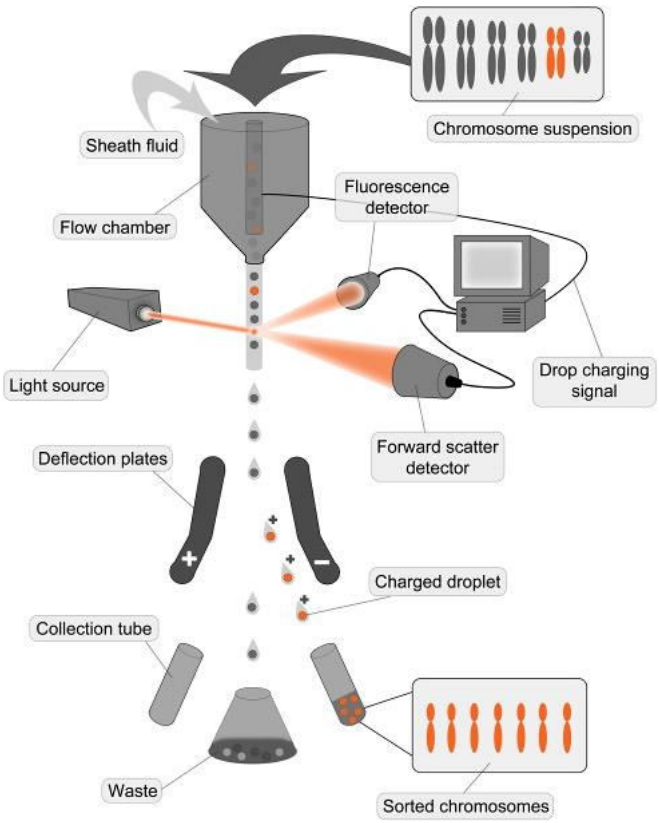


**Figure 15**: The mechanismus of flow sorting (Doležel *et al*., 2014)

While nonparametric flow sorting strategy is based on DNA content, two parameters resolution could be achieved by bivariate analysis of particles that contain two different fluorophores. In replication studies, fluorescently labeled halogenated analogs incorporated into newly synthesized DNA fiber are used (Bohmer *et* Ellwart, 1981). Bivariate flow sorting allows us to distinguish cells going through the cell cycle based on direct measurement of the DNA content increase and the cohort labeling of replicated cells. Halogenated DNA analogs (BrdU, EdU) has been successfully used in animal (Bohmer *et* Ellwart, 1981) as well as in plant research (Lucretti *et al*., 1999), and proved to be a powerful tool to study DNA replication program (Hayashi *et al*., 2013). In plants, the combination of EdU labeling of root meristematic cells followed by flow cytometry analysis was used to analyze the duration of cell cycle and S-phase, and further sorting of nuclei representing different stages of S phase was used for studies of DNA replication in time and space by application of microscopic techniques and Repli-seq as well (for example Mickelson-Young *et al.*, 2016).

### 2.5.5 Cytogenetic and microscopic approaches used in DNA replication studies

Fluorescence in situ hybridization (FISH) is the most popular method for *in situ* localization of different types of DNA or RNA sequences. In combination with immunostaining, *in situ* hybridization can be used to study interactions of proteins with specific DNA sequences and their organization on chromosomes or in interphase nuclei. Although 'classical' FISH represents an extremely versatile method with a wide spectrum of applications, including analysis of chromatin organization in three-dimensional space, which is enabled by use of confocal microscopy and/or by super resolution microscopy.

#### 2.5.5.1 RGEN-ISL

The discovery of type II clustered regularly interspaced short palindromic repeats (CRISPR)- associated caspase 9 (Cas9) system opened a new field for the fluorescence detection of genomic loci in living (Dreissig *et al*., 2017) and fixed non-denatured plant cells (Ishii *et al*., 2019). CRISPR/Cas9 system and its fluorescent labeling are based on the property of designed CRISPR RNA (crRNA). This RNA contains 20 nucleotides long spacer that is complementary to a DNA sequence and

provides the target specificity of the Cas9 system. To find the specific DNA the Cas9 nuclease requires a guide RNA (gRNA) that is composed of crRNA, fluorescently labeled trans-activating crRNA (tracrRNA), and protospacer adjacent motif (PAM) (Ishii *et al*., 2019). This specific complex is formed by the hybridization of the designed crRNA in combination with the fluorescently labeled tracrRNA (Ishii *et al*., 2019). The crRNA contains a 20-nucleotide guide sequence called spacer and the PAM, a short G-rich motif that is positioned next to the gRNA-specific part of the target sequence (Figure 16).

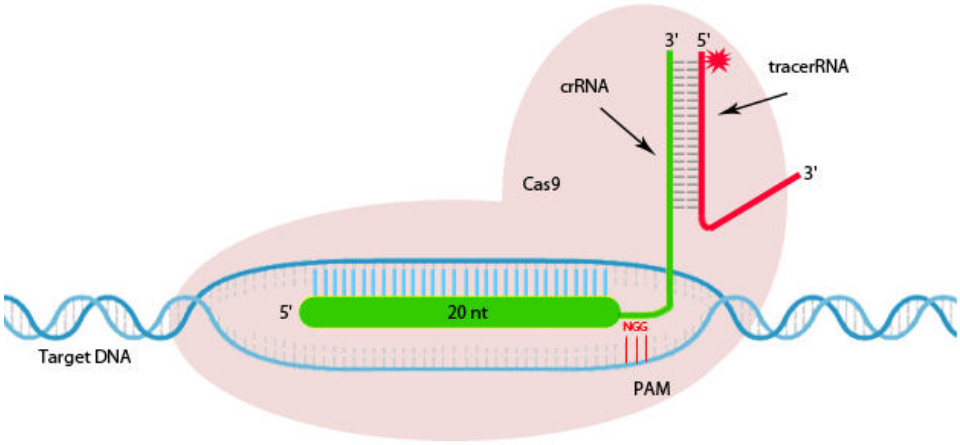


**Figure 16**: The principle of fluorescent labeling using the CRISPR-Cas9 method so-called RGEN-ISL (Němečková *et al*., 2019)

In contrast to classical fluorescence *in situ* hybridization (FISH), RGEN-ISL does not require DNA denaturation for hybridization. Therefore, observation of non-denatured chromatin structure is possible. Due to non-denaturing conditions, RGEN-ISL has a broad range of adaptability and has been used for immunofluorescence detection (Ishii *et al*., 2019). In the present thesis, the protocol for RGEN-ISL was optimized. Non-denaturing labeling was used for the detection of maize Knob repeats together with immunolabeling and EdU labeling to detect specific repeats, histone marks, and DNA replication sites. Even more, differences between chromatin ultrastructure after RGEN-ISL and subsequent FISH on fixed chromosomes were compared applying high-resolution microscopy (SIM) (Němečková *et al*., 2019).

#### 2.5.5.2 Three-dimensional FISH (3D FISH)

Based on well-optimized FISH approaches and due to the question about higher chromatin organization and its behaving during the cell cycle, three-dimensional FISH (3D-FISH) was used for the first time in 1977 (Bass *et al*., 1997). 3D-FISH discovery is based on a previous experiment, which revealed the possibility of specific staining of *Drosophila* polytene chromosomes mounted in a stable environment of polyacrylamide gel (Urata *et al*., 1995). Individual particles such as chromosomes or nuclei are fixed using formaldehyde and embedded in polyacrylamide gel, which allows further immunostaining or fluorescence *in situ* hybridization with specific probes (Howe *et al*., 2013). Polyacrylamide properties provide optically clear sectioning with confocal microscopy and were used in the plant kingdom for the first time to analyze telomeres positioning during the meiotic prophase I in maize (Bass *et al*., 1997). 3D pictures are created based on acquiring of the objects by confocal, or super-resolution microscopy, when individual layers are captured and subsequently composed in the 3D model using mathematic software like for example, Imaris (Bitplane), LAS X (Leica), or ImageJ (Bass *et al*. 1997, Howe *et al*., 2013; 2014; Perničková *et al.* 2019; Koláčková *et al.* 2019).

As was mention before, the flow cytometry is widely used for sorting of specific particles, such as nuclei in different stages of the cell cycle or mitotic chromosomes. This approach was also used in DNA replication studies to analyze the spatiotemporal pattern of DNA replication (Bass *et al*., 2015). With this aim, nuclei of different stages of the cell cycle were sorted, embedded in the gel, and specific pattern for early, middle and late S phase was observed in maize applying confocal and high-resolution microscopy (SIM) (Bass *et al*., 2015).

In the present thesis, the replication profile of seven selected plant species with contrasting genome sizes was analyzed. Replication timing for telomeres and centromeres togethere with the spatial organization was revealed by applying confocal microscopy.

#### 2.5.5.3 Combination of immunolocalization and FISH in 3D

The stability of polyacrylamide gel is one of the undisputed advantages that also allow protein detection in three space of interphase nuclei or on chromosomes.

A combination of immunolocalization and polyacrylamide gel was successfully used by studies of Phillips *et al.* (2010, 2013), where proteins of synaptonemal complex (ZYP1, Asy1) were mapped in 3D space of barley nuclei.

Additionally, three-dimensional visualization of protein-DNA interactions can be achieved using a combination of immunolabeling and FISH (Figure 17). This protocol combines already mentioned 3D FISH with specific labeling of the target proteins (Murphy *et al*., 2014).

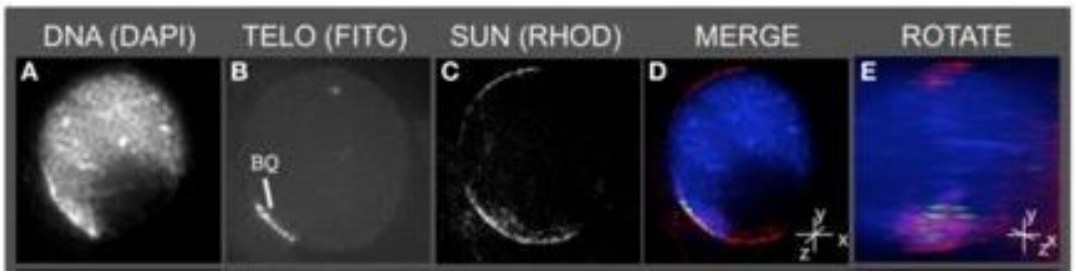


**Figure 17**: Protein immunolocalization (SUN) (C) followed by 3D telomere FISH (TELO) (B) location of meiotic anthers from maize (A) (Murphy *et al*., 2014).

In the present thesis, the combination of fluorescent immunolocalisation and FISH labeling was used to analyze 3D organisation of centromeric and telomeric region in 3D space of nuclei of seven selected plant species. Even more, with the use of EdU incubation, conserved dynamic of DNA replication in selected species was reveald (Němečková *at el*., 2020).

#### 2.5.5.4 Confocal microscopy and high-resolution microscopy

Confocal microscopy is an optical imaging technique, in which a spatial pinhole is used to block out-of-focus light during image capturing (Pawley, 2006). Confocal scanning microscopy allows capturing multiple two-dimensional pictures in different depths of the sample that enabled tree dimension structure reconstruction at the end. This technique is used in different scientific fields including plant cytogenetics studies. For instance, in plants, confocal sectioning was used by Bass *et al*. (2014) to study the replication pattern and replication timing of selected repetitive DNA sequences in 3D space of the nucleus of maize.

In general, microscopy deals with resolution problems caused by the diffraction limit defined by Ernst Abbe (1873), which allows obtaining resolution

~200 nm laterally and ~600 nm in the axial dimension in biological specimens (Pawley, 1995). Analysis of protein and DNA interactions, detailed chromatin structure was until recently limited due to limitations caused by the refraction limit of the light. This limitation in fluorescence microscopy was overcome in 2014 by Betzich, Moerner, and Hell, and awarded by the Nobel Prize (Möckl, 2014). They bring a new "nano dimension" in optical fluorescence microscopy.

Nowadays, several high-resolution (super-resolution) microscopy techniques exist and can be divided based on main two principles: 1) localization microscopy and, 2) based on structuring the illumination light (reviewed in Schubert *et al*., 2017). Localization microscopy is based on the principle of photoactivation, when a photoactivable molecule switches to the bright stage, are imaged and bleached (Komis *et al*., 2015). The resolution of photoactivated localization microscopy (PALM) can reach 20 nm in the lateral speciemen in biological samples (Komis *et al*., 2015). Stochastic optical reconstruction microscopy (STORM) is based on the localization of individual fluorophores in the specimen with subdiffraction precision.

The second set of nanoscopy techniques is based on structuring the illumination light done by confocal microscopy like stimulated-emission depletion (STED) or in the widefield configuration as structured-illumination microscopy (SIM) (Rego *et al*., 2012; Dodgson *et al*., 2015). Structured illumination microscopy based on the wide-field microscopy principle acquires a set of raw images that are finally proceeded by a computer algorithm to generate the resulted image. Raw images are generated by illuminating the sample with interference-generated light, and a stripe pattern is created (so-called Moiré effect). This Moiré pattern contains downshifted high-frequency information (Dodgson *et al*., 2015). The final reconstructed picture can reach about 110-130 nm in lateral and about 250 nm in axial specimens (2-fold improvement than confocal microscope). Sample preparation for fixed material is not limited, compatible with commercially available fluorophores, standard fixative, and labeling method used in conventional microscopy preparation (reviewed in Schubert 2017).

Stimulated emission depletion microscopy (STED) acquires data using the confocal system, and the final picture is based on the optical property of the microscope. The Princip of STED is based on acquiring a sample with spatially arranged light comprising two different laser beams (Müller *et al*., 2012). The laser beam of the excitation line corresponds to the excitation maximum of the

fluorophore, and the second beam, the depletion line, in engineered into the doughnut shape through a phase mask to surround the excitation beam (Komis *et al*., 2015). Based on it, a very small spot of emission can be confirmed (Komis *et al*., 2015). Final resolution about 50 nm in lateral and about 130 nm is an axial plan that can be reached, which corresponds to almost 3-fold improvement than a confocal microscope. Sample preparation is more limited, due to phototoxicity. Depletion laser works with high intensity that requires stable fluorescent days resistant to bleaching. The multicolor resolution could be achieved with two days depleted by the same laser (Müller *et al*., 2012; Dodgson *et al*., 2015).

Using STORM microscopy, histone variants H3.1 and H3.3 in Hella cells outside the S phase and in early, middle, and late S phase were analyzed with a resolution about 40 nm (Clément *et al*., 2018). The first application of Higher-resolution SIM microscopy in plants was used in the replication study of maize by Bass *et al*. (2015); and more recently, Dvořáčková *et al*. (2018) used SIM microscopy to study the localization of replicated 45S DNA loci in intra- and extranucleolar regions in *Arabidopsis* nuclei (Dvořáčková *et al*., 2018).

### 2.5.6 Analysis of DNA replication using next generation sequencing

The whole-genome profiling of replication activity through individual stages of S phase can be analyzed using the Repli-seq method based on EdU labeling, flow sorting, immunoprecipitation, library construction followed next generation sequencing (see Figure 18 A). The Illumina sequencing of replicated DNA sequences was developed of human cells of cell suspension by Hansen *et al.* (2010) and later modified for plant cells (Wear *et al*. 2017).

The Repli-seq procedure is based on newly synthesized DNA labeling (e.g. by EdU) and further analysis of the cell cycle using flow cytometry. The FACS analysis is used to sort individual stages of interphase with the aim to isolate genome regions that are replicated during the individual stages of the S phase (Figure 18 B). After DNA isolation from flow sorted nuclei, DNA is fragmented and sequences labeled by EdU are separated from a non-replicated (un-labeled) DNA fragments using immunoprecipitation. Selected DNA fragments corresponding to DNA sequences that are replicated during the individual phases of phase as well as DNA fragments corresponding to G1 nuclei are then used for illumining libraries

preparation and sequencing. Further bioinformatic processing is based on aligning the Illumina reads to reference genome sequence and identification of replication timing of regions of interest (Figure 18 C). Recently, Repli-seq analysis was used in 3 studies focused on *Arabidopsis*, maize, and endoreduplication in maize (Wear *et al*., 2017; Concia *et al*. 2018).

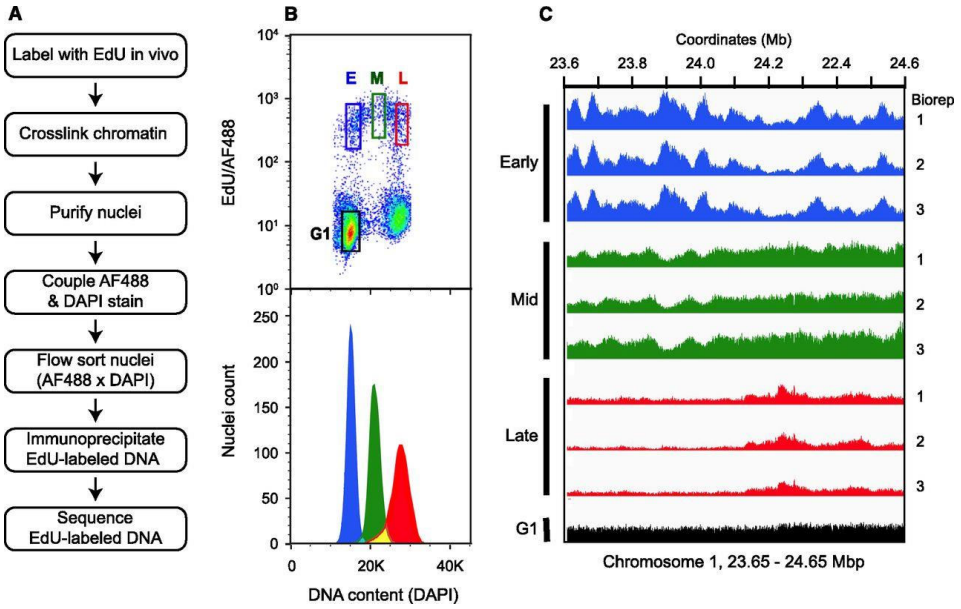


**Figure 18:** The experimental pipeline of *Arabidopsis* Repli-seq experiment (Concia *et al*., 2018)

## 2.6 References


**Abbe E** (1873) Beiträge zur Theorie des Mikroskops und der mikroskopischen Wahrnehmung. *Archiv für mikroskopische Anatomie* **9(1)**: 413-468.

**Achar YJ**, Foiani M (2017) Coordinating replication with transcription. In *DNA Replication* Pp 455-487 Springer Singapore.

**Ananiev EV**, Phillips RL, Rines HW (1998) Complex structure of knob DNA on maize chromosome 9: retrotransposon invasion into heterochromatin. *Genetics* **149(4)**: 2025-2037.

**Aparicio OM**, Weinstein DM, Bell SP (1997) Components and dynamics of DNA replication complexes in *S. cerevisiae*: redistribution of MCM proteins and Cdc45p during S phase. *Cell* **91(1)**: 59-69.

**Aparicio T**, Ibarra A, Méndez J (2006) Cdc45-MCM-GINS, a new power player for DNA replication. *Cell division* **1(1)**: 18.

**Armanios M**, Blackburn EH (2012) The telomere syndromes. *Nature Reviews Genetics* **13(10)**: 693-704.

**Armstrong SJ**, Franklin FC, Jones GH (2001) Nucleolus-associated telomere clustering and pairing precede meiotic chromosome synapsis in *Arabidopsis thaliana*. *Journal of Cell Science* **114**: 4207–4217.

**Ausiannikava D**, Allers T (2017) Diversity of DNA replication in the Archaea. *Genes* **8(2)**: 56.

**Balakrishnan L**, Bambara RA (2011) Eukaryotic lagging strand DNA replication employs a multi-pathway mechanism that protects genome integrity. *Journal of Biological Chemistry* **286(9)**: 6865-6870.

**Bar-Ziv R**, Voichek Y, Barkai N (2016) Chromatin dynamics during DNA replication. *Genome research* **26(9)**: 1245-1256.

**Baskin JM**, Prescher JA, Laughlin ST, Agard NJ, Chang PV, Miller IA, Lo A, Codelli JA, Bertozzi CR (2007) Copper-free click chemistry for dynamic *in vivo* imaging. *Proceedings of the National Academy of Sciences* **104**: 16793–16797.

**Bass HW**, Hoffman GG, Lee TJ, Wear EE, Joseph SR, Allen GC, Hanley-Bowdoin L, Thompson WF (2015) Defining multiple, distinct, and shared spatiotemporal patterns of DNA replication and endoreduplication from 3D image analysis of developing maize (*Zea mays* L.) root tip nuclei. *Plant molecular biology* **89(4-5)**: 339-351.

**Bass HW**, Marshall WF, Sedat JW, Agard DA, Cande WZ (1997) Telomeres cluster de novo before the initiation of synapsis: a three-dimensional spatial analysis of telomere positions before and during meiotic prophase. *The Journal of cell biology* ***137*****(1)**: 5-18.

**Bass HW**, Wear EE, Lee TJ, Hoffman GG, Gumber HK, Allen GC, Thompson WF, Hanley-Bowdoin L (2014) A maize root tip system to study DNA replication programmes in somatic and endocycling nuclei during plant development. *Journal of experimental botany* **65(10)**: 2747-2756.

**Bastia D**, Zaman S (2014) Mechanism and physiological significance of programmed replication termination. In *Seminars in cell & developmental biology* **(30)**: 165-173. Academic Press.

**Bell O**, Schwaiger M, Oakeley EJ, Lienert F, Beisel C, Stadler MB, Schübeler D (2010) Accessibility of the *Drosophila* genome discriminates PcG repression, H4K16 acetylation and replication timing. *Nature structural & molecular biology* **17(7)**: 894.

**Belmont AS**, Bruce K (1994) Visualization of G1 chromosomes: a folded, twisted, supercoiled chromonema model of interphase chromatid structure. *The Journal of cell biology* **127(2)**: 287-302.

**Beltz RE**, Visser DW (1955) Growth Inhibition of Escherichia-Coli by New Thymidine Analogs. *Journal of the American Chemical Society* **77**: 736–738.

**Bernstein H**, Payne CM, Bernstein C, Garewal H, Dvorak K (2008) Cancer and aging as consequences of un-repaired DNA damage. *New Research on DNA Damages. New York, NY, USA: Nova Science Publishers*, 1-47.

**Beseda T**, Cápal P, Kubalová I, Schubert V, Doležel J, Šimková H (2020) Mitotic chromosome organization: General rules meet species-specific variability. *Computational and Structural Biotechnology Journal* **18**: 1311-1319.

**Bintu B**, Mateo LJ, Su JH, Sinnott-Armstrong NA, Parker M, Kinrot S, Yamaya K, Boettiger AN, Zhuang X (2018) Super-resolution chromatin tracing reveals domains and cooperative interactions in single cells. *Science* **362***:* 6413.

**Bohmer RM**, Ellwart J (1981) Cell cycle analysis by combining the 5-bromodeoxyuridine/33258 Hoechst technique with DNA-specific ethidium bromide staining. *Cytometry* **2**: 31–34.

**Bolzer A**, Kreth G, Solovei I, Koehler D, Saracoglu K, Fauth C, Müller S, Eils R, Cremer C, Spiecher MR, Cremer T (2005) Three-dimensional maps of all chromosomes in human male fibroblast nuclei and prometaphase rosettes. *PloS Biology* **3**: e157.

**Bory S**, Catrice O, Brown S, Leitch IJ, Gigant R, Chiroleu F, grison M, Duval MF, Besse, P (2008) Natural polyploidy in *Vanilla planifolia* (Orchidaceae). *Genome* **51(10)**: 816-826.

**Bracht JR**, Fang W, Goldman AD, Dolzhenko E, Stein EM, Landweber LF (2013) Genomes on the edge: programmed genome instability in ciliates. *Cell **152*(3)**: 406-416.

**Breuer C**, Braidwood L, Sugimoto K (2014) Endocycling in the path of plant development. *Current opinion in plant biology* **17**: 78-85.

**Brosh RM**, Majumdar A, Desai S, Hickson ID, Bohr VA, Seidman MM (2001) Unwinding of a DNA triple helix by the Werner and Bloom syndrome helicases. *Journal of Biological Chemistry* **276(5)**: 3024-3030.

**Brown SC**, Bourge M, Maunoury N, Wong M, Wolfe Bianchi M, Lepers-Andrzejewski S, Besse P, Siljak-Yakovlev, Dron M, Satiat-Jeunemaître, B (2017) DNA remodeling by strict partial endoreplication in orchids, an original process in the plant kingdom. *Genome Biology and Evolution* ***9*(4)**: 1051-1071.

**Brustel J**, Kirstein N, Izard F, Grimaud C, Prorok P, Cayrou C, Schotta G, FAbdelsamie A, Déjardin J, Méchali M, Baldacci G, Sardet C, Cadoret JC, Schepers A, Julien E (2017) Histone H4K20 tri-methylation at late-firing origins ensures timely heterochromatin replication. *The EMBO journal* **36(18)**: 2726-2741.

**Bryan TM** (2020) G-Quadruplexes at Telomeres: Friend or Foe? *Molecules* **25(16)**: 3686.

**Bryant JA**, Aves SJ. 2011. Initiation of DNA replication: functional and evolutionary aspects. *Annals of Botany* **107**: 1119–1126.

**Burgers PM**, Kunkel TA (2017) Eukaryotic DNA replication fork. *Annual review of biochemistry* **86**: 417-438.

**Cai S**, Chen C, Tan ZY, Huang Y, Shi J, Gan L (2018) Cryo-ET reveals the macromolecular reorganization of *S. pombe* mitotic chromosomes in vivo. *Proceedings of the National Academy of Sciences* ***115*(43)**: 10977-10982.

**Cairns J** (1962) The bacterial chromosome and its manner of replication as seen by autoradiography. *Journal of Mollecular Biology* **6**: 208–213.

**Cairns J** (1966) Autoradiography of HeLa cell DNA. *Journal of Mollecular Biology* **15**: 372–373.

**Caputi FF**, Candeletti S, Romualdi P (2017) Epigenetic approaches in neuroblastoma disease pathogenesis. In *Neuroblastoma-Current State and Recent Updates*. IntechOpen.

**Carey MF**, Peterson CL, Smale ST (2009). Chromatin immunoprecipitation (chip). *Cold Spring Harbor Protocols* ***2009*(9)**: pdb-prot5279.

**Carrano AV**, Gray JW, Langlois RG, Burkhart-Schult, KJ, Van Dilla MA (1979). Measurement and purification of human chromosomes by flow cytometry and sorting. *Proceedings of the National Academy of Sciences*, **76(3)**: 1382-1384.

**Casjens S** (1998). The diverse and dynamic structure of bacterial genomes. *Annual review of genetics*, 32(1): 339-377.

**Clément C**, Orsi GA, Gatto A, Boyarchuk E, Forest A, Hajj B, Miné-Hattab J, Garnier M, Gurard-Levin ZA, Quivy JP, Almouzni G (2018). High-resolution visualization of H3 variants during replication reveals their controlled recycling. *Nature communications* **9(1)**: 1-17.

**Clowes FAL** (1971) The proportion of cells that divide in root meristems of *Zea mays* L. Annals of Botany **35**: 249–261.

**Concia L**, Brooks AM, Wheeler E, Zynda GJ, Wear EE, LeBlanc C, Song J, Lee TJ, Pascuzzi PE, Martienssen RA, Vaughn MW, Thompson WF, Hanley-Bowdoin L (2018) Genome-wide analysis of the Arabidopsis replication timing program. *Plant physiology* **176(3)**, 2166-2185.

**Costa A**, Hood IV, Berger JM (2013) Mechanisms for initiating cellular DNA replication. *Annual review of biochemistry* **82**: 25-54.

**Costas C**, de la Paz Sanchez M, Stroud H, Yu Y, Oliveros JC, Feng S, Benguria A, López-Vidriero I, Zhamg X, Solano R, Jacobsen SE, Gutierrez C (2011). Genome-wide mapping of Arabidopsis thaliana origins of DNA replication and their associated epigenetic marks. *Nature structural & molecular biology*, **18(3)**, 395.

**Cremer M**, Cremer T (2019) Nuclear compartmentalization, dynamics, and function of regulatory DNA sequences. *Genes, Chromosomes and Cancer* **58(7)**: 427-436.

**Cremer T**, Cremer C (2001) Chromosome territories, nuclear architecture and gene regulation in mammalian cells. *Nature reviews genetics* **2(4)**: 292-301.

**Cremer T**, Cremer M (2010). Chromosome territories. *Cold Spring Harbor perspectives in biology* **2(3)**: a003889.

**Crosetto N**, Bienko M (2020). Radial organization in the mammalian nucleus. *Frontiers in Genetics* **11**: 1-10.

**Daban JR** (2015) Stacked thin layers of metaphase chromatin explain the geometry of chromosome rearrangements and banding. *Scientific Reports* **5**: 14891.

**Dalgaard JZ**, Eydmann T, Koulintchenko M, Sayrac S, Vengrova S, Yamada-Inagawa T (2009) Random and site-specific replication termination. In *DNA Replication* Pp. 35-53. Humana Press.

**Daniell H**, Lin CS, Yu M, Chang WJ (2016) Chloroplast genomes: Diversity, evolution, and applications in genetic engineering. *Genome Biology* **17:** 1-29.

**Davis AF**, Clayton DA (1996) In situ localization of mitochondrial DNA replication in intact mammalian cells. *Journal of Cell Biology* **135**: 883–893.

**de la Paz Sanchez M**, Costas C, Sequeira-Mendes J, Gutierrez C (2012) Regulating DNA replication in plants. *Cold Spring Harbor Perspectives in Biology* **4(12)**: a010140.

**Dekker J**, Heard E (2015) Structural and functional diversity of Topologically Associating Domains. *FEBS letters* **589(20)**: 2877-2884.

**Dekker J**, Rippe K, Dekker M, Kleckner N (2002) Capturing chromosome conformation. *Science* **295(5558)**: 1306-1311.

**Del Priore L**, Pigozzi MI (2014). Histone modifications related to chromosome silencing and elimination during male meiosis in Bengalese finch. *Chromosoma* **123**:293–302.

**Dellino GI**, CittaroD, Piccioni R, Luzi L, Banfi S, Segalla S, Cesaroni M, Mendoza-Maldonado R, Giacca M, Pelicci PG (2013) Genome-wide mapping of human DNA-replication origins: levels of transcription at ORC1 sites regulate origin selection and replication timing. *Genome Research* **23**: 1–11.

**Dewar JM**, Walter JC (2017) Mechanisms of DNA replication termination. *Nature Reviews Molecular Cell Biology* **18(8)**: 507-516.

**Diaz-Perez SV**, Ferguson DO, Wang C, Csankovszki G, Wang C, Tsai SC, Dutta D, Perez V, Kim S, Eller CD, Salstrom J, Ouyang Y, Teitell MA, Kaltenboeck B, Chess A, Huang S, Marahrens Y (2006) A deletion at the mouse Xist gene exposes trans-effects that alter the heterochromatin of the inactive X chromosome and the replication time and DNA stability of both X chromosomes. *Genetics* **174(3)**: 1115-1133.

**Dillinger S**, Straub T, Nemeth A (2017) Nucleolus association of chromosomal domains is largely maintained in cellular senescence despite massive nuclear reorganisation. *PLoS One* **12(6)**: e0178821.

**Dixon JR**, Gorkin DU, Ren B (2016) Chromatin domains: the unit of chromosome organization. *Molecular cell* **62(5)**: 668-680.

**Dixon JR**, Selvaraj S, Yue F, Kim A, Li Y, Shen Y, Hu M, Liu JS, Ren B (2012) Topological domains in mammalian genomes identified by analysis of chromatin interactions. *Nature* **485(7398)**: 376-380.

**Dobrzynska A**, Gonzalo S, Shanahan C, Askjaer P (2016) The nuclear lamina in health and disease. *Nucleus 7*: 233–248.

**Dodgson J**, Chessel A, Cox S, Salas REC (2015) Super-resolution microscopy: SIM, STED and localization microscopy. In *Advanced Microscopy in Mycology* pp 47-60. Springer, Cham.

**Doğan ES**, Liu C (2018) Three-dimensional chromatin packing and positioning of plant genomes. *Nature plants **4*****(8)**: 521-529.

**Doležel J** (1991) Flow cytometric analysis of nuclear DNA content in higher plants.

*Phytochemical Analysis*, doi: 10.1002/pca.2800020402.

**Doležel J**, Vrána J, Cápal P, Kubaláková M, Burešová V, Šimková H (2014) Advances in plant chromosome genomics.. *Biotechnology Advances* **32**: 122-136.

**Dong F,** Jiang J (1998) Non-Rabl patterns of centromere and telomere distribution in the interphase nuclei of plant cells. *Chromosome Research* **6**: 551–558.

**Dong P,** Tu X, Chu P, Lü P, Zhu N, Grierson D, Du B, Li P, Zhong S (2017) 3D chromatin architecture of large plant genomes determined by local A/B compartments. *Molecular Plant* **10**: 1497–1509.

**Dorn A**, Puchta H (2019) DNA Helicases as Safekeepers of Genome Stability in Plants. *Genes* **10(12)**: 1028.

**Downing M**, Schweigert BS (1956) Role of vitamin B12 in nucleic acid metabolism. IV. Metabolism of C14-labeled thymidine by Lactobacillus leichmannii. *Journal of Biological Chemistry* **220**: 521–526.

**Dreissig S**, Schiml S, Schindele P, Weiss O, Rutten T, Schubert V, Gladilin E, Mette MF, Puchta H, Houben A (2017). Live-cell CRISPR imaging in plants reveals dynamic telomere movements. *The Plant Journal* **91(4)**: 565-573.

**Dresselhaus T**, Srilunchang KO, Leljak-Levanić D, Schreiber DN, Garg P (2006) The fertilization-induced DNA replication factor MCM6 of maize shuttles between cytoplasm and nucleus, and is essential for plant growth and development. *Plant physiology* **140(2)**: 512-527.

**Dubochet J**, Adrian M, Chang JJ, Homo JC, Lepault J, McDowall AW, Schultz P (1988) Cryo-electron microscopy of vitrified specimens. *Quarterly Reviews of Biophysics* **21**:129–228.

**Dvořáčková M,** Raposo B, Matula P, Fuchs J, Schubert V, Peška V, Desvoyes B, Gutierrez C, and Fajkus J (2018) Replication of ribosomal DNA in Arabidopsis occurs both inside and outside the nucleolus during S phase progression. *Journal of Cell Science* **131 (2)**, 1-12.

**Edgar BA**, Zielke N, Gutierrez C (2014) Endocycles: a recurrent evolutionary innovation for post-mitotic cell growth. *Nature reviews Molecular cell biology* **15(3)**: 197-210.

**Eltsov M**, Maclellan KM, Maeshima K, Frangakis AS, Dubochet J (2008) Analysis of cryo-electron microscopy images does not support the existence of 30-nm chromatin fibers in mitotic chromosomes in situ. *Proceedings of the National Academy of Sciences* **105**:19732–19737.

**Falkenberg M** (2018) Mitochondrial DNA replication in mammalian cells: overview of the pathway. *Essays in Biochemistry* **62(3)**:287-296.

**Finch JT**, Klug A (1976) Solenoidal model for superstructure in chromatin. *Proceedings of the National Academy of Sciences* **73(6)**: 1897-1901.

**Fragkos M**, Ganier O, Coulombe P, Méchali M (2015) DNA replication origin activation in space and time. *Nature Reviews Molecular Cell Biology* **16(6)**: 360-374.

**Fransz P,** De Jong JH, Lysak M, Castiglione MR, Schubert I (2002) Interphase chromosomes in Arabidopsis are organized as well defined chromocenters from which euchromatin loops emanate. *Proceedings of the National Academy of Sciences* **99**: 14584–14589.

**Friedkin M**, Tilson D, Roberts D (1956) Studies of deoxyribonucleic acid biosynthesis in embryonic tissues with thymidine-C14. *Journal of Biological Chemistry* **220**: 627–637.

**Friedkin M**, Wood HI (1956) Utilization of thymidine-C14 by bone marrow cells and isolated thymus nuclei. *Journal of Biological Chemistry* **220**: 639–651

**Fussell CP** (1992) Rabl distribution of interphase and prophase telomeres in *Allium cepa* not altered by colchicine and/or ultracentrifugation. *American Journal of Botany* **79**, 771–777.

**Fussner E**, Strauss M, Djuric U, Li R, Ahmed K, Hart M, Ellis J, BazettJones DP (2012) Open and closed domains in the mouse genome are configured as 10-nm chromatin fibres. EMBO Reports **13**:992–996.

**Galli E**, Ferat JL, Desfontaines JM, Val ME, Skovgaard O, Barre FX, Possoz C (2019) Replication termination without a replication fork trap. *Scientific reports* **9(1)**: 1-11.

**Gambus A** (2017) Termination of eukaryotic replication forks. In *DNA Replication* pp. 163-187. Springer, Singapore.

**Gandarillas A**, Molinuevo R, Sanz-Gómez N (2018) Mammalian endoreplication emerges to reveal a potential developmental timer. *Cell Death & Differentiation* ***25*****(3)**: 471-476.

**Gent JI**, Dong Y, Jiang J, Dawe RK (2012) Strong epigenetic similarity between maize centromeric and pericentromeric regions at the level of small RNAs, DNA methylation and H3 chromatin modifications. *Nucleic acids research* **40(4)**: 1550-1560.

**Ghirlando R**, Felsenfeld G (2016) CTCF: making the right connections. *Genes & development* **30(8)**: 881-891.

**Gibcus JH**, Samejima K, Goloborodko A, Samejima I, Naumova N, Nuebler J, Kanemaki M, Xie L, Paulson JR, Earnshaw WC, Mirny LA, Dekker J (2018) A pathway for mitotic chromosome formation. *Science* ***359*****(6376)**: eaao6135.

**Gilbert DM** (2010a) Evaluating genome-scale approaches to eukaryotic DNA replication. *Nature Reviews Genetics* **11**, 673–684.

**Gilbert DM** (2010b) Cell fate transitions and the replication timing decision point. *The Journal of Cell Biology* **191(5)**: 899.

**Gilbert N**, Boyle S, Fiegler H, Woodfine K, Carter NP, Bickmore WA (2004) Chromatin architecture of the human genome: gene-rich domains are enriched in open chromatin fibers. *Cell* **118(5)**: 555-566.

**Gilmour DS**, Lis JT (1984) Detecting protein-DNA interactions *in vivo*: Distribution of RNA polymerase on specific bacterial genes. *Proceedings og the National Academy of Scences* **81**: 4275–4279.

**Gilmour DS**, Lis JT (1985) *In vivo* interactions of RNA polymerase II with genes of *Drosophila melanogaster*. *Molecular and Cellular Biology* **5**: 2009– 2018.

**Gilmour DS**, Lis JT (1986) RNA polymerase II interacts with the promoter region of the noninduced hsp70 gene in *Drosophila melanogaster* cells. *Molecular and Cellular Biology* **6**: 3984–3989.

**Gilson E**, Géli V (2007) How telomeres are replicated. *Nature reviews Molecular cell biology* **8(10)**: 825-838.

**Gowrishankar J** (2015) End of the beginning: elongation and termination features of alternative modes of chromosomal replication initiation in bacteria. *PLoS Genetics* **11(1)**: e1004909.

**Grasser F**, Neusser M, Fiegler H, Thormeyer T, Cremer M, Carter NP, Cremer T, Müller S (2008) Replication-timing-correlated spatial chromatin arrangements in cancer and in primate interphase nuclei. *Journal of Cell Science* **121**: 1876–1886.

**Gratzner HG**, Leif RC, Ingram DJ, Castro A (1975) The use of antibody specific for bromodeoxyuridine for the immunofluorescent determination of DNA replication in single cells and chromosomes. *Experimental Cell Research* **95**: 88–94.

**Greider CW**, Blackburn EH (1989) A telomeric sequence in the RNA of Tetrahymena telomerase required for telomere repeat synthesis. *Nature* **337(6205)**: 331-337.

**Grewal SI**, Jia S (2007) Heterochromatin revisited. *Nature Reviews Genetics* **8(1)**: 35-46.

**Grob S**, Grossniklaus U (2017) Chromosome conformation capture-based studies reveal novel features of plant nuclear architecture. *Current opinion in plant biology* **36**: 149-157.

**Guelen L**, Pagie L, Brasset E, Meuleman W, Faza M B, Talhout W, Eussen BH, de Klein A, Wessels L, de Laat W, van Steensel B (2008) Domain organization of human chromosomes revealed by mapping of nuclear lamina interactions. *Nature* **453(7197)**: 948-951.

**Han Y**, Zhang T, Thammapichai P, Weng Y, Jiang J (2015) Chromosome-specific painting in Cucumis species using bulked oligonucleotides. *Genetics* ***200*****(3)**: 771-779.

**Handoko L**, Xu H, Li G, Ngan CY, Chew E, Schnapp M, Lee CWH, Ye C, Ping JLH, Mulawadi F, Wong E, Sheng J, Zhang Y, Poh T, Chan CS, Kunarso G, Shahab A, Bourque G, Cacheux-Rataboul V, Sung WK Ruan Y, Wei CL (2011) CTCF-mediated functional chromatin interactome in pluripotent cells. *Nature genetics* **43(7)**: 630-638.

**Hansen JC**, Connolly M, McDonald CJ, Pan A, Pryamkova A, Ray K, Seidel E, Tamura S, Rogge R, Maeshima K (2018) The 10-nm chromatin fiber and its relationship to interphase chromosome organization. *Biochemical Society Transactions*, **46(1)**: 67-76.

**Hansen RS**, Thomas S, Sandstrom R, Canfield TK, Thurman RE, Weaver M, Dorscher MO, Gartel SM, Stamatoyannopoulos JA (2010) Sequencing newly replicated DNA reveals widespread plasticity in human replication timing. *Proceedings of the National Academy of Sciences* **107(1)**: 139-144.

**Harr JC**, Luperchio TR, Wong X, Cohen E, Wheelan SJ, Reddy KL (2015) Directed targeting of chromatin to the nuclear lamina is mediated by chromatin state and A-type lamins. *Journal of Cell Biology* **208(1)**: 33-52.

**Harrison GE**, Heslop-Harrison JS (1995) Centromeric repetitive DNA sequences in the genus Brassica. *Theoretical and Applied Genetics* **90**: 157–165.

**Hawkins M**, Retkute R, Müller CA, Saner N, Tanaka TU, de Moura AP, Nieduszynski CA (2013) High-resolution replication profiles define the stochastic nature of genome replication initiation and termination. *Cell reports* **5(4)**: 1132-1141.

**Hayashi K**, Hasegawa J, Matsunaga S (2013) The boundary of the meristematic and elongation zones in roots: endoreduplication precedes rapid cell expansion. *Scientific Reports* **3**: 2723.

**Heitz E** (1928) Das heterochromatin der moose. I. Jb. wiss. Bot. **69**: 762–818.

**Heslop-Harrison JS** (1991) The molecular cytogenetics of plants. *Journal of Cell Science* **100(1)**: 15-21.

**Heun P**, Laroche T, Raghuraman MK, Gasser SM (2001) The positioning and dynamics of origins of replication in the budding yeast nucleus. *The Journal of cell biology* **152(2)**: 385-400.

**Hirano T** (2016) Condensin-based chromosome organization from bacteria to vertebrates. *Cell* **164(5)**: 847-857.

**Holt IJ** (2009) Mitochondrial DNA replication and repair: all a flap. *Trends in biochemical sciences* **34(7)**: 358-365.

**Holt IJ**, Reyes A (2012) Human mitochondrial DNA replication. *Cold Spring Harbor perspectives in biology* **4(12)**: a012971.

**Hoo JJ**, Cramer H (1971) On the position of chromosomes in prepared mitosis figures of human fibroblasts. *Humangenetik* **13**: 166–170.

**Houtgraaf JH**, Versmissen J, van der Giessen WJ (2006) A concise review of DNA damage checkpoints and repair in mammalian cells. *Cardiovascular Revascularization Medicine* **7(3)**: 165-172.

**Howe ES, Murphy SP, Bass H W.** 2013. Three-dimensional acrylamide fluorescence in situ hybridization for plant cells. *Plant meiosis*. Humana Press, Totowa, NJ, 53–66.

**Hozier J**, Renz M, Nehls P (1977) The chromosome fiber: evidence for an ordered superstructure of nucleosomes. *Chromosoma* **62(4)**: 301-317.

**Hřibová E**, Holušová K, Trávníček P, Petrovská B, Ponert J, Šimková H, Kubátová B, Jersáková J, Čurn V, Suda J, Doležel J, Vrána J (2016) The enigma of progressively partial endoreplication: new insights provided by flow cytometry and next-generation sequencing. *Genome Biology and Evolution* **8**: 1996-2005.

**Hsieh THS**, Weiner A, Lajoie B, Dekker J, Friedman N, Rando OJ (2015). Mapping nucleosome resolution chromosome folding in yeast by micro-C. *Cell* **162(1)**: 108-119.

**Hu B**, Wang N, Bi X, Karaaslan ES, Weber AL, Zhu W, Berendzen KW, Liu C (2019) Plant lamin-like proteins mediate chromatin tethering at the nuclear periphery. *Genome biology* **20(1)**: 87.

**Huberman JA**, Riggs AD (1966) Autoradiography of chromosomal DNA fibers from Chinese hamster cells. *Proceedings of the National Academy of Sciences* **55**: 599–606.

**Chai W**, Du Q, Shay JW, Wright WE (2006). Human telomeres have different overhang sizes at leading versus lagging strands. *Molecular cell* **21(3)**: 427-435.

**Chen C**, Lim HH, Shi J, Tamura S, Maeshima K, Surana U, Gan L, Cohen-Fix O (2016) Budding yeast chromatin is dispersed in a crowded nucleoplasm *in vivo*. *Molecular biology of the Cell* **27**:3357–3368.

**Chevalier C**, Nafati M, Mathieu-Rivet E, Bourdon M, Frangne N, Cheniclet C, Renaudin JP, Gévaudant F, Hernould M (2011) Elucidating the functional role of endoreduplication in tomato fruit development. *Annals of Botany* **107(7)**: 1159-1169.

**Chicano A**, Daban JR (2019) Chromatin plates in the interphase nucleus. *FEBS letters* **593(8)**: 810-819.

**Choe KN**, Moldovan GL (2017) Forging ahead through darkness: PCNA, still the principal conductor at the replication fork. *Molecular cell* **65(3)**: 380-392.

**Idziak D**, Robaszkiewicz E, Hasterok R (2015) Spatial distribution of centromeres and telomeres at interphase varies among *Brachypodium* species. *Journal of Experimental Botany* **66**: 6623–6634.

**Ishii T**, Schubert V, Khosravi S, Dreissig S, Metje-Sprink J, Sprink T, Fuchs J, Meister A, Houben A (2019) RNA-guided endonuclease–in situ labelling (RGEN-ISL): a fast CRISPR/Cas9-based method to label genomic sequences in various species. *The New phytologist* **222(3)**: 1652.

**Jackson DA**, Pombo A (1998) Replicon clusters are stable units of chromosome structure: evidence that nuclear organization contributes to the efficient activation and propagation of S phase in human cells. *The Journal of cell biology* **140(6)**: 1285-1295.

**Jacob F**, Brenner S, Cuzin F (1963) On the regulation of DNA synthesis in bacteria: the hypothesis of the replicon. *Cold Spring Harbor Symposia of Quantitative Biology* **256**: 298–300.

**Janssen A**, Colmenares SU, Karpen GH (2018) Heterochromatin: guardian of the genome. *Annual review of cell and developmental biology* **34**: 265-288.

**Jasencakova Z**, Meister A, Schubert I. (2001) Chromatin organization and its relation to replication and histone acetylation during the cell cycle in barley. *Chromosoma* **110**: 83–92.

**Jasencakova Z**, Soppe WJ, Meister A, Gernand D, Turner BM, Schubert I (2003) Histone modifications in Arabidopsis–high methylation of H3 lysine 9 is dispensable for constitutive heterochromatin. *The Plant Journal* **33(3)**: 471-480.

**Jiang J** (2019) Fluorescence in situ hybridization in plants: recent developments and future applications. *Chromosome Research* **27(3)**: 153-165.

**Johnson DS**, Mortazavi A, Myers RM, Wold B (2007) Genome-wide mapping of *in vivo* protein-DNA interactions. *Science **316*(5830)**:1497-1502.

**Joti Y**, Hikima T, Nishino Y, Kamada F, Hihara S, Takata H, Ishikawa T, Maeshima K (2012) Chromosomes without a 30-nm chromatin fiber. Nucleus **3**:404–410.

**Joubes J**, Chevalier C (2000) Endoreduplication in higher plants. In *The plant cell cycle* (pp. 191-201). Springer, Dordrecht.

**Jowhar Z**, Shachar S, Gudla PR, Wangsa D, Torres E, Russ JL, pegoraro G, Ried T, raznahan A, Misteli T (2018) Effects of human sex chromosome dosage on spatial chromosome organization. *Molecular Biology of the Cell* **29**: 2458–2469.

**Kamm A,** Galasso I, Schmidt T, Heslop-Harrison JS (1995) Analysis of a repetitive DNA family from *Arabidopsis arenosa* and relationships between *Arabidopsis* species. *Plant Molecular Biology* **27**: 853–862.

**Kaplan DL**, Bastia D (2009) Mechanisms of polar arrest of a replication fork. *Molecular microbiology* ***72*****(2)**: 279-285.

**Kizilyaprak C**, Spehner D, Devys D, Schultz P (2010) *In vivo* chromatin organization of mouse rod photoreceptors correlates with histone modifications. *PloS one* **5(6)**: e11039.

**Kohlmeier F**, Maya-Mendoza A, Jackson DA (2013) EdU induces DNA damage response and cell death in mESC in culture. *Chromosome Research* **21**: 87–100.

**Koláčková V**, Perničková K, Vrána J, Duchoslav M, Jenkins G, Phillips D, Turkosi E, Šamajová O, Sedlářová M, Šamaj J, Doležel J, Kopecký D (2019) Nuclear Disposition of Alien Chromosome Introgressions into Wheat and Rye Using 3D-FISH. *International journal of molecular sciences* **20(17)**: 4143.

**Komis G**, Šamajová O, Ovečka M, Šamaj J (2015). Super-resolution microscopy inplant cell imaging. *Trends in plant science* **20(12)**: 834-843.

**Kondorosi E**, Kondorosi A (2004) Endoreduplication and activation of the anaphase-promoting complex during symbiotic cell development. *FEBS letters* ***567*****(1)**: 152-157.

Kornberg RD, Lorch Y (1999) Twenty-five years of the nucleosome, fundamental particle of the eukaryote chromosome. *Cell* ***98*****(3)**: 285-294.

**Kosak ST**, Groudine M (2004) Form follows function: The genomic organization of cellular differentiation. *Genes & development* **18(12)**: 1371-1384.

**Langmore JP**, Schutt C (1980) The higher order structure of chicken erythrocyte chromosomes *in vivo*. *Nature* **288(5791)**: 620-622.

**Lee TJ**, Pascuzzi PE, Settlage SB, Shultz RW, Tanurdzic M, Rabinowicz PD, Menges M, Zheng P, Main D, Murray JAH, Sosinski B, Allen GC, Martinssen RA, Hanley-Bowdoin L, Vaughn MW, Thomspon WF (2010) *Arabidopsis thaliana* chromosome 4 replicates in two phases that correlate with chromatin state. *PLoS Genetetics* ***6*****(6)**: e1000982.

**Lentz SI**, Edwards JL, Backus C, McLean LL, Haines KM, Feldman EL (2010) Mitochondrial DNA (mtDNA) Biogenesis: Visualization and Duel Incorporation of BrdU and EdU Into Newly Synthesized mtDNA *In Vitro*. Journal of Histochemistry & Cytochemistry **58**: 207–218.

**Li F**, Chen J, Izumi M, Butler MC, Keezer SM, Gilbert DM (2001) The replication timing program of the Chinese hamster beta-globin locus is established coincident with its repositioning near peripheral heterochromatin in early G1 phase. *The Journal of Cell Biology* **154**: 283–292.

**Li J**, Santoro R, Koberna K, Grummt I (2005) The chromatin remodeling complex NoRC controls replication timing of rRNA genes. *The EMBO journal* **24(1)**: 120-127.

**Li Q**, Zhou H, Wurtele H, Davies B, Horazdovsky B, Verreault A, Zhang Z (2008) Acetylation of histone H3 lysine 56 regulates replication-coupled nucleosome assembly. *Cell* **134(2)**: 244-255.

**Lieberman-Aiden E**, van Berkum NL, Williams L, Imakaev M, Ragoczy T, Telling A, Amit I, Lajoie BR, Sabo PJ, Dorschner MO, Sandstrom R, Bernstein B, Bender A, Groundine M, Gnirke A, Stamatoyannopoulos J, Mirny LA, Lander ES, Dekker J **(**2009) Comprehensive mapping of long-range interactions reveals folding principles of the human genome. *Science* **326**: 289–293.

**Ligasová A**, Koberna K (2018) DNA Replication: From Radioisotopes to Click Chemistry. *Molecules **23*(11)**: 3007.

**Liu C**, Cheng YJ, Wang JW, Weigel D (2017) Prominent topologically associated domains differentiate global chromatin packing in rice from *Arabidopsis*. *Nature plants **3*(9)**: 742-748.

**Lucretti S**, Nardi L, Nisini P, Moretti F, Gualberti G, Dolezel J (1999) Bivariate flow cytometry DNA/BrdUrd analysis of plant cell cycle. *Methods in Cell Science* **21**:155–166.

**Lundberg A** (2019). Transcriptional gene signatures: passing the restriction point for routine clinical implementation.

**Lysak MA**, Fransz PF, Ali HBM, Schubert I (2001) Chromosome painting in *Arabidopsis thaliana*. *The Plant Journal* **28(6)**: 689-697.

**Maeshima K**, Ide S, Babokhov M (2019) Dynamic chromatin organization without the 30-nm fiber. *Current opinion in cell biology* **58**: 95-104.

**Maeshima K**, Imai R, Tamura S, Nozaki T (2014) Chromatin as dynamic 10-nm fibers. *Chromosoma* **123(3)**: 225-237.

**Maeshima K**, Laemmli UK (2003) A two-step scaffolding model for mitotic chromosome assembly. *Developmental cell* **4(4)**: 467-480.

**Maeshima K**, Tamura S, Hansen J C, Itoh Y (2020) Fluid-like chromatin: Toward understanding the real chromatin organization present in the cell. *Current Opinion in Cell Biology* **64**: 77-89.

**Magdalou I**, Lopez BS, Pasero P, Lambert SA (2014). The causes of replication stress and their consequences on genome stability and cell fate. In *Seminars in cell & developmental biology* **30** Pp. 154-164. Academic Press.

**Magnusson J**, Orth M, Lestienne P, Taanman JW (2003) Replication of mitochondrial DNA occurs throughout the mitochondria of cultured human cells. Experimental Cell Research **289**: 133–142.

**Mandáková T**, Lysak MA (2008) Chromosomal phylogeny and karyotype evolution in x= 7 crucifer species (Brassicaceae). *The Plant Cell* **20(10)**: 2559-2570.

**Mantiero D**, Mackenzie A, Donaldson A, Zegerman P (2011) Limiting replication initiation factors execute the temporal programme of origin firing in budding yeast. *EMBO Journal* **30**: 4805–4814.

**Manton I** (1950) The spiral structure of chromosomes. *Biological Reviews* **25(4)**: 486-508.

**Marczynski GT**, Shapiro L (1993) Bacterial chromosome origins of replication. *Current opinion in genetics & development* **3(5)**: 775-782.

**Marchal C**, Sima J, Gilbert DM (2019) Control of DNA replication timing in the 3D genome. *Nature Reviews Molecular Cell Biology*, 1-17.

**Markaki Y**, Gunkel M, Schermelleh L, Beichmanis S, Neumann J, Heidemann M., Leonhardt H, Eick D, Cremer C, Cremer T (2010) Functional nuclear organization of transcription and DNA replication a topographical marriage between chromatin domains and the interchromatin compartment. In *Cold Spring Harbor symposia on quantitative biology* **75**: Pp 475-492. Cold Spring Harbor Laboratory Press.

**Martínez P**, Blasco M A (2015) Replicating through telomeres: a means to an end. *Trends in biochemical sciences* **40(9)**: 504-515.

**Masai H**, Matsumoto S, You Z, Yoshizawa-Sugata N, Oda M (2010) Eukaryotic chromosome DNA replication: where, when, and how?. *Annual review of biochemistry 79*.

**Matheson TD**, Kaufman PD (2016) Grabbing the genome by the NADs. *Chromosoma* **125(3)**: 361-371.

**Mayer R**, Brero A, von Hase J, Schroeder T, Cremer T, Dietzel S (2005) Common themes and cell type specific variations of higher order chromatin arrangements in the mouse. *BMC Cell Biol*ogy **6**: 44.

**McCulloch SD**, Kunkel TA (2008) The fidelity of DNA synthesis by eukaryotic replicative and translesion synthesis polymerases. *Cell research* **18(1)**: 148-161.

**McDowall AW**, Smith JM, Dubochet J (1986) Cryo-electron microscopy of vitrified chromosomes *in situ*. *EMBO Journal* **5**:1395–1402.

**McGuffee SR**, Smith DJ, Whitehouse I (2013) Quantitative, genome-wide analysis of eukaryotic replication initiation and termination. *Molecular cell* **50(1)**: 123-135.

**McHenry CS** (2011) DNA replicases from a bacterial perspective. *Annual review of biochemistry* **80**: 403-436.

**McKee BD** (2004) Homologous pairing and chromosome dynamics in meiosis and mitosis. *Biochimca et Biophysica Acta* **1677**:165–180.

**Meuleman W**, Peric-Hupkes D, Kind J, Beaudry J B, Pagie L, Kellis M,Reinders M, Wessels L, van Steensel B (2013) Constitutive nuclear lamina–genome interactions

are highly conserved and associated with A/T-rich sequence. *Genome research* **23(2)**: 270-280.

**Mickelson-Young L**, Wear E, Mulvaney P, Lee TJ, Szymanski ES, Allen G, Hanley-Bowdoin L, Thompson W (2016) A flow cytometric method for estimating S-phase duration in plants. *Journal of Experimental Botan*y **67**: 6077–6087.

**Miotto B**, Ji Z, Struhl K (2016) Selectivity of ORC binding sites and the relation to replication timing, fragile sites, and deletions in cancers. Proceedings of the national Academy of Scence **113**: E4810-9.

**Mirkin EV**, Mirkin SM (2007) Replication fork stalling at natural impediments. *Microbiology and molecular biology reviews* **71(1)**: 13-35.

**Möckl L**, Lamb DC, Bräuchle C (2014) Super-resolved fluorescence microscopy: nobel Prize in Chemistry 2014 for Eric Betzig, Stefan Hell, and William E. Moerner. *Angewandte Chemie Internation Edition in English* **53**: 13972–13977.

**Mora L**, Sánchez I, Garcia M, Ponsà M (2006) Chromosome territory positioning of conserved homologous chromosomes in different primate species. *Chromosoma* **115**: 367–375.

**Moreno A**, Carrington JT, Albergante L, Al Mamun M, Haagensen EJ, Komseli ES, Gorgoulis VG, Newman TJ, Blow JJ (2016) Unreplicated DNA remaining from unperturbed S phases passes through mitosis for resolution in daughter cells. *Proceedings of the National Academy of Sciences* **113(39)**: E5757-E5764.

**Morley SA**, Ahmad N, Nielsen BL (2019) Plant organelle genome replication. *Plants* **8(10)**: 358.

**Morley SA**, Nielsen BL (2016) Chloroplast DNA copy number changes during plant development in organelle DNA polymerase mutants. *Frontiers in Plant Science* **7**: 57.

**Müller T**, Schumann C, Kraegeloh A (2012) STED microscopy and its applications: new insights into cellular processes on the nanoscale. *ChemPhysChem* **13(8)**: 1986-2000.

**Murphy SP**, Gumber HK, Mao Y, Bass HW (2014) A dynamic meiotic SUN belt includes the zygotene-stage telomere bouquet and is disrupted in chromosome segregation mutants of maize (*Zea mays* L.). *Frontiers in plant science* **5**: 314.

**Naumova N**, Imakaev M, Fudenberg G, Zhan Y, Lajoie BR, Mirny LA, Dekker J (2013) Organization of the mitotic chromosome. *Science* **342(6161)**: 948-953.

**Němečková A**, Koláčková V, Vrána J, Doležel J, Hřibová E (2020) DNA replication and chromosome positioning throughout the interphase in three-dimensional space of plant nuclei. *Journal of Experimental Botany*, doi.org/10.1093/jxb/eraa370

**Němečková A**, Wäsch C, Schubert V, Ishii T, Hřibová E, Houben A (2019) CRISPR/Cas9-based RGEN-ISL allows the simultaneous and specific visualization of proteins, DNA repeats, and sites of DNA replication. *Cytogenetic and Genome Research* **159(1)**: 48-53.

**Németh A**, Conesa A, Santoyo-Lopez J, Medina I, Montaner D, Péterfia B, Solovei I, Cremer T, Dopazo J, Längst G (2010) Initial genomics of the human nucleolus. *PLoS Genetetics* **6(3)**: e1000889.

**Neylon C**, Kralicek AV, Hill TM, Dixon NE (2005) Replication termination in *Escherichia coli*: structure and antihelicase activity of the Tus-Ter complex. *Microbiology and molecular biology reviews* **69(3)**: 501-526.

**Nishino Y**, Eltsov M, Joti Y, Ito K, Takata H, Takahashi Y, Hihara S, Frangakis AS, Imamoto N, Ishikawa T, Maeshima K (2012) Human mitotic chromosomes consist predominantly of irregularly folded nucleosome fibres without a 30-nm chromatin structure. *EMBO Journal* **31**:1644–1653.

**Nozaki T**, Imai R, Tanbo M, Nagashima R, Tamura S, Tani T, Joti Y, Tomita M, Hibino K, Kanemaki MT, Wendt KS, Okada Y, Nagai T, Maeshima K (2017) Dynamic organization of chromatin domains revealed by super-resolution live-cell imaging. *Molecular cell* **67(2)**: 282-293.

**O'Donnell M**, Langston L, Stillman B (2013) Principles and concepts of DNA replication in bacteria, archaea, and eukarya. *Cold Spring Harbor perspectives in biology* **5(7)**: a010108.

**Oakley AJ** (2019) A structural view of bacterial DNA replication. *Protein Science* **28(6)**: 990-1004.

**Ockey CH** (1969) Human chromosome identification and the pattern of DNA replication in fibroblasts from an XXY male. a quantitative autoradiographic study of early and late synthesis. *Cytogenetics* **8**: 272–295.

**Oehlmann M**, Score AJ, Blow JJ (2004) The role of Cdc6 in ensuring complete genome licensing and S phase checkpoint activation. *The Journal of cell biology* **165(2)**: 181-190.

**Ohnuki Y** (1968) Structure of chromosomes. *Chromosoma* **25(4)**: 402-428.

**Okazaki R**, Okazaki T, Sakabe K, Sugimoto K, Sugino A (1968) Mechanism of DNA chain growth. I. Possible discontinuity and unusual secondary structure of newly synthesized chains. *Proceedings of the National Academy of Science* **59**: 598–605.

**Okazaki T**, Okazaki R (1969) Mechanism of DNA chain growth. IV. Direction of synthesis of T4 short DNA chains as revealed by exonucleolytic degradation. *Proceedings of the National Academy of Science* **64**: 1242–1248.

**Olins AL**, Olinsb DE (1974) Spheroid chromatin units (ν bodies). *Science* **183(4122)**: 330-332.

**Olins DE**, Olins AL (2003) Chromatin history: our view from the bridge. *Nature reviews Molecular cell biology* **4(10)**: 809-814.

**Ono T**, Losada A, Hirano M, Myers MP, Neuwald AF, Hirano T (2003) Differential contributions of condensin I and condensin II to mitotic chromosome architecture in vertebrate cells. *Cell* **115(1)**: 109-121.

**Palmer JD** (1985) Comparative Organization of Chloroplast Genomes. Annual Review of Genetics **19**: 325–354.

**Palmer JD**, Stein DB (1986) Conservation of Chloroplast Genome Structure among Vascular Plants. Curr. Genet. 1986, 10, 823–833.

**Paulson JR**, Laemmli UK (1977) The structure of histone-depleted metaphase chromosomes. *Cell* **12(3)**: 817-828.

**Pawley J** (2006) *Handbook of biological confocal microscopy* 236. Springer Science & Business Media.

**Pawley JB** (1995) *Handbook of Biological Confocal Microscopy*. New York, NY: Plenum Press.

**Peacock WJ**, Dennis ES, Rhoades MM, Pryor AJ (1981) Highly repeated DNA sequence limited to knob heterochromatin in maize. *Proceedings of the National Academy of Sciences* **78(7)**: 4490-4494.

**Pecinka A**, Schubert V, Meister A, Kreth G, Klatte M, Lysak MA, Fuchs J, Schubert I (2004) Chromosome territory arrangement and homologous pairing in nuclei of *Arabidopsis thaliana*. Chromosoma **113(5)**:258-269

**Peric-Hupkes D**, Meuleman W, Pagie L, Bruggeman SW, Solovei I, Brugman W, Solovei I, Brugman W, Gräf S, Flicek P, Kerkhoven RM, van Lohuizen, Reinders M, Wessels L, van Steensel B (2010) Molecular maps of the reorganization of genome-nuclear lamina interactions during differentiation. *Molecular cell* **38(4)**: 603-613.

**Perničková K**, Koláčková V, Lukaszewski AJ, Fan C, Vrána J, Duchoslav M, Jenkins G, Philips D, Šamajová O, Sedlářová M, Šamaj J, Doležel J, Kopecký D (2019) Instability of alien chromosome introgressions in wheat associated with improper positioning in the nucleus. *International journal of molecular sciences* **20(6)**: 1448.

**Petryk N**, Kahli M, d'Aubenton-Carafa Y, Jaszczyszyn Y, Shen Y, Silvain M, Thermes C, Chen CL, Hyrien O (2016) Replication landscape of the human genome. *Nature communications* **7(1)**: 1-13.

**Phillips D**, Nibau C, Ramsay L, Waugh R, Jenkins G (2010) Development of a molecular cytogenetic recombination assay for barley. *Cytogenetic and genome research* **129(1-3)**: 154-161.

**Phillips D**, Wnetrzak J, Nibau C, Barakate A, Ramsay L, Wright F, Higgins JD, Perry RM, Jenkins G (2013) Quantitative high resolution mapping of HvMLH3 foci in barley pachytene nuclei reveals a strong distal bias and weak interference. *Journal of experimental botany* **64(8)**: 2139-2154.

**Picard F**, Cadoret J C, Audit B, Arneodo A, Alberti A, Battail C, Duret L, Prioleau MN (2014) The spatiotemporal program of DNA replication is associated with specific combinations of chromatin marks in human cells. *PLoS Genetetics* **10(5)**: e1004282.

**Pickersgill H**, Kalverda B, De Wit E, Talhout W, Fornerod M, van Steensel B (2006) Characterization of the *Drosophila melanogaster* genome at the nuclear lamina. *Nature genetics* ***38*****(9)**: 1005-1014.

**Picot J**, Guerin CL, Le Van Kim C, Boulanger CM (2012) Flow cytometry: retrospective, fundamentals and recent instrumentation. *Cytotechnology* **64(2)**: 109-130.

**Piskadlo E**, Tavares A, Oliveira RA (2017) Metaphase chromosome structure is dynamically maintained by condensin I-directed DNA (de) catenation. *Elife* ***6***: e26120.

**Plohl M**, Luchetti A, Meštrović N, Mantovani B (2008) Satellite DNAs between selfishness and functionality: structure, genomics and evolution of tandem repeats in centromeric (hetero) chromatin. *Gene* ***409*****(1-2)**: 72-82.

**Poirier MG**, Marko JF (2002) Mitotic chromosomes are chromatin networks without a mechanically contiguous protein scaffold. *Proceedings of the National Academy of Sciences* **99(24)**: 15393-15397.

**Pombo A**, Dillon N (2015) Three-dimensional genome architecture: players and mechanisms. *Nature reviews Molecular cell biology* **16(4)**: 245-257.

**Pontvianne F**, Carpentier MC, Durut N, Pavlištová V, Jaške K, Schořová Š, Parrinello H, Rohmer M, Pakaard CS, Fojtová M, Fajkus J, Sáez-Vásquez J (2016) Identification of nucleolus-associated chromatin domains reveals a role for the nucleolus in 3D organization of the *A. thaliana* genome. *Cell reports* **16(6)**: 1574-1587.

**Pontvianne F**, Grob S (2020) Three-dimensional nuclear organization in *Arabidopsis thaliana*. *Journal of Plant Research* **24**: 507-521.

**Poonperm R**, Takata H, Hamano T, Matsuda A, Uchiyama S, Hiraoka Y, Fukui K (2015) Chromosome scaffold is a double-stranded assembly of scaffold proteins. *Scientific reports* **5(1)**: 1-10.

**Pope BD**, Gilbert DM (2013) The replication domain model: regulating replicon firing in the context of large-scale chromosome architecture. *Journal of Molecular Biology* **425**: 4690–4695.

**Pope BD**, Ryba T, Dileep V, Yue F, Wu W, Denas O, Vera DL, Wang Y, Hansen S, Canfield TK, Thurman RE, Cheng Y, Gülsoy G, Dennis JH, Snyder MP, Stamatoyannopoulos JA, Taylor J, Hardison RC, Kahveci T, Ren B, Gilbert MD (2014) Topologically associating domains are stable units of replication-timing regulation. *Nature* ***515*****(7527)**: 402-405.

**Prieto EI**, Maeshima K (2019) Dynamic chromatin organization in the cell. *Essays in biochemistry* **63(1)**: 133-145.

**Prieto P**, Shaw P, Moore G (2004) Homologue recognition during meiosis is associated with a change in chromatin conformation. *Nature Cell Biology* **6**: 906.

**Quinet M**, Angosto T, Yuste-Lisbona FJ, Blanchard-Gros R, Bigot S, Martinez JP, Lutts S (2019) Tomato fruit development and metabolism. *Frontiers in Plant Science* **10**: 1554.

**Rabl C** (1885) Uber zelltheilung. *Morphologisches Jahrbuch* ***10***: 214-330.

**Raghuraman MK**, Brewer BJ, Fangman WL (1997) Cell cycle-dependent establishment of a late replication program. *Science* **276(5313)**: 806-809.

**Rao SS**, Huang SC, St Hilaire BG, Engreitz JM, Perez EM, Kieffer-Kwon KR, Sanborn AL, Johnstone SE, Bascom GD, Bochkov ID, Huang X, Shamim MS, Shin J, Turner D, Ye Z, Omer AD, Robinson JT, Schlick T, Bernstein BE, Casellas R, Lander ES, Aiden EL (2017) Cohesin loss eliminates all loop domains. *Cell* ***171*****(2)**: 305-320.

**Rao SS**, Huntley MH, Durand NC, Stamenova EK, Bochkov ID, Robinson JT, Sanborn AL, Machol I, Omer AD, Lander ES, Aiden EL (2014) A 3D map of the human genome at kilobase resolution reveals principles of chromatin looping. *Cell* **159(7)**: 1665-1680.

**Rattner JB**, Lin CC (1985) Radial loops and helical coils coexist in metaphase chromosomes. *Cell* ***42*****(1)**: 291-296.

**Rawlins DJ**, Highett MI, Shaw PJ (1991) Localization of telomeres in plant interphase nuclei by in situ hybridization and 3D confocal microscopy. *Chromosoma* **100**: 424–431.

**Rego EH**, Shao L, Macklin JJ, Winoto L, Johansson GA, Kamps-Hughes N, Davidson MW, Gustafsson MG (2012) Nonlinear structured-illumination microscopy with a photoswitchable protein reveals cellular structures at 50-nm resolution. *Proceedings of the National Academy of Sciences* ***109*****(3)**: E135-E143.

**Rhind N**, Gilbert DM (2013) DNA replication timing. *Cold Spring Harbor perspectives in biology* ***5*****(8)**: a010132.

**Ribas-Mundo M** (1966) DNA replication patterns of normal human leukocyte cultures. Time sequence of DNA synthesis in relation to the H3-thymidine incorporation over the nucleolus. *Blood* **28(6)**: 891–900.

**Rivin CJ**, Cullis CA, Walbot V (1986) Evaluating quantitative variation in the genome of *Zea mays*. *Genetics* ***113*(4)**: 1009-1019.

**Robinson NP**, Bell SD (2007) Extrachromosomal element capture and the evolution of multiple replication origins in archaeal chromosomes. *Proceedings of National Academy of Science* **104**: 5806–5811.

**Robinson PJ**, Fairall L, Huynh VA, Rhodes D (2006) EM measurements define the dimensions of the "30-nm" chromatin fiber: evidence for a compact, interdigitated structure. *Proceedings of the National Academy of Sciences* **103(17)**: 6506-6511.

**Rosenbusch BE**, Schneider M, Hanf V (1998) Tetraploidy and partial endoreduplication in a tripronuclear zygote obtained after intracytoplasmic sperm injection. *Fertility and sterility* **69(2)**: 344-346.

**Sabelli PA**, Larkins BA (2009) The contribution of cell cycle regulation to endosperm development. *Sexual Plant Reproduction* ***22*(4)**: 207-219.

**Salic A**, Mitchison TJ (2008) A chemical method for fast and sensitive detection of DNA synthesis *in vivo*. *Proceedings of the National Academy of Sciences* **105**: 2415–2420.

**Sanborn AL**, Rao SS, Huang SC, Durand NC, Huntley MH, Jewett AI, Bochkov ID, Chinnappan D, Cutkosky A, Li J, Geeting KP, Gnirke A, Melnikov A, McKenna D, Stamenova EK, Lander ES, Aiden EL (2015) Chromatin extrusion explains key features of loop and domain formation in wild-type and engineered genomes. *Proceedings of the National Academy of Sciences* ***112*(47)**: E6456-E6465.

**Santoro R**, Li J, Grummt I (2002) The nucleolar remodeling complex NoRC mediates heterochromatin formation and silencing of ribosomal gene transcription. *Nature Genetics* **32**: 393–396.

**Santos AP**, Shaw P (2004) Interphase chromosomes and the Rabl configuration: does genome size matter? *Journal of Microscopy* **214**: 201–206.

**Sawicki DL**, Erlanger BF, Beiser SM (1971) Immunochemical detection of minor bases in nucleic acids. *Science* **174**: 70–72.

**Sexton T**, Cavalli G (2015) The role of chromosome domains in shaping the functional genome. *Cell* **160**: 1049–1059.

**Sexton T**, Yaffe E, Kenigsberg E, Bantignies F, Leblanc B, Hoichman M, Parrinello H, Tanay A, Cavalli G (2012) Three-dimensional folding and functional organization principles of the *Drosophila* genome. *Cell* **148(3)**: 458-472.

**Shultz RW**, Tatineni VM, Hanley-Bowdoin L, Thompson WF (2007) Genome-wide analysis of the core DNA replication machinery in the higher plants Arabidopsis and rice. *Plant Physiology* **144(4)**: 1697-1714.

**Schalch T**, Duda S, Sargent DF, Richmond TJ (2005) X-ray structure of a tetranucleosome and its implications for the chromatin fibre. *Nature **436*(7047)**: 138-141.

**Scheffer MP**, Eltsov M, Frangakis AS (2011) Evidence for short-range helical order in the 30-nm chromatin fibers of erythrocyte nuclei. *Proceedings of the National Academy of Sciences* **108(41)**: 16992-16997.

**Schepers A**, Papior P (2010) Why are we where we are? Understanding replication origins and initiation sites in eukaryotes using ChIP-approaches. *Chromosome research* **18(1)**: 63-77.

**Schubert I**, Shaw P (2011) Organization and dynamics of plant interphase chromosomes. *Trends in Plant Science* **16**: 273–81.

**Schubert V** (2017) Super-resolution microscopy–applications in plant cell research. *Frontiers in plant science* **8**: 531.

**Schubert V**, Rudnik R, Schubert I (2014) Chromatin associations in Arabidopsis interphase nuceli. *Fronties in Genetics* **5**:389.

**Schwartz M**, Zlotorynski E, Kerem B (2006) The molecular basis of common and rare fragile sites. *Cancer letters* **232(1)**: 13-26.

**Sinai MIT**, Kerem B (2018) DNA replication stress drives fragile site instability. *Mutation Research/Fundamental and Molecular Mechanisms of Mutagenesis* **808**: 56-61.

**Sirbu BM**, Couch FB, Feigerle JT, Bhaskara S, Hiebert SW, Cortez D (2011). Analysis of protein dynamics at active, stalled, and collapsed replication forks. *Genes & development* **25(12)**: 1320-1327.

**Skinner BM**, Völker M, Ellis M, Griffin DK (2009) An appraisal of nuclear organisation in interphase embryonic fibroblasts of chicken, turkey and duck. *Cytogenetetic and Genome Research* **126**: 156–164.

**Smith JJ**, Antonacci F, Eichler EE, Amemiya CT (2009) Programmed loss of millions of base pairs from a vertebrate genome. *Proceedings of the National Academy of Sciences* **106**:11212–11217.

**Solomon MJ**, Larsen PL, Varshavsky A. 1988. Mapping protein-DNA interactions *in vivo* with formaldehyde: Evidence that histone H4 is retained on a highly transcribed gene. *Cell* **53**: 937–947.

**Song C**, Zhang S, Huang H (2015) Choosing a suitable method for the identification of replication origins in microbial genomes. *Frontiers in microbiology* **6**: 1049.

**Song F**, Chen P, Sun D, Wang M, Dong L, Liang D, Xu RM, Zhu P, Li G (2014) Cryo-EM study of the chromatin fiber reveals a double helix twisted by tetranucleosomal units. *Science **344*(6182)**: 376-380.

**Spielmann M**, Lupiáñez DG, Mundlos S (2018). Structural variation in the 3D genome. *Nature Reviews Genetics **19*(7)**, 453-467.

**Stillman B** (2008) DNA polymerases at the replication fork in eukaryotes. *Molecular cell* **30(3)**: 259-260.

**Strohner R**, Nemeth A, Jansa P, Hofmann-Rohrer U, Santoro R, Längst G, Grummt I (2001) NoRC—a novel member of mammalian ISWI-containing chromatin remodeling machines. *EMBO Journal* **20(17)**: 4892–4900.

**Suda J**, Kron P, Husband BC, Trávníček P (2007) Flow cytometry and ploidy: applications in plant systematics, ecology and evolutionary biology. *Flow cytometry with plant cells: analysis of genes, chromosomes and genomes*, 103-130.

**Suda J**. 2004. An employment of flow cytometry into plant biosystematics. PhD thesis, MS., Depon. Prague: Dept. of Botany, Faculty of Science Charles University.

**Sugimoto K**, Okazaki T, Imae Y, Okazaki R (1969) Mechanism of DNA chain growth, III. Equal annealing of T4 nascent short DNA chains with the separated complementary strands of the phage DNA. *Proceedings of the National Academy of Scences* **63**: 1343–1350.

**Sugimoto K**, Okazaki T, Okazaki R (1968) Mechanism of DNA chain growth, II. Accumulation of newly synthesized short chains in E. coli infected with ligase-defective T4 phages *Proceedings of the National Academy of Scences* **60**: 1356–1362.

**Sugimoto N**, Maehara K, Yoshida K, Ohkawa Y, Fujita M (2018) Genome-wide analysis of the spatiotemporal regulation of firing and dormant replication origins in human cells. *Nucleic acids research* **46(13)**: 6683-6696.

**Sugiura M** (1995) The chloroplast genome. *Essays in Biochemistry* **30**: 49–57.

**Sun HB**, Shen J, Yokota H (2000) Size-dependent positioning of human chromosomes in interphase nuclei. *Biophysical journal* **79(1)**: 184-190.

**Sun M**, Biggs R, Hornick J, Marko JF (2018) Condensin controls mitotic chromosome stiffness and stability without forming a structurally contiguous scaffold. *Chromosome Research* **26(4)**: 277-295.

**Sutherland GR** (2003) Rare fragile sites. *Cytogenetic and genome research* **100(1-4)**: 77-84.

**Szabo Q**, Bantignies F, Cavalli G (2019) Principles of genome folding into topologically associating domains. *Science advances* **5(4)**: eaaw1668.

**Szabo Q**, Jost D, Chang JM, cattoni JM, Papadopoulos GL, Bonec B, Sexton T, Gurgo J, Jacquier C, Nollmann M, Bantignies F, Cavalli G (2018) TADs are 3D structural units of higher-order chromosome organization in *Drosophila*. *Science Advances* **4**: eaar8082.

**Šimoníková D**, Němečková A, Karafiátová M, Uwimana B, Swennen R, Doležel J, Hřibová E (2019) Chromosome painting facilitates anchoring reference genome sequence to chromosomes in situ and integrated karyotyping in Banana (Musa Spp.). *Frontiers in Plant Science* **10**: 1503.

**Tanabe H**, Habermann FA, Solovei I, Cremer M, Cremer T (2002) Nonrandom radial arrangements of interphase chromosome territories: evolutionary considerations and functional implications. *Mutatation Research* **504**:37–45.

**Taylor JH**, Woods PS, Hughes WL (1957) The Organization and Duplication of Chromosomes as Revealed by Autoradiographic Studies Using Tritium-Labeled Thymidinee. *Proceedings of The National Academy of Science* **43**: 122–128.

**Techer H**, Koundrioukoff S, Azar D, Wilhelm T, Carignon S, Brison O, Debatisse M, Le Tallec B (2013) Replication dynamics: Biases and robustness of DNA fiber analysis. *Journal of Molecular Biology* **425**: 4845–4855.

**Tiang CL**, He Y, Pawlowski WP (2012) Chromosome organization and dynamics during interphase, mitosis, and meiosis in plants. *Plant Physiology* **158(1)**:26-34.

**Trávníček P**, Kubátová B, Čurn V, Rauchová J, Krajníková E, Jersáková J, Suda J (2011) Remarkable coexistence of multiple cytotypes of the Gymnadenia conopsea aggregate (the fragrant orchid): evidence from flow cytometry. *Annals of Botany **107*(1)**: 77-87.

**Trávníček P**, Ponert J, Urfus T, Jersáková J, Vrána J, Hřibová E, Doležel J, Suda J (2015) Challenges of flow-cytometric estimation of nuclear genome size in orchids, a plant group with both whole-genome and progressively partial endoreplication. *Cytometry Part A **87*(10)**: 958-966.

**Urata Y**, Parmelee SJ, Agard DA, Sedat JW (1995) A three-dimensional structural dissection of *Drosophila* polytene chromosomes. *The Journal of cell biology* **131(2)**: 279-295.

**van Holde K**, Zlatanova J (2007) Chromatin fiber structure: where is the problem now? *Seminars in Cell and Developmental Biology* **18**:651–658.

**van Koningsbruggen S**, Gierliński M, Schofield P, Martin D, Barton GJ, Ariyurek Y, den Dunnen, Lamond AI (2010) High-resolution whole-genome sequencing reveals that specific chromatin domains from most human chromosomes associate with nucleoli. *Molecular biology of the cell* **21(21)**: 3735-3748.

**Van Steensel B**, Belmont AS (2017) Lamina-associated domains: links with chromosome architecture, heterochromatin, and gene repression. *Cell **169*(5)**: 780-791.

**Velappan Y**, Signorelli S, Considine MJ (2017) Cell cycle arrest in plants: what distinguishes quiescence, dormancy and differentiated G1?. *Annals of botany **120*(4)**: 495-509.

**Vertii A**, Ou J, Yu J, Yan A, Pagès H, Liu H, Zhu LJ, Kaufman, PD (2019) Two contrasting classes of nucleolus-associated domains in mouse fibroblast heterochromatin. *Genome research **29*(8)**: 1235-1249.

**Visvanathan A**, Ahmed K, Even-Faitelson L, Lleres D, Bazett-Jones DP, Lamond AI (2013). Modulation of higher order chromatin conformation in mammalian cell nuclei can be mediated by polyamines and divalent cations. *PLoS One*, **8(6)**: e67689.

**Wang J**, Davis RE (2014) Programmed DNA elimination in multicellular organisms. Current opinion in Genetics Development **27**:26–34.

Wanner G, Formanek H (2000) A new chromosome model. *Journal of structural biology* **132(2)**: 147-161.

**Watson JD**, Crick FH (1953) Molecular structure of nucleic acids: a structure for deoxyribose nucleic acid. *Nature* **171(4356)**: 737-738.

**Wear EE**, Song JZ, Zynda GJ, LeBlanc C, Lee TJ, Mickelson-Young L, Concia L, Mulvaney P, Szymansi ES, Allen GC, Martinssen RA, Vaughn MW, Hanley-Bowdoin L, Thomspon WF (2017) Genomicanalysis of the DNA replication timing program during mitotic S phase in maize (*Zea mays*) root tips. *The Plant Cell* **29**, 2126–2149.

**Weierich C**, Brero A, Stein S, von Hase J, Cremer C, Cremer T, Solvei I (2003) Three-dimensional arrangements of centromeres and telomeres in nuclei of human and murine lymphocytes. Chromosome Res. Int. J. Mol. Supramol. Evol. Asp. *Chromosome Biology* **11**: 485–502.

**Wen B**, Wu H, Shinkai Y, Irizarry RA, Feinberg AP (2009) Large histone H3 lysine 9 dimethylated chromatin blocks distinguish differentiated from embryonic stem cells. *Nature genetics* **41(2)**: 246-250.

**Werner JE**, Kota RS, Gill BS, Endo TR (1992) Distribution of telomeric repeats and their role in the healing of broken chromosome ends in wheat. *Genome* **35**: 844–848.

**Wilkins TA**, Rajasekaran, K, Anderson DM (2000) Cotton biotechnology. *Critical Reviews in Plant Sciences* **19(6)**: 511-550.

**Wolfgruber TK**, Sharma A, Schneider KL, Albert PS, Koo DH, Shi J, Gao Zhi, Han F, Lee H, Xu R, Allison J, Jiang J, Dawe KR, Presting GG (2009) Maize centromere structure and evolution: sequence analysis of centromeres 2 and 5 reveals dynamic loci shaped primarily by retrotransposons. *PLoS Genet **5*(11)**: e1000743.

**Woodcock CL**, Frado LL, Rattner JB (1984) The higher-order structure of chromatin: evidence for a helical ribbon arrangement. *Journal of Cell Biology* **99**: 42–52.

**Xiang W**, Roberti MJ, Hériché JK, Huet S, Alexander S, Ellenberg J (2018) Correlative live and super-resolution imaging reveals the dynamic structure of replication domains. *Journal of Cell Biology*, **217(6)**: 1973-1984.

**Zeman MK**, Cimprich KA (2014) Causes and consequences of replication stress. *Nature cell biology* **16(1)**: 2-9.

**Zhang W**, Yi C, Bao W, Liu B, Cui J, Yu H, u, Cao X, Gu M, Liu M, Cheng Z (2005) The transcribed 165-bp CentO satellite is the major functional centromeric element in the wild rice species *Oryza punctata*. *Plant physiology* **139(1)**: 306-315.

**Zynda GJ**, Song J, Concia L, Wear EE, Hanley-Bowdoin L, Thompson WF, Vaughn MW (2017) Repliscan: a tool for classifying replication timing regions. *BMC Bioinformatics* 18(1): 362.

# 3 AIMS OF THE THESIS

## I Specific visualization of proteins, DNA repeats, and sites of DNA replication in maize using non-denaturing conditions

The first aim of the thesis was to establish a combination of labeling techniques allowing *in situ* studies in non-denaturing conditions with the use of the RGEN-ISL approach.

## II Comparison of DNA replication time in seven phylogenetically related species with differeces in genome sizes

The second aim of the work was to analyze replication timing of DNA sequences specific for centromeric and telomeric regions and to examine if differences in the genome size, chromosome number, and repetitive DNA organization in their nuclear genomes influence the replication timing, and have an effect on the 3D organization of chromatin in the interphase nucleus.

# 4 RESULTS

## 4.1 Summary

In this thesis, I focused on the comparison of DNA replication in space and time in seven related plant species differing in their genome size. The first goal of the current work was to established a combination of non-denaturing labeling techniques to visualize the spatiotemporal organization of the genome. This aim runs in parallel with the study focused on the dynamic of DNA replication in the 3D space of cell nuclei during different stages of the S phase.

To establish a new labeling protocol, discover of CRISPR-Cas9-based RNA guided endonuclease-in situ labeling (RGEN-ISL) was utilized. We used repeat specific gRNA for maize 180-bp knob repeat. The combination of RGEN-ISL and 5-ethynyl-2-deoxyuridine (EdU) was used for the detection of replication in maize. Even more, a triple combination of RGEN-ISL, EdU, and immunostaining was established. The replication of heterochromatin Knob repeats was combined with chromatin histone marks effect. A possible contribution of H3K9me2 in the early replication of heterochromatin in maize was found and simultaneously, the opposite function of H3K4me2 was found in the late replicating euchromatin in maize.

Moreover, the influence of denaturation on the morphology of chromatin was examined using super-resolution microscopy (SIM) with a resolution of about ~ 120 – 140 nm. In the case of non-denaturing conditions, chromatin maintained more compact, whereas in the classical denaturing condition of standard FISH procedure chromatin was flattened and impaired (Němečková *et al*., 2019).

A comparison study of seven selected species revealed surprisingly conserved dynamics of DNA replication in all species, although they differ in interphase chromatin arrangement and genome size as well. Telomere replication timing was established for the first part of the S phase, mostly for the early and middle phases. The only exception was found in rye, where the telomeric regions contained large heterochromatin blocks. As we showed, those telomeric regions that were closely connected to the heterochromatin blocks were replicated preferentially during the late S phase. The largest proportion of centromeric region, labeled by immunostaining with CENH3, was found in the middle and late S phase, although

the replication starts already in the early S phase. Moreover, a stable orientation of centromeric and telomeric regions was observed through all stages of the interphase.

## 4.2 Original papers

4.2.1 CRISPR/Cas9-Based RGEN-ISL Allows the Simultaneous and Specific Visualization of Proteins, DNA Repeats, and Sites of DNA Replication (Appendix I)

4.2.2 DNA replication and chromosome positioning throughout the interphase in three-dimensional space of plant nuclei (Appendix II)

### 3.2.1. CRISPR/Cas9-Based RGEN-ISL Allows the Simultaneous and Specific Visualization of Proteins, DNA Repeats, and Sites of DNA Replication

Němečková A, Wäsch Ch, Schubert V, Ishii T, Hřibová E, Houben, A

Cytogenetic and Genome Research, 159: 48-53, 2019

doi: 10.1159/000502600

IF: 1.114

**Abstract:**

Visualizing the spatiotemporal organization of the genome will improve our understanding of how chromatin structure and function are intertwined. Here, we describe a further development of the CRISPR/Cas9-based RNA-guided endonuclease-in situ labeling (RGEN-ISL) method. RGEN-ISL allowed the differentiation between vertebrate-type (TTAGGG)n and Arabidopsis-type (TTTAGGG)n telomere repeats. Using maize as an example, we established a combination of RGEN-ISL, immunostaining, and EdU labeling to visualize in situ specific repeats, histone marks, and DNA replication sites, respectively. The effects of the non-denaturing RGEN-ISL and standard denaturing FISH on the chromatin structure were compared using super-resolution microscopy. 3D structured illumination microscopy revealed that denaturation and acetic acid fixation impaired and flattened the chromatin. The broad range of adaptability of RGEN-ISL to different combinations of methods has the potential to advance the field of chromosome biology.

### 3.2.2 DNA replication and chromosome positioning throughout the interphase in three-dimensional space of plant nuclei

Němečková A, Koláčková V, Vrána J, Doležel J, Hřibová E

Journal of Experimental Botany, 2020

doi: doi:10.1093/jxb/eraa370

IF: 5.908

**Abstract:**

Despite much recent progress, our understanding of the principles of plant genome organization and its dynamics in three-dimensional space of interphase nuclei remains surprisingly limited. Notably, it is not clear how these processes could be affected by the size of a plant's nuclear genome. In this study, DNA replication timing and interphase chromosome positioning were analyzed in seven *Poaceae* species that differ in their genome size. To provide a comprehensive picture, a suite of advanced, complementary methods was used: labeling of newly replicated DNA by ethynyl-2'-deoxyuridine, isolation of nuclei at particular cell cycle phases by flow cytometric sorting, three-dimensional immunofluorescence *in situ* hybridization, and confocal microscopy. Our results revealed conserved dynamics of DNA replication in all species, and a similar replication timing order for telomeres and centromeres, as well as for euchromatin and heterochromatin regions, irrespective of genome size. Moreover, stable chromosome positioning was observed while transitioning through different stages of interphase. These findings expand upon earlier studies in suggesting that a more complex interplay exists between genome size, organization of repetitive DNA sequences along chromosomes, and higher order chromatin structure and its maintenance in interphase, albeit controlled by currently unknown factors.

## 4.3 Conference presentations

### 4.3.1 Replication of DNA repeats in time and space

(poster presentation; Appendix III)

### 4.3.2 DNA replication timing program in barley (*Hordeum vulgare*).

(poster presentation: Appendix IV)

### 4.3.3 Chromatin arrangement across the whole cell cycle in the Poaceae family

(poster presentation: Appendix V)

### 4.3.4 Replication of DNA repeats in time and space

(oral presentation)

### 4.3.5 3D organizace chromozómů v buněčném jádře obilovin.

(oral presentation)

### 3.3.1 Replication of DNA repeats in time and space

Němečková A, Vrána J, Doležel J, Hřibová E

In: Abstract of the: „Plant Genome Stability and Change“.
IPK Gatersleben, Germenay, 2018

**Abstract:**

Genetic information is replicated during S phase of cell cycle and the process is under strict control. In plants, the time course of DNA replication has been studied in detail only in maize. To provide more insights, we set up to study the replication of a set of DNA repeats, including those playing a role in telomere and centromere organization, tandem organized units of rDNA sequences and other tandem repeats in two closely related plant species differing in genome size. *Brachypodium distachyon* has a small genome and low proportion of DNA repeats (1C ~355 Mb, ~30% repeats) while *Hordeum vulgare* has a large genome (1C ~5100 Mb) with a high proportion of DNA repeats (more than 80%). In order to study DNA replication of the selected DNA repeats in time and space we combined flow cytometry and 3D acrylamide FISH. Cell cycle transition was followed by incorporation of 5-ethynyl-2'-deoxyuridine (EdU) into newly synthesized DNA, and the nuclei at different stages of cell cycle (G1, G2, very early, early, middle, late and very late S-phase). The sorted nuclei were used for 3D FISH with probes for the DNA repeats and rRNA genes. Our work revealed complex patterns of DNA replication in different stages of S phase. During the early S phase, the signals of EdU labeled replicating chromatin were localized to particular foci and separated from non-replicating chromatin labeled by DAPI. This contrasted with the late S phase, when the signals of EdU labeled replicating chromatin overlapped with DAPI-stained heterochromatin. In middle S phase, the most of the chromatin is replicated, no specific pattern of EdU labeled versus DAPI stained chromatin was observed. These results indicated that highly heterochromatic regions were replicated in late S phase. 3D acrylamide FISH with the probes specific to different DNA repeats and rDNA sequences revealed a more complex mode of their replication during the S phase. While 5S rRNA genes were replicated during early S phase, 45S rRNA genes were replicated during all

stages of S phase. Nevertheless, a majority of them were replicated in very late S phase, probably reflecting the presence of large amounts of pseudogenic 45S rDNA units. The LTR retrotransposon Cereba, which localizes preferentially to centromeric regions of *H. vulgare* replicated during all stages of S phase and sub-telomeric satellite repeats psc119 is replicated during the early and middle S phase. These results provide the first picture of the complexity of DNA replication in time and nuclear space, which reflects different types of DNA sequences and their role in genome organization and function.

### 3.3.2 DNA replication timing program in barley (*Hordeum vulgare*)

Čížková J, Němečková A, Vrána J, Doležel J, Hřibová E

In: International Conference on Polyploidy

Ghent, Belgium, 2019

**Abstract:**

Nuclear genome is replicated during the S phase of cell cycle under strict rules, which ensure accuracy and completeness of this important process. Replication timing programs have been described in prokaryotes, yeasts and many animal species. In plants, DNA replication was analysed in detail only in species with relatively small genomes, such as maize and *Arabidopsis*. To provide more insights, we studied the replication machinery in barley, a representative of plants with large genome (1C ~ 5100 Mb) and high proportion of DNA repeats (~ 84%). In order to study DNA replication in time and space we combined flow sorting of EdU-labeled nuclei, 3D acrylamide FISH and Repli-seq. Nuclei at different stages of the cell cycle (G1, G2, early, middle and late S-phase) were isolated and used for 3D FISH with probes specific to different DNA repeats and rRNA genes. We observed that replication process of different DNA repeats varied in time, e.g., centromeric retrotransposon Cereba was replicated during all stages of S phase, while sub-telomeric satellite repeat psc119 was replicated during the early and middle S phase. Difference in replication timing was observed also for rRNA genes, while 5S rRNA genes were replicated during early S phase, majority of 45S rRNA genes were replicated in late S phase, probably reflecting the presence of large amounts of pseudogenic 45S rDNA units. Genome-wide replication timing program in barley was described based on Repli-seq, which identified genomic regions that replicate predominantly during early, middle and late S-phase. Our results provide the first picture of the complexity of DNA replication in barley, reflecting different types of DNA sequences and their role in genome organization.

### 3.3.3 Chromatin arrangement across the whole cell cycle in the *Poaceae* family

Němečková A., Vrána J, Doležel J, Hřibová E

In: Abstract of the „MEETING OF THE GPZ GROUP, CYTOGENETICS 2019“.

Dresden, Germany, 2019

**Abstract:**

In 1885, Carl Rabl observed a particular arrangement of chromosomes in interphase nuclei, later named after him. Almost one and half century later, our understanding of the spatial organization of interphase chromosomes remains sketchy. Among other, it is believed that the Rabl configuration is typical for plants with genomes larger than 4000 Mb, and absent in species with genomes smaller than 1000 Mb, and that the Rabl configuration is not preserved in all tissues and organs of an organism. In order to provide more insights, we studied nuclear chromatin organization in root tip meristem cells at different stages of cell cycle in seven species from the *Poaceae* family. Following labeling by EdU, cell nuclei were sorted using flow cytometry and microscopically analyzed after 3D FISH with probes for telomeres, centromeres and 45S rDNA. While in species with relatively small genomes (*Brachypodium*, rice and maize), replicating chromatin concentrated to small regions resembling islands, the replicating chromatin was more dispersed and localized to many small loci in species with large genomes (barley, wheat, rye and oat). A combination of EdU labeling and 3D FISH on sorted nuclei revealed Rabl configuration during the whole S phase in all species except rice. Apart from the analysis of chromosome spatial organization, we analyzed the replication of 45S rRNA genes which are localized in nucleoli. 45S rDNA was replicated during late S phase with the exception of *Brachypodium*, in which the replication of 45S rDNA started already in the middle S phase.

### 3.3.4 Replication of DNA repeats in time and space

Němečková A, Vrána J, Doležel J, Hřibová Eva

In: Praha, Czech Republic, 2018

**Abstract:**

Genetic information is replicated during S phase of cell cycle and the process is under strict control. Most of our knowledge about genome replication comes from animals studies but in plants, the time course of DNA replication has been studied in detail only in maize and *Arabidopsis*. To provide more insights, we set up to study the replication machinery in *Hordeum vulgare*, a plant representative with large genome (1C ~5100 Mb) and high proportion of DNA repeats (more than 80 %). In order to study DNA replication in time and space we combined flow cytometry, 3D acrylamide FISH and Repli-seq. Cell cycle transition was followed by incorporation of 5-ethynyl-2'-deoxyuridine (EdU) into newly synthesized DNA, and the nuclei at different stages of cell cycle (G1, G2, very early, early, middle, late and very late S-phase). In order to study replication of DNA repeats, we sorted nuclei from all 9 phases of the cell cycle and used them for 3D FISH with probes for the DNA repeats and rRNA genes. 3D acrylamide FISH with the probes specific to different DNA repeats and rDNA sequences revealed a more complex mode of their replication during the S phase. While 5S rRNA genes were replicated during early S phase, majority of 45S rRNA genes were replicated in very late S phase, probably reflecting the presence of large amounts of pseudogenic 45S rDNA units. The LTR retrotransposon Cereba, which localizes preferentially to centromeric regions of *H. vulgare* replicated during all stages of S phase and sub-telomeric satellite repeats psc119 is replicated during the early and middle S phase. The work on replication of specific DNA repeats by 3D FISH was completed by the analysis of genome-wide replication timing in barley by Repli-seq procedure. Our results provide the first picture of the complexity of DNA replication in time and nuclear space, which reflects different types of DNA sequences and their role in genome organization and function in barley.

### 3.3.5 3D organizace chromozómů v buněčném jádře obilovin

Němečková A, Hřibová E

In: 53. výroční cytogenetická conference

Olomouc, Czech Republic, 2020

[In Czech]

**Abstrakt:**

První hypotézu uspořádání chromozómů v interfázním jádře přinesl již v roce 1885 Carl Rabl, který pomocí optického mikroskopu pozoroval dělící se buňky mloka. Jeho hypotézy byly potvrzeny až aplikací cytogenetických studií na člověku, živočiších a některých rostlinných druzích, která obsahovaly velké chromozómy. Tyto studie ukázaly, že chromozómy jsou v interfázním jádře organizovány tak, že centromerické a telomerické oblasti leží na opačných pólech interfázních jader – tzv. Rabl konfigurace. Pozdější studie odhalily že rostlinné druhy s malým genomem, jako např. *Arabidopsis thaliana*, mají chromozómy v interfázním jádře organizovány do tzv. Růžicové struktury (Rosette-like structure), kdy jsou centromerické oblasti lokalizovány na periferii jádra a telomerické oblasti se nachází v blízkosti jadérka.

Cílem naší studie byla analýza uspořádání interfázních chromozómů u sedmi zástupců lipnicovitých, včetně hospodářsky významných obilovin, které se liší velikostí jaderných genomů, množství repetitivních sekvencí DNA, počtem a morfologií chromozómů. Za tímto účelem bylo využito značení nově se replikujících oblastí DNA pomocí 5-ethynyl-2'-deoxyuridinu (EdU), analýzy buněčného cyklu a třídění jader specifických pro různé fáze buněčného cyklu pomocí průtokové cytometrie, trojdimenzionální fluorescenční *in situ* hybridizace (3D FISH) a konfokální mikroskopie.

Naše výsledky odhalili konzervovanou dynamiku DNA replikace u všech analyzovaných rostlinných druhů a velmi podobnou dobu replikace centromerických a telomerických oblastí chromozómů. Navíc třídění jader a následná 3D cytogenetická analýza odhalila stabilní pozici chromozómů v průběhu rozdílných fází (G1, S, G2) interfázního jádra.

Získané výsledky rozšiřují dosavadní znalosti o uspořádání interfázních chromozómů rostlin, a ukazují, že na uspořádání rostlinných interfázních

chromozómů má vliv nejen velikost genomu, či velikost chromozómů, ale také přítomnost a organizace repetitivních sekvencí DNA a organizace samotného chromatinu v průběhu interfáze buněčného cyklu.

# 5 CONCLUSIONS

## 5.1 Specific visualization of proteins, DNA repeats, and sites of DNA replication in maize using non-denaturing conditions

A combination of three methods was established under non-denaturing conditions that became a valuable tool for the simultaneous detection of specific DNA repeats, proteins, and DNA replication sites.

## 5.2.Comparison of DNA replication time in seven phylogenetically related species with differences in genome sizes.

Replication timing of centromeric and telomeric regions in seven selected plant species using a combination of EdU labeling, flow sorting, and 3D-immuno-FISH localization was established. Simultaneous detection in 3D space of nuclei, where the chromatin structure is preserved, was proved as a powerful tool for analysis of the spatiotemporal pattern of DNA replication, and chromatin organization during interphase.

# 6 LIST OF ABBREVIATIONS

| | |
|---|---|
| A | adenine |
| 3C | chromosome confirmation capture |
| 3D | tree dimensional |
| 3D-SIM | tree dimensional structured illumination microscopy |
| BAC | bacterial artificial chromosome |
| bp | base pairs |
| BrdU | 5-bromodeoxyuridine |
| C | cytosine |
| Cas9 | CRISPR associated protein 9 |
| CENH3 | centromere-specific variant of histone H3 |
| CRISPR | clustered regularly interspersed palindromic repeats |
| crRNA | CRISPR ribonucleic acid |
| ChIP | chromatin immunoprecipitation |
| ChIP-chip | chromatin immunoprecipitation analysed on microarrays |
| ChiP-seq | chromatin immunoprecipitation sequencing |
| CT | chromosome territories |
| CTRs | constant timing region |
| cpDNA | chloroplast deoxyribonucleic acid |
| ddNTP | dideoxynucleotide |
| DNA | deoxyribonucleic acid |
| dsDNA | double strand deoxyribonucleic acid |
| EdU | 5-ethynyl-2-deoxyuridine |
| ESI | electron spectroscopic imaging |

| | |
|---|---|
| FCM | flow cytometry |
| FISH | fluorescence *in situ* hybridization |
| FLIM | fluorescence-lifetime imaging microscopy |
| FRET | fluorescence resonance energy transfer |
| G | guanine |
| gRNA | guide ribonucleic acid |
| Hi-C | chromosome-conformation-base mapping |
| kb | kilobase pairs |
| LAD | lamina associated domain |
| MAR | matrix attachment region |
| Mb | megabase pairs |
| mtDNA | mitochondrial deoxyribonucleic acid |
| NAD | nucleolus associated domains |
| NGS | next generation sequencing |
| Nm | nano-metr |
| oriC | replication origin |
| ORs | origins of replication |
| PALM | photoactivated localisation microscopy |
| PAM | protospacer adjacent motif |
| Pre-RC | pre-replication complex |
| PCR | polymerase chain reaction |
| PPE | progressively partial endoreplication |
| rRNA | ribosomal ribonucleic acid |
| RNA | ribonucleic acid |

| | |
|---|---|
| Repli-seq | genome-wide analysis of replication timing by next generation sequencing |
| RPA | replication protein A |
| SAXS | small angel X-ray scattering |
| SIM | structured illumination microscopy |
| STED | stimulated emission depletion microscopy |
| STORM | stochastic optical reconstruction microscopy |
| T | thymine |
| TAD | topologically associating domain |
| TTR | timing transition region |
| tracrRNA | trans-activating CRISPR ribonucleic acid |
| UV | ultraviolet |

# 7 LIST OF APPENDICES

## Original Papers

Appendix I: CRISPR/Cas9-Based RGEN-ISL Allows the Simultaneous and Specific Visualization of Proteins, DNA Repeats, and Sites of DNA Replication

Appendix II: DNA replication and chromosome positioning throughout the interphase in three-dimensional space of plant nuclei

## Published Posters

Appendix III: Replication of DNA repeats in time and space

Appendix IV: DNA replication timing program in barley (*Hordeum vulgare*).

Appendix V: Chromatin arrangement across the whole cell cycle in the *Poaceae* family

# APPENDIX I

## CRISPR/Cas9-Based RGEN-ISL Allows the Simultaneous and Specific Visualization of Proteins, DNA Repeats, and Sites of DNA Replication

Němečková A, Wäsch C, Schubert V, Ishii, T, Hřibová E, Houben A.

Cytogenetic and Genome Research, 159, 48-53, 2019

doi: 10.1159/000502600

IF: 1.114

**Original Article**

Cytogenetic and Genome Research

Cytogenet Genome Res 2019;159:48–53
DOI: 10.1159/000502600

Accepted: August 3, 2019
Published online: October 12, 2019

# CRISPR/Cas9-Based RGEN-ISL Allows the Simultaneous and Specific Visualization of Proteins, DNA Repeats, and Sites of DNA Replication

Alžběta Němečková[a, b] Christina Wäsch[a] Veit Schubert[a] Takayoshi Ishii[c]
Eva Hřibová[b] Andreas Houben[a]

[a]Leibniz Institute of Plant Genetics and Crop Plant Research (IPK) Gatersleben, Seeland, Germany; [b]Institute of Experimental Botany, Czech Academy of Sciences, Center of the Region Haná for Biotechnological and Agricultural Research, Olomouc, Czech Republic; [c]Arid Land Research Center (ALRC), Tottori University, Tottori, Japan

**Keywords**
CRISPR/Cas9 · DNA replication · FISH · Immunostaining · RGEN-ISL · Super-resolution microscopy

**Abstract**
Visualizing the spatiotemporal organization of the genome will improve our understanding of how chromatin structure and function are intertwined. Here, we describe a further development of the CRISPR/Cas9-based RNA-guided endonuclease-in situ labeling (RGEN-ISL) method. RGEN-ISL allowed the differentiation between vertebrate-type $(TTAGGG)_n$ and *Arabidopsis*-type $(TTTAGGG)_n$ telomere repeats. Using maize as an example, we established a combination of RGEN-ISL, immunostaining, and EdU labeling to visualize in situ specific repeats, histone marks, and DNA replication sites, respectively. The effects of the non-denaturing RGEN-ISL and standard denaturing FISH on the chromatin structure were compared using super-resolution microscopy. 3D structured illumination microscopy revealed that denaturation and acetic acid fixation impaired and flattened the chromatin. The broad range of adaptability of RGEN-ISL to different combinations of methods has the potential to advance the field of chromosome biology.


Since the 1990s, fluorescence in situ hybridization (FISH) has been widely used for the visualization of specific DNA sequences in fixed nuclei and chromosomes. In that process, a DNA denaturation step using heat, formamide, or sodium hydroxide is necessary to allow probe hybridization. However, these treatments may affect the native structure of chromatin. Nowadays, with the improved ultrastructural investigation possibilities via super-resolution microscopy and a high interest in analyzing the real native chromatin structure, its arrangement, and modifications during the cell cycle, more sensitive techniques for chromatin labeling are required.

The discovery and application of the type II clustered regulatory interspaced short palindromic repeat (CRISPR)-associated caspase 9 (Cas9) system for genome editing was the starting point to employ this system also for the fluorescence detection of genomic loci in living [Chen et al., 2013; Anton et al., 2014; Dreissig et al., 2017] and fixed non-denatured animal and plant cells [Deng et al., 2015; Ishii et al., 2019].

The principle of fluorescence labeling using the CRISPR/Cas9 system is based on the property of designed CRISPR RNA (crRNA), which contains a spacer complementary to a DNA sequence and provides the target specificity of the Cas9 system (Fig. 1). To find the target



E-Mail karger@karger.com
www.karger.com/cgr

Andreas Houben
Leibniz Institute of Plant Genetics and Crop Plant Research (IPK)
Corrensstrasse 3
OT Gatersleben, DE–06466 Seeland (Germany)
E-Mail houben@ipk-gatersleben.de

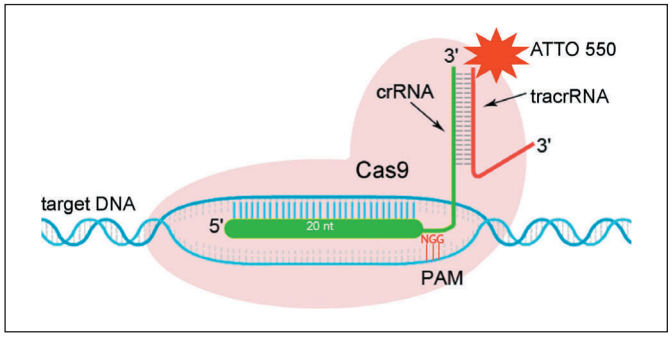


**Fig. 1.** The principle of fluorescence labeling of genomic DNA using the CRISPR-Cas9-based RGEN-ISL method. The crRNA: tracrRNA complex uses optimized Alt-R crRNA and ATTO 550-labeled tracrRNA sequences that hybridize and then form a complex with Cas9 endonuclease to guide targeted binding to genomic DNA. The binding site is specified by the protospacer element of the crRNA (green bar). This element recognizes 19 or 20 nt on the opposite strand of the NGG PAM site. The PAM site must be present immediately downstream of the protospacer element that binding can occur.

DNA, the Cas9 nuclease requires a guide RNA (gRNA) which is composed of crRNA, fluorescently labeled *trans*-activating crRNA (tracrRNA), and a protospacer adjacent motif (PAM). This specific complex is formed by hybridization of the designed crRNA in combination with the fluorescently labeled tracrRNA [Ishii et al., 2019]. The crRNA contains a 20-nucleotide guide sequence called spacer and the PAM, a short G-rich motif which is positioned next to the gRNA-specific part of the target sequence.

To further develop the CRISPR/Cas9-based RNA-guided endonuclease-in situ labeling (RGEN-ISL) method for the detection of high-copy DNA, we employed telomere and maize 180-bp knob [Peacock et al., 1981; Ananiev et al., 1998] repeat-specific gRNAs. We established a combination of RGEN-ISL, immunostaining, and 5-ethynyl-deoxyuridine (EdU) labeling to detect specific repeats, histone marks, and DNA replication sites, respectively. We compared the effect of non-denaturing RGEN-ISL and standard denaturing FISH on the structure of chromatin using super-resolution microscopy.

## Materials and Methods

*Material*

Nuclei and chromosomes of *Zea mays* L. (genotype B73) and *Scadoxus multiflorus* (Martyn) Raf. (also known as *Haemanthus multiflorus*) were used.

*Sample Preparation*

Maize nuclei and chromosomes were isolated from root meristems and leaves of young seedlings. *S. multiflorus* nuclei were isolated from roots of mature plants. Leaves were fixed for 30 min in Tris buffer with 2% formaldehyde (10 mM Tris, 10 mM $Na_2EDTA$, 100 mM NaCl, 0.1% Triton X-100, 2% formaldehyde, pH 7.5 [prepared from formaldehyde solution 37%, Carl Roth GmbH, cat. No. 7398.1]) at 4°C. The first 5 min of fixation were done under vacuum condition using a Vacufuge concentrator (Eppendorf, model 5301) according to Doležel et al. [1992]. After fixation, leaves were washed 3 times in Tris buffer, using a rotating shaker (100 rpm) on ice. For the preparation of chromosomes and nuclei from the root meristems, Tris buffer with 3% formaldehyde was used for 35 min (5 min under vacuum and 30 min on ice only) for fixation. The meristems of four 1-cm-long root tips were chopped into thin slices with a razor blade in 500 µL LB01 buffer (15 mM Tris, 2 mM $Na_2EDTA$, 0.5 mM spermine tetrahydrochloride, 80 mM KCl, 20 mM NaCl, 15 mM β-mercaptoethanol, 0.1% Triton X-100, pH 7.5) [Doležel et al., 1989]. The suspension was passed through a 35-µm nylon mesh, and nuclei and chromosomes were spun onto standard microscopic slides using a Thermo Shandon Cytospin 3 (700 rpm for 5 min for leaf- and 400 rpm for 5 min for root-derived material). The slides were checked by phase contrast microscopy and kept in ice-cold 1× PBS. Before use, slides were washed in 1× PBS for 5 min on ice while shaking (100 rpm).

*RNA-Guided Endonuclease-in situ Labeling*

Target-specific crRNAs for the 180-bp maize knob repeat [Peacock et al., 1981] and the vertebrate telomere repeat were designed using the software crCRISPRdirect (https://crispr.dbcls.jp/) (online suppl. Table 1; for all online suppl. material, see www.karger.com/doi/10.1159/000502600). We employed the 2-part gRNA (crRNA and tracrRNA) system (Alt-R® CRISPR-Cas9, Integrated DNA Technologies, https://eu.idtdna.com) for RGEN-ISL according to Ishii et al. [2019]. For the assembly of 10 µM gRNA, 1 µL 100 µM crRNA, 1 µL 100 µM ATTO550-labeled tracrRNA, and 8 µL duplex buffer were used. Afterwards, the gRNA was denatured for 5 min at 95°C to hybridize. In the next step, the ribonucleoprotein (RNP) complex was prepared: 1 µL 10 µM gRNA, 1 µL 6.25 µM dCas9 proteins (D10A and H840A; Novateinbio, PR-137213), 10 µL 10× Cas9 buffer (200 mM Hepes pH 7.5, 1 M KCl, 50 mM $MgCl_2$, 50% (v/v) glycerol, 10% BSA, and 1% Tween 20), 10 µL 10 mM DTT, and 80 µL double distilled water were mixed, incubated at 26°C for 10 min, and stored at 4°C. Per slide, 100 µL of 1× Cas9 buffer/1 mM DTT was applied for 2 min at room temperature. The slides were tilted to remove the buffer, and 25 µL RNP complex per slide was applied. Slides were covered with parafilm and kept in a humid chamber at 26°C for 2–4 h, or at 4°C overnight. After incubation, the slides were washed in ice-cold 1× PBS for 5 min. To prevent the dissociation of the RNP complex, post-fixation was performed with 4% formaldehyde in 1× PBS for 5 min on ice. Then, the slides were washed with 1× PBS for 5 min on ice and dehydrated in ethanol (70, 90, and 96%; 2 min each) at room temperature. Slides were embedded and counterstained with DAPI in Vectashield mounting medium (Vector Laboratories, Burlingame, CA, USA).

*Combination of RGEN-ISL and FISH*

After RGEN-ISL, the slides were fixed in 4% formaldehyde in 1× PBS for 5 min and treated with freshly prepared ethanol:glacial

acetic acid (3:1) at room temperature for 7 h in the dark. Then, the slides were dehydrated in an ethanol series (70, 90, and 96%; 2 min each) at room temperature. After brief drying, 15 µL of a prehybridization solution of DS20 (20% dextran sulfate [Sigma-Aldrich, cat. No. D8906], 50% deionized formamide [Sigma-Aldrich, cat. No. 4767], 300 mM NaCl, 30 mM tri-sodium citrate dehydrate, 50 mM phosphate buffer, pH 7.0) was applied per slide and covered with a 22 × 22 mm cover slip for overnight incubation at 37°C. The next day, coverslips were removed, and the slides were washed in 2× SSC with 0.1% Triton and 2× SSC at room temperature for 5 min each, and dehydrated in an ethanol series (70, 90, and 96%; 2 min each) at room temperature. After short drying, DNA was denatured in 0.2 N NaOH/70% ethanol at room temperature for 3 min and then dehydrated sequentially in an ethanol series. The hybridization solution consisting of 15 µL DS20 and 1 µL of probe specific for the 180-bp Knob 2 (oligo probe FAM-GAAGGCTAACACCTACGGATTTTTGACCAAGAAATGGTCTCCACCAGAAATCCAAAAAT [Zhu et al., 2017]) was denatured at 95°C for 5 min, immediately transferred on ice, and kept for 5 min. The hybridization mix was applied to the slide, covered with a coverslip, and hybridized overnight in a humid chamber at 37°C. The next day, slides were washed in 2× SSC with 0.1% Triton X-100 and 2× SSC at room temperature for 5 min each. Slides were dehydrated using the ethanol series and finally embedded and counterstained with DAPI in Vectashield mounting medium.

*Combination of DNA Replication Analysis and RGEN-ISL*

Roots of 3-day-old maize seedlings were incubated with 20 µM EdU solution (baseclick GmbH, cat. No. BCK-EdU647) in $ddH_2O$ (stock solution contains 10 mM EdU in DMSO) for 30 min at 28°C. Then, the roots were washed thoroughly in $H_2O$, and the nuclei were prepared as described for RGEN-ISL.

*Combination of DNA Replication Analysis, Immunostaining, and RGEN-ISL*

Slides carrying nuclei isolated from EdU-treated roots were washed for 5 min in ice-cold 1× PBS and incubated with 70 µL of primary antibodies per slide (1:100 dilution, anti-methylation H3K9me2 and H3K4me2 [Abcam, cat. No. Ab1220 and Ab7766]) at 4°C overnight in a humid chamber. The next day, the slides were washed twice for 5 min in 1× PBS, and then 100 µL of 1× Cas9 buffer per slide was used for equilibration for 2 min. After that, 25 µL of the RNP complex together with the secondary antibody anti-rabbit Alexa 488 (1:200 dilution; Jackson ImmunoResearch Laboratories, cat. No. 711-545-152) was applied per slide. First the RNP complex was prepared, afterwards the secondary antibodies were diluted in the RNP mix. Slides were covered with parafilm and incubated overnight at 4°C in a humid chamber. For the visualization of the EdU-incorporated DNA, the slides were washed in 1× PBS on a shaker (5 min; 100 rpm), and the freshly prepared EdU reaction cocktail (250 µL per slide) for detection was applied, covered with parafilm, and incubated for 30 min at 28°C in a humid chamber protected from light. After incubation, the reaction cocktail was removed, and the slides were washed for 5 min in 1× PBS on a shaker (100 rpm). Post-fixation was performed with 4% formaldehyde in 1× PBS for 5 min on ice. Then, the slides were washed in 1× PBS for 5 min on ice and dehydrated in ethanol (70, 90, 96%; 2 min each) at room temperature. The slides were embedded and counterstained with DAPI in Vectashield.

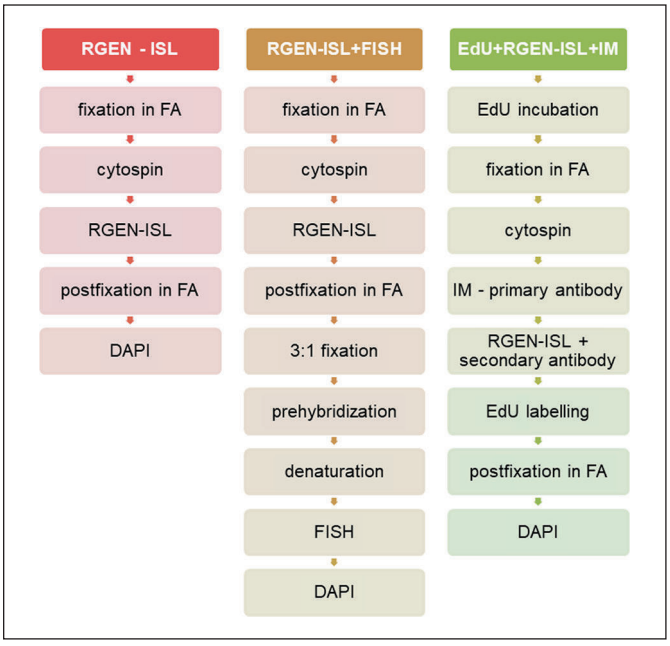


**Fig. 2.** Workflow of RGEN-ISL and its combination with FISH (RGEN-ISL + FISH) and with EdU-based DNA replication analysis and immunolabeling (EdU + RGEN-ISL + IM). FA, formaldehyde; IM, immunolabeling.

All protocols for RGEN-ISL and its combination with FISH (RGEN-ISL + FISH) and with EdU-based DNA replication analysis and immunolabeling (EdU + RGEN-ISL + IM) are summarized in Figure 2.

*Microscopy*

Widefield fluorescence imaging was performed using an Olympus BX61 microscope equipped with an ORCA-ER CCD camera (Hamamatsu). All images were acquired in grayscale and pseudocolored with Adobe Photoshop 6 (Adobe Systems). To analyze the ultrastructure and spatial arrangement of signals and chromatin at a lateral resolution of ~120 nm (super-resolution, achieved with a 488-nm laser), spatial structured illumination microscopy (3D-SIM) was applied using a Plan-Apochromat 63×/1.4 oil objective of an Elyra PS.1 microscope system and the software ZENblack (Carl Zeiss GmbH). Image stacks were captured separately for each fluorochrome using 561-, 488-, and 405-nm laser lines for excitation and appropriate emission filters. Maximum intensity projections were calculated based on 3D-SIM image stacks employing the ZENblack software [Weisshart et al., 2016].

## Results and Discussion

*RGEN-ISL and FISH Signals Differ at the Subchromosomal Level*

The 180-bp knob repeat of maize [Peacock et al., 1981; Ananiev et al., 1998] was used to compare the structure

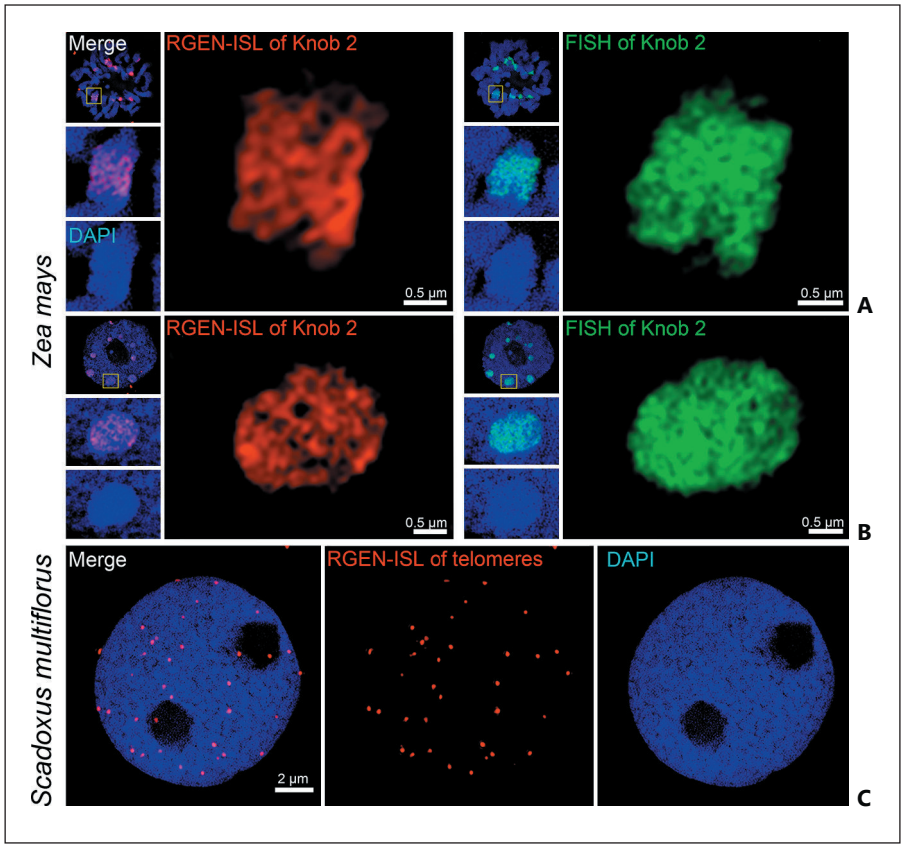


**Fig. 3.** Application of RGEN-ISL for the detection of high copy repeats. **A**, **B** Comparison of the chromatin ultrastructure after Knob 2-specific labeling by RGEN-ISL (red) and subsequent FISH (green) of fixed chromosomes (**A**) and interphase nuclei of maize (**B**). **C** Nucleus of *S. multiflorus* exhibiting vertebrate-specific telomere signals. To analyze the ultrastructure and spatial arrangement of signals and chromatin at a lateral resolution of ~140 nm, 3D structured illumination microscopy was applied. A higher resolution is achieved by FAM labeling (~120 nm).

of chromatin and fluorescence signals after applying the newly developed RGEN-ISL method and standard FISH. Specific gRNAs (Knob 1, Knob 2, Knob 3) which differ in GC content, PAM, melting temperature, and target copy number were designed (online suppl. Table 1). A positive correlation between signal intensity and reliability of designed probes and their copy number of target repeats was observed as the Knob 2-specific gRNA with the highest copy number resulted in the strongest signals (online suppl. Fig. 1). A negative correlation between RGEN-ISL signal intensity and the degree of chromatin structure preservation was found as previously noted by Ishii et al. [2019]. Fixation of leaf tissue in 2% formaldehyde resulted in the strongest RGEN-ISL signals, but the chromatin structure was of low quality. The opposite was observed using 4% formaldehyde-fixed nuclei. Application of 3% formaldehyde fixation in combination with a Knob 2-specific gRNA provided the most reliable result in all experiments (online suppl. Fig. 2).

To evaluate the influence of denaturation on the morphology of chromatin, non-denaturing RGEN-ISL was performed first and super-resolution microscopy (3D-SIM) images were acquired. Afterwards, the same specimen was used for standard FISH, recorded again, and the images were compared. The depicted overall morphology of chromosomes and nuclei was similar for both methods (Fig. 3A, B). However, the application of 3D-SIM revealed subtle differences. The width of chromosomes increased after standard FISH, and the chromosome structure labeled by DAPI was less defined (Fig. 3A). It seems that FISH, a method which is based on denaturation and acetic acid fixation, impaired and flattened the chromatin. In case of non-denaturing RGEN-ISL, the chromatin structure stays more compact. FISH-positive chromosome regions were about one fifth larger in total. Hence, RGEN-ISL is the method of choice for the visualization of repeats if the ultrastructure of chromatin is of interest.

*RGEN-ISL Enables the Detection of Vertebrate-Type Telomeres in* S. multiflorus

The chromosome termini of the blood lily *S. multiflorus* (2n = 18) are sealed by vertebrate-type $(TTAGGG)_n$ and not *Arabidopsis*-type $(TTTAGGG)_n$ telomere repeats [Monkheang et al., 2016]. To check whether a visualiza-

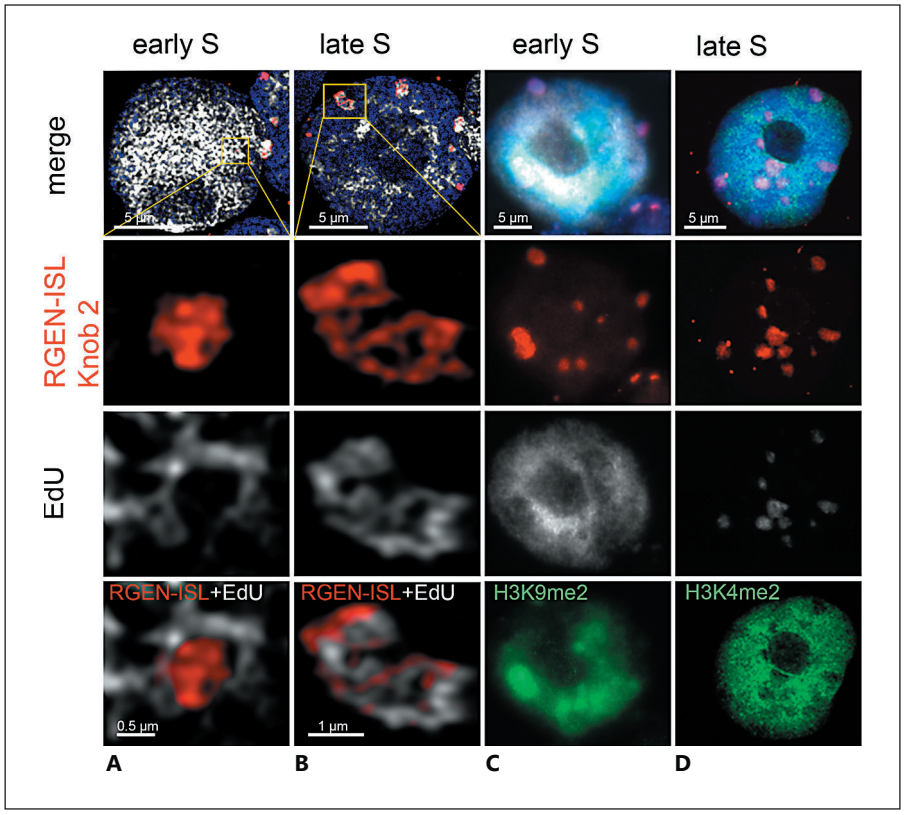


**Fig. 4.** RGEN-ISL in combination with EdU-based DNA replication analysis (EdU + RGEN-ISL) (**A**, **B**) and immunolabeling (EdU + RGEN-ISL + IM) (**C**, **D**) using maize nuclei. **A** The early replicating nucleus shows euchromatin labeling by EdU (white), whereas the Knob 2 repeats marked by RGEN-ISL (red) are not yet replicated. **B** The late replicating nucleus shows Knob 2 repeat-specific EdU labeling. **C** After triple staining of early S phase, the late replicating Knob 2 repeats are free of EdU, but stained by anti-histone H3K9me2. **D** During late S phase the late replicating Knob 2 repeats are EdU marked and free of anti-histone H3K4me2 signals. **A**, **B** 3D structured illumination microscopy. **C**, **D** Standard fluorescence microscopy.

tion of this repeat is possible by RGEN-ISL, *Arabidopsis* and vertebrate telomere-specific gRNAs were used. Telomere signals were only detected with the vertebrate telomere-specific gRNA (Fig. 3C; online suppl. Fig. 3). The RGEN-ISL resulted in 29.6 dot-like signals per nucleus ($n = 50$). A slightly higher number of telomere signals per nucleus (32.2) was found after standard FISH ($n = 50$). Hence, RGEN-ISL allows the differentiation between vertebrate-type $(TTAGGG)_n$ and *Arabidopsis*-type $(TTTAGGG)_n$ telomere repeats.

*Combination of RGEN-ISL and DNA Replication Analysis*

The combination of FISH and EdU-based DNA replication detection has been used to determine the replication timing of defined genomic sequences [Klemme et al., 2013]. To test whether RGEN-ISL could be used instead of FISH, maize roots were pulse-labeled with 20 µM EdU. After application of RGEN-ISL, the EdU click-reaction was performed without a negative effect on the RGEN-ISL signal intensity. Post-fixation with 4% formaldehyde before EdU labeling, reduced the EdU click-reaction efficiency and resulted in a weaker EdU signal. Therefore, the final post-fixation step should be done after both methods were employed. SIM shows clearly the overlap between the Knob 2 signals and EdU-labeled chromatin in the late phase of replication (Fig. 4B) and no colocalization during early replication (Fig. 4A). Using this fast, reproducible, and sensitive technique, we were able to deliver in only 1 week the same information as obtained after a laborious repli-Seq project in maize, in which it was shown that the Knob 180-bp repeat is replicated in late S phase [Wear et al., 2017].

*Combination of EdU-Based DNA Replication Analysis, RGEN-ISL, and Indirect Immunostaining*

Finally, we tested whether the combined EdU-based replication analysis and RGEN-ISL-based DNA detection could be linked with indirect immunolabeling to visualize the replication behavior of knob repeats and the distribution of post-translational histone marks simultaneously. Therefore, maize nuclei after EdU-pulse labeling were isolated, and RGEN-ISL was employed in combination with immunostaining. The triple combination resulted in knob-specific RGEN-ISL signals colocalizing with early and late replicating histone H3K9me2 and

H3K4me2 chromatin, respectively (Fig. 4C, D). It is possible that H3K9me2 contributes to the early replication of heterochromatin in maize. Contrary, H3K4me2 may have an opposite function H3K4me2 may have an opposite function in late replicating euchromatin. To conclude, a triple combination method under non-denaturing conditions for the simultaneous detection of specific DNA repeats, proteins, and DNA replication sites has been developed.


## Acknowledgements

We would like to thank Sylvia Swetik and Katrin Kumke (IPK Gatersleben, Germany) for technical assistance.


## Statement of Ethics

The authors have no ethical conflicts to disclose.

## Disclosure Statement

The authors have no conflicts of interest to declare.


## Funding Sources

This work was supported by the Czech Science Foundation, grant "Spatial and temporal characterisation of DNA replication in phylogenetically related plant species with contrasting genome sizes" (17-14048S), the ERASMUS+ student traineeship mobility program, and the DFG (Ho1779/28-1).


## Author Contributions

A.H. designed the experiments. A.N., C.W., and V.S. conducted the study and processed the data. A.N., C.W, and A.H. wrote the manuscript. A.N., C.W., V.S., T.I., E.H., and A.H. discussed the results and contributed to manuscript writing. All authors read and approved the final manuscript.

## References


Ananiev EV, Phillips RL, Rines HW: Complex structure of knob DNA on maize chromosome 9. Retrotransposon invasion into heterochromatin. Genetics 149: 2025–2037 (1998).

Anton T, Bultmann AS, Leonhardt H, Markaki Y: Visualization of specific DNA sequences in living mouse embryonic stem cells with a programmable fluorescent CRISPR/Cas system. Nucleus 5:163–172 (2014).

Chen B, Gilbert LA, Cimini BA, Schnitzbauer J, Zhang W, et al: Dynamic imaging of genomic loci in living human cells by an optimized CRISPR/Cas system. Cell 155:1479–1491 (2013).

Deng WL, Shi XH, Tjian R, Lionnet T, Singer RH: CASFISH: CRISPR/Cas9-mediated in situ labeling of genomic loci in fixed cells. Proc Natl Acad Sci USA 112:11870–11875 (2015).

Doležel J, Binarová P, Lucretti S: Analysis of nuclear DNA content in plant cells by flow-cytometry. Biol Plant 31:113–120 (1989).

Doležel J, Čihalíková J, Lucretti S: A high-yield procedure for isolation of metaphase chromosomes from root tips of *Vicia faba* L. Planta 188:93–98 (1992).

Dreissig S, Schiml S, Schindele P, Weiss O, Rutten T, et al: Live-cell CRISPR imaging in plants reveals dynamic telomere movements. Plant J 91:565–573 (2017).

Ishii T, Schubert V, Khosravi S, Dreissig S, Metje-Sprink J, et al: RNA-guided endonuclease – in situ labelling (RGEN-ISL): a fast CRISPR/Cas9-based method to label genomic sequences in various species. New Phytol 222: 1652–1661 (2019).

Klemme S, Banaei-Moghaddam AM, Macas J, Wicker T, Novak P, Houben A: High-copy sequences reveal distinct evolution of the rye B chromosome. New Phytol 199:550–558 (2013).

Monkheang P, Chaveerach A, Sudmoon R, Tanee T: Karyotypic features including organizations of the 5S, 45S rDNA loci and telomeres of *Scadoxus multiflorus* (Amaryllidaceae). Comp Cytogenet 10:637–646 (2016).

Peacock WJ, Dennis ES, Rhoades MM, Pryor AJ: Highly repeated DNA sequence limited to knob heterochromatin in maize. Proc Natl Acad Sci USA 78:4490–4494 (1981).

Wear EE, Song J, Zynda GJ, LeBlanc C, Lee TJ, et al: Genomic analysis of the DNA replication timing program during mitotic S phase in maize (*Zea mays*) root tips. Plant Cell 29: 2126–2149 (2017).

Weisshart K, Fuchs J, Schubert V: Structured illumination microscopy (SIM) and photoactivated localization microscopy (PALM) to analyze the abundance and distribution of RNA polymerase II molecules on flow-sorted *Arabidopsis* nuclei. Bio-protocol 6:e1725 (2016). http://www.bio-protocol.org/e1725

Zhu M, Du P, Zhuang L, Chu C, Zhao H, Qi Z: A simple and efficient non-denaturing FISH method for maize chromosome differentiation using single-strand oligonucleotide probes. Genome 60:657–664 (2017).

## APPENDIX II

# DNA replication and chromosome positioning throughout the interphase in three-dimensional space of plant nuclei

Němečková A, Koláčková V, Vrána J, Doležel J, Hřibová E

Journal of Experimental Botany, 2020

doi:10.1093/jxb/eraa370

IF: 5.908

*Journal of Experimental Botany*
doi:10.1093/jxb/eraa370 Advance Access Publication 17 August, 2020

RESEARCH PAPER

# DNA replication and chromosome positioning throughout the interphase in three-dimensional space of plant nuclei

**Alžběta Němečková, Veronika Koláčková, Jan Vrána, Jaroslav Doležel and Eva Hřibová*,**

Institute of Experimental Botany of the Czech Academy of Sciences, Centre of the Region Haná for Biotechnological and Agricultural Research, Olomouc, Czech Republic

* Correspondence: hribova@ueb.cas.cz

Received 2 April 2020; Editorial decision 24 July 2020; Accepted 31 July 2020

Editor: Frank Wellmer, Trinity College Dublin, Ireland

## Abstract

**Despite much recent progress, our understanding of the principles of plant genome organization and its dynamics in three-dimensional space of interphase nuclei remains surprisingly limited. Notably, it is not clear how these processes could be affected by the size of a plant's nuclear genome. In this study, DNA replication timing and interphase chromosome positioning were analyzed in seven *Poaceae* species that differ in their genome size. To provide a comprehensive picture, a suite of advanced, complementary methods was used: labeling of newly replicated DNA by ethynyl-2'-deoxyuridine, isolation of nuclei at particular cell cycle phases by flow cytometric sorting, three-dimensional immunofluorescence *in situ* hybridization, and confocal microscopy. Our results revealed conserved dynamics of DNA replication in all species, and a similar replication timing order for telomeres and centromeres, as well as for euchromatin and heterochromatin regions, irrespective of genome size. Moreover, stable chromosome positioning was observed while transitioning through different stages of interphase. These findings expand upon earlier studies in suggesting that a more complex interplay exists between genome size, organization of repetitive DNA sequences along chromosomes, and higher order chromatin structure and its maintenance in interphase, albeit controlled by currently unknown factors.**

**Keywords:** DNA replication, EdU labeling, flow cytometry, *Poaceae*, Rabl configuration, S phase, three-dimensional fluorescence *in situ* hybridization (3D-FISH).

## Introduction

One of the exciting features of eukaryotic genomes is the organization in three-dimensional (3D) space of cell nuclei and spatial changes in genome organization during the cell cycle. The chromatin arrangement and positioning of individual chromosomes in interphase nuclei was a great enigma until recently. Nevertheless, already in 1885, based on microscopic observations of dividing cells of *Salamandra maculata* and *Proteus anguinus*, Carl Rabl had predicted that chromosome positioning in interphase nuclei follows their orientation in the preceding mitosis (reviewed by Cremer *et al.*, 2006). His hypothesis was later confirmed by cytogenetic studies in humans, animals, as well as in some plants

Abbreviations: 3C, chromosome confirmation capture; 3D, three-dimensional; EdU, 5-ethynyl-2'-deoxyuridine; FISH, fluorescence *in situ* hybridization; Hi-C, chromosome confirmation base mapping; PAA, polyacrylamide; ROI, region of interest; TAD, topologically associating domain.

with larger chromosomes, which shed more light on the clustering of centromeric and telomeric regions at opposite poles of interphase nuclei (Cremer *et al.*, 1982; Schwarzacher and Heslop-Harrison, 1991; Werner *et al.*, 1992). This chromosome arrangement was accordingly dubbed the Rabl configuration. Yet a different interphase chromosome arrangement was observed in the model plant *Arabidopsis thaliana*, which has a small genome (1C ~157 Mb), for which the centromeres are located at the nuclear periphery but the telomeres congregate around the nucleolus (Armstrong *et al.*, 2001; Fransz *et al.*, 2002). Centromeric heterochromatin forms dense bodies, called chromocenters, while euchromatin domains form 0.2–2 Mb loops that are organized into rosette-like structures (Fransz *et al.*, 2002; Pecinka *et al.*, 2004; Tiang *et al.*, 2012; Schubert *et al.*, 2014). Nonetheless, despite this difference, chromosomes also preferentially occupy distinct regions (chromosome territories) in plant species.

According to several studies, chromatin arrangement in interphase nuclei of wheat (*Triticum aestivum*), oat (*Avena sativa*), and rice (*Oryza sativa*), and in particular their centromere–telomere orientation, may be tissue specific and cell cycle dependent (Dong and Jiang, 1998; Prieto *et al.*, 2004; Santos and Show, 2004). While a majority of nuclei in somatic cells of rice, a species with a small genome (1C ~490 Mb, Bennett *et al.*, 1976), do lack Rabl configuration, in some tissues, such as pre-meiotic cells in anthers or xylem precursor cells, rice chromosomes seem to assume the Rabl configuration (Prieto *et al.*, 2004; Santos and Show, 2004). Chromosome arrangement following the Rabl configuration and orientation in somatic cell nuclei was also observed in other plants whose genomes are small, including *Brachypodium distachyon* (1C ~355 Mb) (Idziak *et al.*, 2015). However, according to Catalán *et al.* (2012), the majority of cell types in *B. stacei* and *B. hybridum*, which also have small genomes (1C ~276 Mb and 1C ~619 Mb, respectively), did not show the Rabl configuration; however, Idziak *et al.* (2015) observed the Rabl configuration in 13% and 17% of root meristem cells in *B. stacei* and *B. hybridum*, respectively. Interestingly, the Rabl configuration has not been found in plants with medium-size genomes, such as tomato (*Solanum tuberosum*, 1C ~900 Mb), and in plants with large genomes, such as onion (*Allium cepa*, 1C ~17 Gb), field bean (*Vicia faba*, 1C ~15 Gb), and pea (*Pisum sativum*, 1C ~4.4 Gb) (Rawlins *et al.*, 1991; Fussell, 1992; Harrison and Heslop-Harrison, 1995; Kamm *et al.*, 1995).

The development of the 3D fluorescence *in situ* hybridization (3D-FISH) method has provided an opportunity to map spatial telomere positions at the prophase stage of meiosis in maize (*Zea mays*; Bass *et al.*, 1997), in addition to *A. thaliana* and an oat addition line containing maize chromosome 9 (Howe *et al.*, 2013). To characterize changes in chromosome positioning in 3D nuclear space throughout interphase, cell nuclei at a particular cell cycle phase can be isolated using flow cytometry. Embedding these flow-sorted nuclei in a polyacrylamide (PAA) gel stabilizes their structure during the 3D-FISH procedure so 3D images of them can be taken by confocal microscopy (Kotogány *et al.*, 2010; Hayashi *et al.*, 2013; Bass *et al.*, 2014; Koláčková *et al.*, 2019).

The chromosome conformation capture (3C) technique (Dekker 2002), and its variants, has enabled the study of spatial chromatin organization in cell nuclei at a higher resolution than via FISH. The so-called Hi-C method (Lieberman-Aiden *et al.*, 2009) can be used to analyze contacts between DNA loci across the whole genome; hence, the contact maps thus obtained describe chromosome contact patterns, genome packing, and 3D chromatin architecture (Dong *et al.*, 2018; Kempfer and Pombo, 2019). Although Hi-C identifies genome loci that are associated in 3D space, it does not provide information on their physical position in nuclei.

The results of 3C techniques have confirmed chromatin's organization into domains containing either active and open chromatin (A compartments), or inactive and closed chromatin (B compartments) (Lieberman-Aiden *et al.*, 2009). In metazoans, these compartments are organized into smaller, self-interacting domains called topologically associated domains (TADs) (Sexton and Cavalli, 2015; Dixon *et al.*, 2016; Sotelo-Silveira *et al.*, 2018). TADs are regulatory landscapes of chromosomes and contain genes that tend to be co-regulated during the cell differentiation process (Dixon *et al.*, 2016, Ramírez *et al.*, 2018; Szabo *et al.*, 2018). Borders of TADs correspond to DNA replication domains (Pope *et al.*, 2014) and may serve as physical barriers to spread activity within the genome (reviewed by Dixon *et al.*, 2016). Recently, Golicz *et al.* (2020) reported association of TADs with differences in transposable element composition, single nucleotide polymorphism (SNP) accumulation, and increased incidence of meiotic crossovers in rice. Despite mounting 3C studies, the evolution of TADs and their function in eukaryotes are still unresolved (Liu *et al.*, 2017; Concia *et al.*, 2020; Golicz *et al.*, 2020). In plants, TADs were not observed in *A. thaliana* (Feng *et al.*, 2014; Wang *et al.*, 2015; Liu *et al.*, 2016), and their presence seems instead to be linked to species with larger genomes (Dong *et al.*, 2017; Liu *et al.*, 2017; Concia *et al.*, 2020; Golicz *et al.*, 2020).

In the majority of cases, spatial chromatin organization in interphase nuclei as revealed by FISH corresponds to the results obtained by Hi-C (Sexton *et al.*, 2012; Dong *et al.*, 2017; Liu *et al.*, 2017; Mascher *et al.*, 2017). The only exception we know of is *A. thaliana*, for which the Hi-C analysis failed to confirm the rosette-like organization of its chromosomal domains. According to the Hi-C approach, telomeres of different chromosomes should cluster, but FISH studies show telomeres surrounding the nucleolus (Feng *et al.*, 2014; Liu and Weigel, 2015).

Several investigations have focused on the organization of chromatin, and its structure and changes during the cell cycle. In mammals, DNA sequences located at interior regions of nuclei undergo replication earlier, while late replication occurs mostly at the nuclear periphery (Gilbert *et al.*, 2010; Bryant and Aves, 2011). Cell cycle kinetics and the progression of cells through the S phase can now be followed in detail, after labeling newly synthesized DNA with a thymidine analog, 5-ethynyl-2'-deoxyuridine (EdU), and conducting bivariate flow cytometric analysis of nuclear DNA content and the amount of incorporated EdU (Mickelson-Young *et al.*, 2016). Such EdU-labeled nuclei can be flow-sorted onto microscope slides and used as templates for FISH, to analyze the replication timing of particular DNA sequences and their positioning in 3D nuclear space (Hayashi *et al.*, 2013; Bass *et al.*, 2014, 2015; Dvořáčková *et al.*, 2018).

DNA replication dynamics were analyzed in detail by microscopy for several plant species, including the monocot species maize and barley (*Hordeum vulgare*) and two dicots, *A. thaliana* and *V. faba* (Jasencakova *et al.*, 2001; Bass *et al.*, 2014; Jacob *et al.*, 2014; Robledillo *et al.*, 2018). In general, different stages of S phase had contrasting DNA replication patterns. The early S phase was characterized by weakly dispersed EdU signals, yet speckled EdU signals were typical for the late S phase, whereas the nuclei in the middle of the S phase were all covered with EdU signals, except for the nucleolar area (Jasencakova *et al.*, 2001; Kotogány *et al.*, 2010; Bass *et al.*, 2014, 2015). Using 3D microscopy to analyze DNA replication dynamics in root meristem cells of maize, Bass *et al.* (2015) described distinct patterns of EdU signal distribution during early and middle S phase. In the former, DNA replication primarily occurred in regions characterized by weak fluorescence of the DNA fluorochrome DAPI; in the latter, it was correlated with strong DAPI signals. Those authors also found that knob regions and centromeric regions associated with heterochromatin were replicated during the late S phase. Based on their results, they proposed a 'mini-domain model', describing how gene islands are replicated in the early S phase, and blocks of repetitive DNA in the middle S phase (Bass *et al.*, 2015).

Interestingly, the dynamics of interphase chromosome positioning during the cell cycle have yet to be studied in plants. To fill this knowledge gap, here we characterized chromosome positioning in 3D nuclear space during the cell cycle and followed DNA replication in centromeric and telomeric regions of grass plants. We examined interphase nuclei of root meristem cells in seven *Poaceae* species differing in nuclear genome size. We labeled newly synthesized DNA by EdU, monitored cell cycle kinetics by flow cytometry, and performed 3D immuno-FISH on flow-sorted nuclei. Chromosome positioning was analyzed in interphase nuclei of root meristem cells in the same *Poaceae* spp. Confocal microscopy of nuclei embedded in a PAA gel allowed us to locate centromeres and telomeres in 3D space and to analyze the replication timing of these chromosome regions. Our results provide new information on chromosome positioning and spatiotemporal patterning of DNA replication of key chromosome domains in plants.

## Material and methods

### *Plant material and germination of seeds*

Plants used included wheat (*Triticum aestivum* L.) cultivar 'Chinese Spring' ($2n=2x=42$), oat (*Avena sativa* L.) cultivar Atego ($2n=2x=42$), barley (*Hordeum vulgare* L.) cultivar 'Morex' ($2n=2x=14$), rye (*Secale cereale* L.) cultivar 'Dánkowskie Diament' ($2n=2x=14$), rice (*Oryza sativa* L.) cultivar 'Nipponbare' ($2n=2x=24$), maize (*Zea mays* L.) line 'B73' ($2n=2x=20$), and *Brachypodium distachyon* L. cultivar 'Bd21' ($2n=2x=10$). All seeds were obtained from the Leibniz Institute of Plant Genetics and Crop Plant Research Genebank (IPK Gaterleben, Germany) except for rice, kindly provided by Professor Takashi Ryu Endo (Kyoto University, Kyoto, Japan), and also wheat, obtained from the Wheat Genetics & Genomic Resources Center (Kansas State University, Manhattan, KS, USA). All seeds were germinated in the dark in a biological incubator at 24 °C, in glass Petri dishes on moistened filter paper, until their primary roots had reached 2.5–4 cm in length.

### *EdU labeling of replicating DNA*

Young seedlings were incubated in 20 μM EdU (Click-iT™ EdU Alexa Fluor™ 488 Flow Cytometry Assay Kit, ThermoFisher Scientific/Invitrogen, Waltham, MA, USA) mixed in $ddH_2O$, for 30 min, at 24 °C. Root tips were excised and fixed in 2% (v/v) formaldehyde in Tris buffer (10 mM Tris, 10 mM $Na_2EDTA$, 100 mM NaCl, 0.1% Triton X-100, pH 7.5) for 20 min at 4 °C, and washed three times in Tris buffer at 4 °C (Doležel *et al.*, 1992). Approximately10 root tips incorporated with EdU were treated with a 0.5 ml Click-iT reaction cocktail (Click-iT™ EdU Alexa Fluor™ 488 Flow Cytometry Assay Kit, ThermoFisher Scientific/Invitrogen), prepared according to the manufacturer's instructions, and incubated for 10 min in a vacuum, followed by their incubation in the dark for 45 min at room temperature. After this labeling, roots were washed three times for 5 min in phosphate-buffered saline (PBS; 10 mM $Na_2HPO_4$, 2 mM $KH_2PO_4$, 137 mM NaCl, 2.7 mM KCl, pH 7.4), on a rotating shaker (160 rpm) at room temperature.

The root tips were mounted in 0.1% agarose (mixed in $ddH_2O$) onto cavity microscopic slides (Paul Marienfeld GmbH & Co. KG, Lauda-Königshofen, Germany) and mounted in Vectashield supplemented with DAPI (Vector Laboratories, Ltd, Peterborough, UK) to stain their chromosomal DNA. These preparations were imaged using a Leica TCS SP8 STED 3X confocal microscope (Leica Microsystems, Wetzlar, Germany), with a ×10/0.4 NA Plan-Apochromat objective (*z*-stacks, pinhole Airy). Image stacks were captured separately for DAPI, using a 405 nm laser, and for the EdU-labeled samples by Alexa Fluor 488, using a 488 nm laser and appropriate optical filters. Typically, image stacks of 36 slides, on average, with 138 μm spacing were acquired. Next, maximum intensity projections were carried out using Leica LAS-X software, with final image processing done in Adobe Photoshop version 6.0 (Adobe Systems Corporation, San Jose, CA, USA).

### *Sorting of nuclei by flow cytometry*

Suspensions of intact nuclei were prepared, according to Doležel *et al.* (1992), from roots of young seedlings in which replicating DNA had been labeled by EdU (as described above). Briefly, ~1 cm long root tips were cut and fixed with 2% (v/v) formaldehyde made in Tris buffer at 4 °C, and washed three times with Tris buffer at 4 °C. Meristematic parts of root tips (~1 mm long) were excised from 70 roots per sample in barley, oat, wheat, and rye, and from 100 roots in rice and *Brachypodium* (see Supplementary Table S1 at *JXB* online). Root meristems were homogenized in 500 μl of LB01 buffer (Doležel *et al.*, 1989), using a Polytron PT 1200 homogenizer (Kinematica AG, Littua, Switzeland), for 13 s at 10 000–24 000 rpm depending on the species (Supplementary Table S1). For maize, 50 root meristems were chopped using a razor blade, following Doležel *et al.* (1989). Each crude homogenate was passed through a 50 μm nylon mesh and its nuclei were pelleted at 500 *g*, at 4 °C for 10 min. The resulting pellet was resuspended in 0.5 ml of Click-iT reaction cocktail, prepared according to the manufacturer's instructions, and the nuclei were incubated in the dark at 24 °C for 30 min. Then, the nuclei were pelleted again, at 500 *g*, for 10 min, resuspended in 500 μl of LB01 buffer, and stained by DAPI (0.2 μg $ml^{-1}$ final concentration). Finally, the suspensions of nuclei were filtered through a 20 μm nylon mesh and analyzed with a FASCAria II SORP flow cytometer and sorter (BD Bioscience, San Jose, CA, USA) equipped with UV (355 nm) and blue (488 nm) lasers. Nuclei representing different phases of the cell cycle were sorted into 1× meiocyte buffer A (1× buffer A salts, 0.32 M sorbitol, 1× DTT, 1× polyamines) (Bass *et al.*, 1997; Howe *et al.*, 2013).

### *Mounting of nuclei in a polyacrylamide gel*

Flow-sorted nuclei were mounted in a 5% PAA gel, as described by Howe *et al.* (2013) and Bass *et al.* (1997), with minor modifications. Briefly, 500 μl of PAA mix containing 15% (w/v) acrylamide/bisacrylamide (akrylamid/bisakrylamid 30% NF ROTIPHORESE (29:1) Roche Applied Science, Penzberg, Germany), 1× Buffer A salts (10× buffer contained 800 mM KCl, 200 mM NaCl, 150 mM PIPES, 20 mM EGTA, 5 mM EDTA, 1 M NaOH, pH 6.8), 1× polyamines (1000× polyamines contained 0.15 M spermine and 0.5 M spermidine), 1× DTT (1000×

DTT contained 1.0 M DTT, 0.01 M NaOAc), 0.32 M sorbitol, and 99 µl of $ddH_2O$ were rapidly combined with 25 µl of freshly prepared 20% ammonium sulfate in $ddH_2O$ and 25 µl of 20% sodium sulfate (anhydrous) in $ddH_2O$. One volume of activated PAA gel mix was mixed with two volumes of flow-sorted nuclei, on a microscopic slide coated with aminoalkylsilane (Sigma-Aldrich, Darmstadt, Germany), and then gently stirred with the pipette tip. The PAA mix was covered with a clean, glass coverslip and allowed to polymerize at 37 °C for ~40 min. The coverslip was removed and silane-coated slides with an acrylamide pad were washed three times, with 1× MBA in a Coplin jar, to remove any non-polymerized acrylamide.

### *Immunostaining and fluorescence in situ hybridization*

To visualize the centromeric regions, slides with the PAA pad were washed in a blocking buffer (phosphate buffer, 1% Triton X-100, 1 mM EDTA) at room temperature for 1 h, after which 100 µl of blocking buffer was added to each slide and it was covered with parafilm for 10 min. Next, 50 µl of diluted anti-OsCenH3 primary antibody (1:100) (Nagaki *et al.*, 2004) was added, covered with parafilm, and incubated at 4 °C in a humid chamber for 12 h. All the slides were then washed in a wash buffer (phosphate buffer, 0.1% Tween, 1 mM EDTA), three times for 15 min and once for 10 min in 2× SSC buffer (2× SSC), and then fixed in 1% (v/v) formaldehyde in 2× SSC for 30 min at room tem perature. After this fixation, each slide was washed three times for 15 min in 2× SSC at room temperature and used for the FISH.

A hybridization mix (35 µl), containing 50% formamide, 2× SSC, and 400 ng of directly labeled telomere oligo-probe $[CCCTAAA]_4$, was added onto a slide with a PAA pad and covered by a glass coverslip. The slides were denatured at 94 °C for 6 min and incubated overnight in a humid chamber at 37 °C. Post-hybridization washing steps consisted of a 5 min wash in 2× SSC; stringent washes of 2× 15 min in 0.1×SSC at 37 °C; then 2× 15 min in 2× SSC at 37 °C, followed by 2× 15 min 2× SSC at room temeperature, and, finally, 1× 15 min in 4× SSC at room temeperature. After completing these washing steps, 100 µl of fluorescently labeled secondary antibody (anti-rabbit Alexa Fluor 546, ThermoFisher Scientific/Invitrogen) diluted 1:250 in blocking buffer (5% BSA with 0.1% Tween dissolved in phosphate buffer) was added to each slide; this was then covered with parafilm and incubated at 37 °C for 3 h. Finally, the preparation was washed in 4× SSC (3× 15 min, room temeperature) and in phosphate buffer (3× 15 min, room temeperature). The PAA pad was mounted in 30 µl of Vectashield with DAPI (Vector Laboratories), covered with a glass coverslip, and sealed with nail polish.

### *Confocal microscopy and image analysis*

Images were acquired using a Leica TCS SP8 STED 3X confocal microscope (Leica Microsystems), equipped with a ×63/1.4 NA Oil Plan-Apochromat objective (*z*-stacks, pinhole Airy) and Leica LAS-X software that included the Leica Lightning module. Image stacks were captured separately for each fluorochrome, by using 647, 561, 488, and 405 nm laser lines for excitation and appropriate emission filters. Typically, image stacks of 100 slides, on average, with 0.2 µm spacing were acquired. The 3D modeling of microscopic images, co-localization analysis, and volume calculations were performed in the Imaris 9.2 software program (Bitplane, Oxford Instruments, Zurich, Switzerland). To estimate co-localization signals, the program's 'Colocalization' function based on Pearson's correlation coefficient was used (Manders *et al.*, 1992). The region of interest (ROI) was individually determined for each nucleus, and likewise for each channel. Importantly, setting the ROI ensures a 'layer by layer' correlation, thus preventing the negative co-localization of the green channel of EdU signals representing another layer. The EdU signals and the volume of each nucleus were both determined based on the primary intensity of fluorophores obtained after the microscopic analysis. The Imaris program's functions 'Surface' and 'Spot detection' were used for modeling the centromere–telomere arrangements; the channel contrast was adjusted using its 'Channel Adjustment' and videos were created using its 'Animation function'. Between 100 and 150 nuclei of each plant species were analyzed.

## Results

Since we studied plant species differing in genome size and root morphology, our experimental protocols had to be individually optimized. While the EdU concentration and incubation times were the same for all seven species, microscopic analysis of their root tips after EdU labeling revealed differences in meristematic zones (Fig. 1). This information proved useful for excising meristematic regions when preparing suspensions of meristem cell nuclei. Another critical step in preparing suspensions of nuclei was the extent of mechanical homogenization applied, which affected both the integrity and yield of nuclei per species (Supplementary Table S1). The thick maize roots were chopped with a razor blade in a nuclei isolation buffer, to obtain sufficient amounts of nuclei suitable for flow cytometry.

DNA replication kinetics in interphase nuclei of root tip meristems during the cell cycle were evaluated after EdU incorporation into replicating DNA. Bivariate flow cytometric analysis of EdU versus DAPI fluorescence resulted in typical 'horseshoe' dot plot patterns (Bass *et al.*, 2014; Hřibová *et al.*, 2016), making it possible to unambiguously distinguish the nuclei at $G_1$ and $G_2$ phases of the cell cycle as well as those in early, middle, and late S phase (Fig. 2). Fluorescent detection

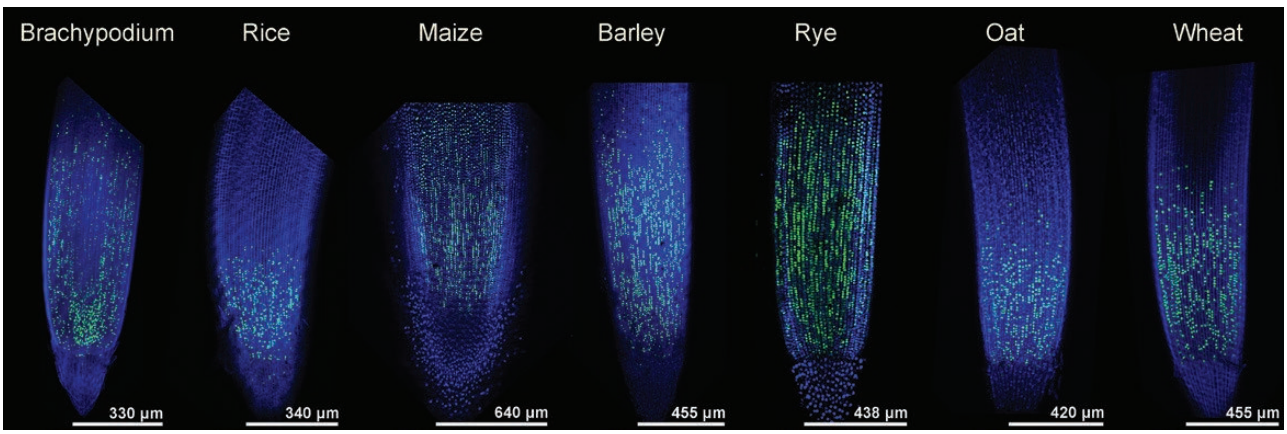


**Fig. 1.** Meristem zones in root tips of seven *Poaceae* species. Roots were incubated with 20 mM EdU for 30 min and the EdU incorporated into replicating DNA was detected by Alexa Fluor 488 (in green). Nuclei were stained with DAPI (blue).

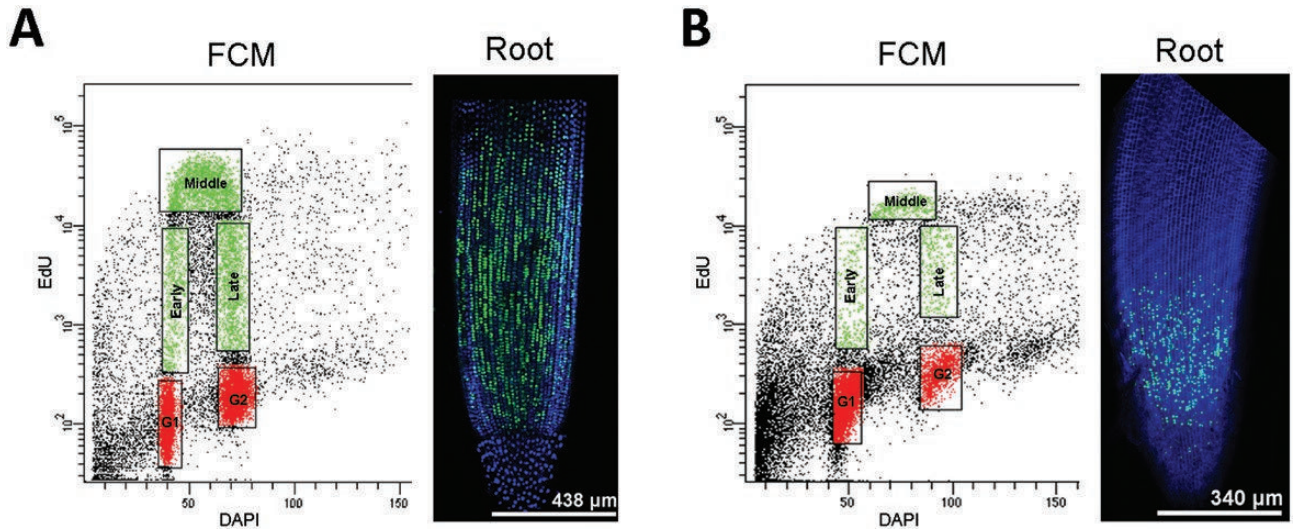


**Fig. 2.** Bivariate, flow cytometric analysis of the cell cycle in rye (A) and rice (B). Roots of young seedlings were incubated with 20 mM EdU for 30 min. EdU in isolated nuclei was detected by Alexa Fluor 488 (in green) and their DNA stained with DAPI (blue). The *x*-axis represents relative DNA content, estimated as the intensity of DAPI fluorescence (linear scale); the *y*-axis shows the extent of EdU incorporation into newly synthesized DNA, quantified by Alexa Fluor 488 fluorescence intensity (log scale). Red boxes in the dot plot show $G_1$ and $G_2$ phase nuclei; green boxes highlight the early, middle, and late S phase nuclei.

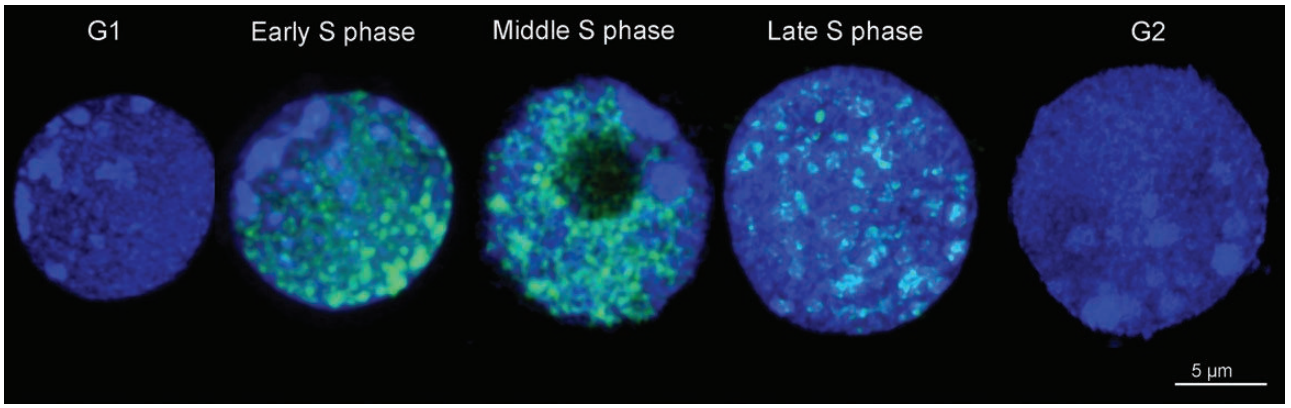


**Fig. 3.** Maximum intensity projection of rye nuclei, in 3D, in different phases of the cell cycle. EdU (in green) was incorporated during a 30 min pulse into newly synthesized DNA. The $G_1$ and $G_2$ phases lacked the green signals of EdU. Changes in DNA replication pattern during early, middle, and late S phase are clearly visible. Note the replication of heterochromatin regions. DNA was stained by DAPI (blue).

of incorporated EdU was useful, not only for flow cytometric analysis and nuclei sorting, but also for microscopy.

### *DNA replication kinetics*

Microscopic analysis of EdU fluorescence in cell nuclei revealed differential replication, such that the early, middle, and late S phase had unique patterns. Weak, discrete signals were typical for the early DNA replication stage, while speckled signals concentrated in particular areas were characteristic of late DNA replication stages. Strong signals dispersed throughout the whole nucleus were observed for the middle S phase (Fig. 3). Overlapping heterochromatin regions and EdU signals in the late S phase indicated that these regions underwent replication later than did euchromatin. EdU signals were also detected inside nucleoli, as discrete and clearly visible spots during both the early and middle S phase. Clear signals were also seen at the periphery of nucleoli in middle and late S phase (Supplementary Fig. S1), suggesting the replication of 45S rDNA loci.

### *Replication timing of centromeric and telomeric regions*

The time at which the centromeric and telomeric regions underwent replication was determined following the microcopy of nuclei at different S phase stages and based on whether EdU overlapped with immunofluorescent signals in centromeric regions and FISH signals in telomeric regions (Fig. 4). Although the replication of centromeric regions was initiated in early S phase, the highest number of centromeric regions underwent replication during middle and late S phase (Figs 4, 5; Supplementary Figs S2–S4). In contrast, prevailing replication of telomeric sequences was observed during both the early and middle S phase. Crucially, this replication pattern of both chromosome domains was seen in all species (Figs 4, 5; Supplementary Figs S4, S5, S7), except rye, for which a minor

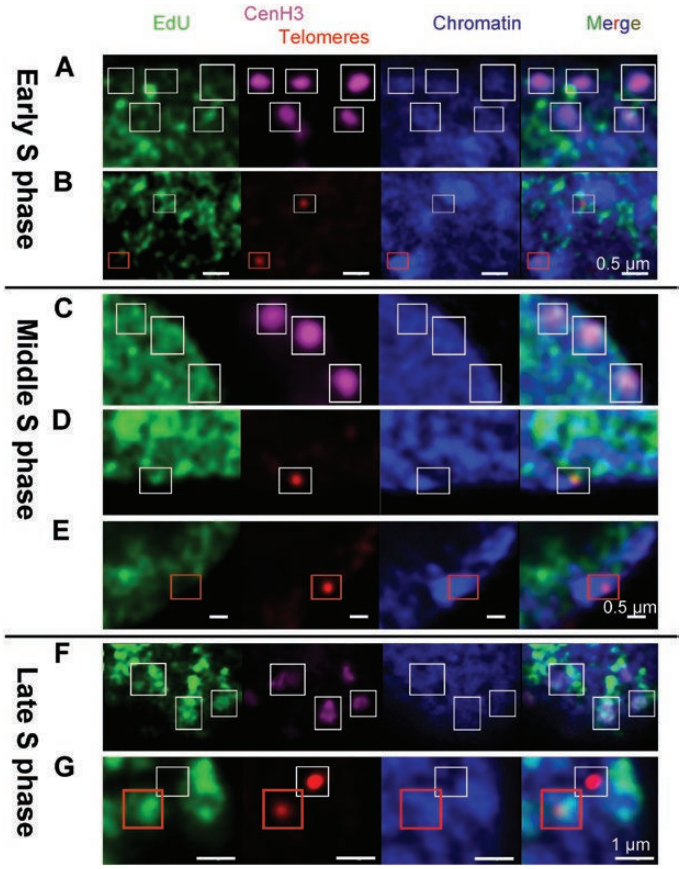


**Fig. 4.** DNA replication in rye nuclei and replication timing of centromeric and telomeric sequences. Co-localization of signals specific to telomeres (in red) and centromeres (pink), with EdU signals corresponding to the replicated DNA (green), was used to describe the pattern of replication timing. In early S phase, centromeric signals (A) as well as telomeric signals, which are connected with heterochromatin regions (B, red rectangle), did not co-localize with EdU. Those telomeric sequences not localized in heterochromatin (B, white rectangle) co-localized with EdU signals, pointing to an ongoing replication process. Co-localization of EdU and centromeric signals is visible in both the middle and late S phase (C, F). Similarly, telomeric sequences attached to heterochromatin regions (red rectangle) co-localized with EdU in middle and late S phase (E, G).

difference was observed in the replication dynamics of its telomeric sequences. Telomeric regions of rye comprise large heterochromatic blocks (Appels *et al.*, 1978; Evtushenko *et al.*, 2016) and, as our results showed, those DNA loci closely connected to a given heterochromatic block (probably flanking regions) were replicated in late S phase, whereas those telomeres situated apart from heterochromatin were replicated earlier, during the middle S phase (Fig. 4B, D, E).

Differentially phasing centromere and telomere replication influenced the overall replication pattern of S phase nuclei, as revealed by EdU (Supplementary Videos S1–S3. The first replication signals observed in nuclei were concentrated at telomeric regions, while the opposite pole of the nucleus where centromeres were localized lacked any EdU signals. By way of analogy, heterochromatin blocks and regions around centromeres replicated during late S phase, whereas the telomeres at the opposite pole of nuclei lacked the replication signals. A majority of nuclear DNA underwent replication during the middle S phase, generating strong EdU signals that spread throughout the whole nuclear volume (Supplementary Videos S4–S6). The images captured of rye are shown in Fig. 4, and Supplementary Figs S2–S7 show those of the remaining six species. The analysis of FISH signals (Fig. 5) showed that co-localization between EdU and centromere fluorescence channels increased from early S phase to middle and late S phase.

### *Chromosome positioning in interphase nuclei*

Localization of centromeres and telomeres during the course of S phase was used to infer chromosome positioning in interphase nuclei. In total, we analyzed 700 nuclei (100 nuclei per species) having spherical shapes, which are typical for the meristem cells of root tips. We confirmed the regular Rabl configuration, when centromeres and telomeres localize at opposite nuclear poles, in the large genomes of wheat, oat, rye, and barley, as well as in *B. distachyon* that has a small genome. In contrast, the chromosomes of rice, with a small genome, and maize, with a relatively large genome, did not assume the proper Rabl configuration (Fig. 6). In all species, their chromosomal arrangements were stable throughout interphase (Fig. 7; Supplementary Fig. S8; Supplementary Videos S1–12).

For the majority of species, the number of fluorescence signals from centromeres and telomeres corresponded to their number of mitotic chromosomes. The only exception was rice, wherein the Rabl configuration was not observed. Here, the telomeric and centromeric signals constituted large, clustered signals randomly distributed in the nucleoplasm (Fig. 6; Supplementary Videos S7–S9). In maize, the centromeres clustered in one region of the nuclei, but the telomeres were randomly dispersed throughout the nucleoplasm (Fig. 6; Supplementary Videos S10–S12).

## Discussion

Mounting evidence suggests a role for spatial chromatin positioning within cell nuclei in gene regulation, an organism's development and growth, and its response to external signals (Lipps *et al.*, 2010; Bonev and Cavalli, 2016; Drinnenberg *et al.*, 2019; Finn and Misteli, 2019). This has spurred interest in better understanding the principles of 3D genome organization, and its dynamics and functional significance. Most studies performed to date were done in humans and some animals, providing a coherent picture of hierarchical folding steps, ranging from nucleosomes to chromosome territories (Bouwman and Laat, 2015; Kempfer and Pombo, 2019). However, the efforts to confirm the functional significance of individual folding steps and chromatin conformation, such as the chromatin loops and TADs, have so far yielded ambiguous results (Dumur *et al.*, 2019). One approach to reveal conserved principles of nuclear organization is to compare the spatial genome organization across metazoan domains. Higher plants offer attractive targets, since they are evolutionarily distant from animals, yet preserve the basic structural features of eukaryotic cell nuclei. Moreover, they exhibit a wide range of genome sizes and ploidy levels (Pellicer and Leitch, 2020).

Research findings in plants suggest the absence of A and B chromatin compartments and a lack of insulator proteins

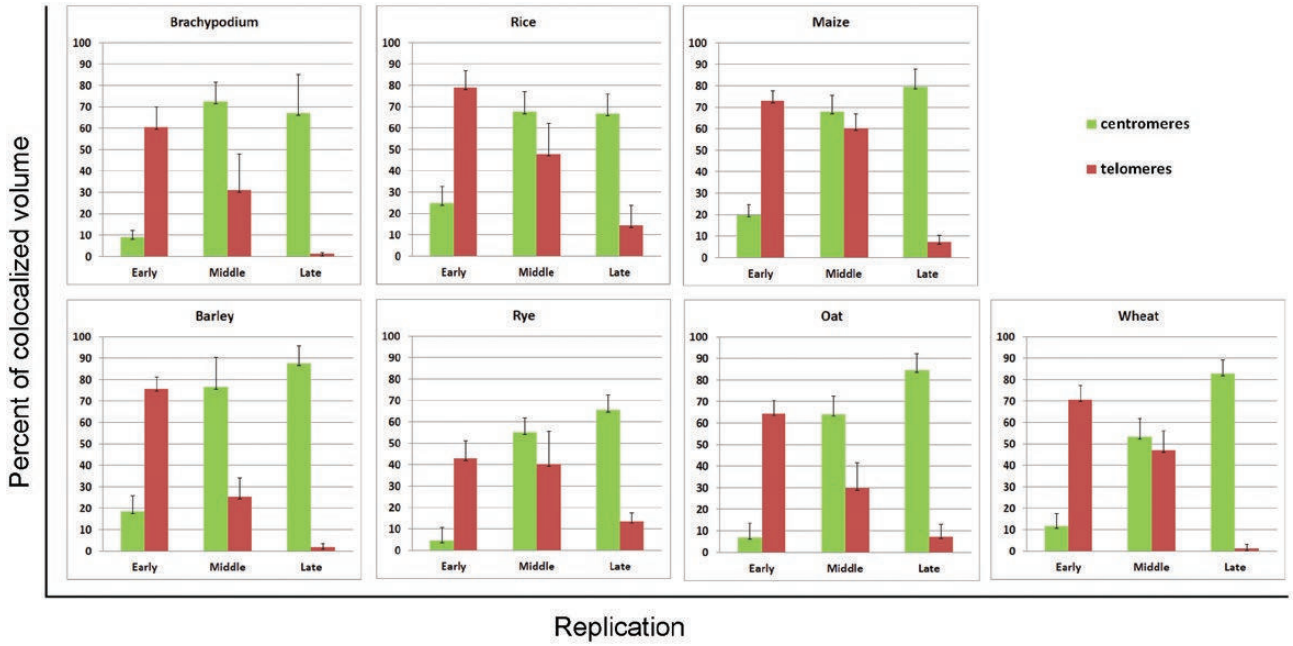


**Fig. 5.** Replication timing of centromeric and telomeric sequences. Replication timing was obtained after the co-localization analysis and volume calculations of 3D models of microscopic images (obtained by Imaris 9.2 software). The columns represent the percentage of co-localized volume of signals from telomeric and centromeric regions and the EdU signals.

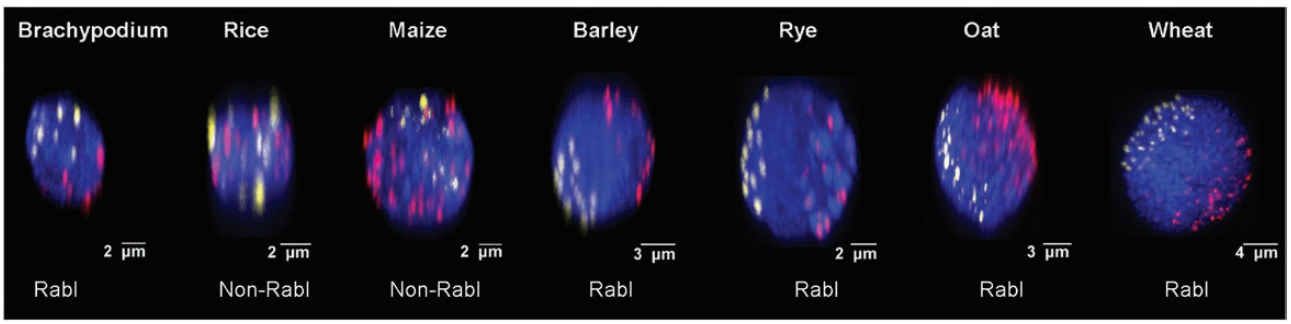


**Fig. 6.** Chromosome positioning in $G_1$ nuclei, estimated according to the positions of telomeres and centromeres. Centromeres were labeled using CenH3 antibody (in yellow) and telomeres were visualized by FISH with an oligonucleotide probe (red). Nuclear DNA was stained with DAPI (blue).

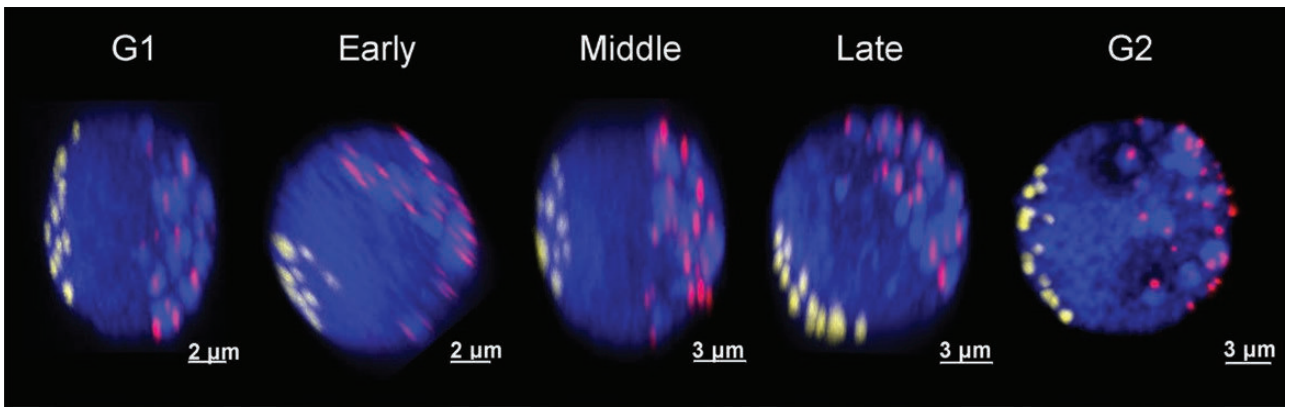


**Fig. 7.** Orientation of chromosomes in interphase nuclei of rye. Centromeres were labeled using CenH3 immunostaining (in yellow) and telomeres were visualized by FISH with an oligonucleotide probe (red). Nuclear DNA was stained with DAPI (blue).

separating TADs that were identified in animals (Dong *et al.*, 2017, 2020; Mascher *et al.*, 2017; Szabo *et al.*, 2018; Dong *et al.*,). Spatial organization and compaction of chromatin in plants could also be affected by ploidy level. Recently, Golicz *et al.* (2020) identified TADs in diploid rice similar to those revealed in *Drosophila* (Ulianov *et al.*, 2015). However, the 3D organization of the large genome of hexaploid wheat, whose chromosomes assume the Rabl configuration, seems more

complex, in that Concia *et al.* (2020) identified three layers of spatial organization of its genome: (sub)genome territories, separation between facultative and constitutive heterochromatin, and micro-compartmentalization of transcriptionally active genes (transcription factories).

The two main types of chromosome arrangement in plant interphase nuclei are the Rabl configuration and a rosette-like structure (Rabl, 1885; Francz *et al.*, 2002; Tiang *et al.*, 2012). The Rabl configuration, where centromeres and telomeres localize at opposite nuclear poles, is considered typical for plants with large genomes. However, this does not seem to be a general rule, as the Rabl configuration was not confirmed in some plants with relatively large genomes, such as maize and sorghum (Anamthawat-Jónsson and Heslop-Harrison, 1990; Schubert and Shaw, 2011; Tiang *et al.*, 2012). The rosette structure, in which the centromeres are located at the nuclear periphery and the telomeres congregate around the nucleolus, has so far been described only in *A. thaliana* (Armstrong *et al.*, 2001; Fransz *et al.*, 2002).

Although a variety of studies have focused on interphase chromosome positioning in plants (e.g. Pecinka *et al.*, 2004; Idziak *et al.*, 2015), except one of maize (Bass *et al.*, 2015), chromosome positioning was not followed throughout the interphase, from $G_1$ to $G_2$ phases of the cell cycle. Here, to obtain a more complete picture, we analyzed the positioning of interphase chromosomes during the cell cycle in root tip meristems of seven *Poaceae* species. These phylogenetically related species have genomes ranging from 355 Mb to 17 Gb/1C in size, with *B. distachyon* serving as a model plant with a small genome (1C ~355 Mb). In all species, we observed a stable arrangement of centromeres and telomeres throughout the interphase (Fig. 7; Supplementary Fig. S8). Based on the positions of telomeres and centromeres, we confirmed the Rabl configuration in *B. distachyon* having a small genome, and in barley, rye, oat, and wheat that feature large genomes (Fig. 6). Our results are in line with findings of Dong and Jiang (1998) and Santos and Shaw (2004), who observed that chromosomes do not assume the Rabl configuration in either rice with a small genome or maize with a moderate genome size (Fig. 6; Supplementary Fig. S8). In both species, some of the centromeric signals clustered at a particular region of the nucleoplasm, indicating a tendency towards Rabl-like polarized organization, but their telomeric signals were dispersed (Fig. 6; Supplementary Fig. S8). One reason for the irregular distribution of rice and maize interphase chromosomes could be the presence of acrocentric chromosomes, as hypothesized by Idziak *et al.* (2015), who observed a disrupted Rabl configurations in *B. stacei* and *B. hybridum* whose karyotypes comprise acrocentric chromosomes.

The association between the 3D genome organization and replication timing has been described in mammals and in *Drosophila*, too (e.g. Zink *et al.*, 1999; Grasser *et al.*, 2008, Hiratani *et al.*, 2010, Weber *et al.*, 2012). With the exception of recent studies on DNA replication timing in maize and *A. thaliana* (Wear *et al.*, 2017; Concia *et al.*, 2018), information on correlations between chromatin compaction and DNA replication timing in plants is generally lacking. A popular approach to study patterns of DNA replication in different regions of cell nuclei is the microscopic detection of thymidine analogs incorporated into the newly synthesized DNA (Gilbert *et al.*, 2010; Bryant and Aves, 2011; Bass *et al.*, 2014, 2015). In mammals, early DNA replication was observed in the interior nuclear regions, while late replication occurred mostly at the nuclear periphery (Li *et al.*, 2001; Pope and Gilbert, 2013). In plants, differences in replication patterns among early, middle, and late S phase were revealed by the fluorescently labeled thymidine analog EdU (Hayashi *et al.*, 2013; Bass *et al.*, 2014, 2015; Dvořáčková *et al.*, 2018). Nevertheless, apart from a few exceptions, the patterns of nuclear DNA replication were analyzed only in plants with small and moderately sized genomes, such as *A. thaliana*, rice, and maize (Hayashi *et al.*, 2013; Bass *et al.*, 2014, 2015; Dvořáčková *et al.*, 2018).

In pioneering work, Cortes *et al.* (1980) used the thymidine analog 5-bromo-2'-deoxyuridine (BrdU) in onion, a species with a large genome, finding a high coincidence between constitutive heterochromatin, including pericentromeric regions, and late replicating DNA. In barley, another species with a large genome, Jasencakova *et al.* (2001) found that DNA replication started at rDNA loci, then continued in the euchromatin and centromeric regions before its completion in pericentromeric heterochromatin. Our observations obtained after EdU labeling of newly replicated DNA agree with the results obtained in maize by Bass *et al.* (2015). Early S phase nuclei were characterized by localized weak signals, whereas strong signals dispersed throughout the whole nucleus were observed in nuclei at middle S phase, but speckled signals concentrated in particular areas were seen at late DNA replication stages (Fig. 3). Since we studied seven species differing in genome size, our results indicate that this pattern of DNA replication is general and does not depend on the amount of nuclear DNA (Supplementary Fig. S9).

We combined EdU labeling with the localization of telomere and centromere regions by FISH, to provide a more detailed view of DNA replication kinetics. We observed contrasting replication timing of telomeres and centromeres in all seven plant species, where the highest intensity of early replication was observed in gene-dense chromosome termini, while the highest intensity of late replicating DNA was typical for pericentromeric regions (Fig. 5). In middle S phase, DNA replication sites were almost evenly distributed along the entire chromosomes and only slightly increased in the interstitial regions of chromosome arms. These findings confirm those recently obtained in *A. thaliana* and maize by Repli-seq analysis that corresponded to the gene density of their chromosome profiles (Wear *et al.*, 2017, Zynda *et al.*, 2017; Concia *et al.*, 2018). Kwasniewska *et al.* (2018) showed that terminal parts of barley chromosomes replicated in early S phase, whole chromosomes were covered with EdU signals at middle S phase, with centromeric parts of chromosomes replicated in late S phase. Those authors reasoned that this chromosome replication profile implied the presence of transcriptionally active genes in the terminal parts of chromosomes along with inactive heterochromatin in the centromeric regions.

To conclude, our study indicates that the spatiotemporal pattern of DNA replication timing during S phase in plants is

conserved and does not depend on their genome size. While the positioning of interphase chromosomes is stable throughout the cell cycle, the relationships between interphase chromosome positioning and genome size seem to be more complex. That other researchers found that chromosome positioning may differ between tissues, and even within tissue of the same plant, suggests that interphase chromosome configuration is not simply the consequence of chromosome orientation in preceding mitosis and that it is controlled by as yet unknown factors.

## Supplementary data

The following supplementary data are available at *JXB* online.

Table S1. Conditions for preparation of suspensions of nuclei from meristem root tip cells after the EdU pulse.

Fig. S1. Replication of 45S rDNA in oat.

Fig. S2. Non-co-localization of CenH3 in early S phase in the seven grass species.

Fig. S3. Co-localization of CenH3 in middle S phase in the seven grass species.

Fig. S4. Co-localization of CenH3 in late S phase in the seven grass species.

Fig. S5. Co-localization of telomeres in early S phase in the seven grass species.

Fig. S6. Co-localization of telomeres in middle S phase in the seven grass species.

Fig. S7. Non-co-localization of telomeres in late S phase in the seven grass species.

Fig. S8. Models of 3D chromosome positioning in interphase nuclei of *B. distachyon*, *O. sativa*, *Z. mays*, *H. vulgare*, *S. cereale*, *A. sativa*, and *T. aestivum*.

Fig. S9. Maximum intensity projection of 3D nuclei from different stages of interphase in *B. distachyon*, *O. sativa*, *Z. mays*, *H. vulgare*, *S. cereale*, *A. sativa*, and *T. aestivum*.

Video S1. Barley nucleus in early S phase.

Video S2. Barley nucleus in middle S phase.

Video S3. Barley nucleus in late S phase.

Video S4. Rye nucleus in early S phase.Video S5. Rye nucleus in middle S phase.

Video S6. Rye nucleus in late S phase.

Video S7. Rice nucleus in $G_1$ phase.

Video S8. Rice nucleus in middle S phase.

Video S9. Rice nucleus in $G_2$ phase.

Video S10. Maize nucleus in $G_1$ phase.

Video S11. Maize nucleus in middle S phase.

Video S12. Maize nucleus in $G_2$ phase.

## Acknowledgements

We are grateful to Dr Kateřina Malínská, for advice on confocal microscopy, and we thank Ms Zdeňka Dubská and Bc. Jitka Weiserová for their excellent technical assistance. We acknowledge the core facility CELLIM of CEITEC, supported in part by the Czech-BioImaging large RI project funded by MEYS CR (grant award LM2015062), for providing us with an imaging facility to use. This work was supported by the Czech Science Foundation (grant award 17-14048S) and by the ERDF project 'Plants as a tool for sustainable global development' (grant award CZ.02.1.01/0.0/0.0/16_019/0000827).

## Author contributions

EH designed the experiments. AN, VK, and JV conducted the study and processed the data. AN and EH wrote the manuscript. AN, VK, JV, JD, and EH discussed the results and contributed to manuscript writing. All authors have read and approved the final manuscript.

## References

**Anamthawat-Jónsson K, Heslop-Harrison JS.** 1990. Centromeres, telomeres and chromatin in the interphase nucleus of cereals. Caryologia **43**, 205–213.

**Appels R, Driscoll C, Peacock WJ.** 1978. Heterochromatin and highly repeated DNA sequences in rye (*Secale cereale*). Chromosoma **70**, 67–89.

**Armstrong SJ, Franklin FC, Jones GH.** 2001. Nucleolus-associated telomere clustering and pairing precede meiotic chromosome synapsis in *Arabidopsis thaliana*. Journal of Cell Science **114**, 4207–4217.

**Bass HW, Hoffman GG, Lee TJ, Wear EE, Joseph SR, Allen GC, Hanley-Bowdoin L, Thompson WF.** 2015. Defining multiple, distinct, and shared spatiotemporal patterns of DNA replication and endoreduplication from 3D image analysis of developing maize (*Zea mays* L.) root tip nuclei. Plant Molecular Biology **89**, 339–351.

**Bass HW, Marshall WF, Sedat JW, Agard DA, Cande WZ.** 1997. Telomeres cluster de novo before the initiation of synapsis: a three-dimensional spatial analysis of telomere positions before and during meiotic prophase. Journal of Cell Biology **137**, 5–18.

**Bass HW, Wear EE, Lee TJ, Hoffman GG, Gumber HK, Allen GC, Thompson WF, Hanley-Bowdoin L.** 2014. A maize root tip system to study DNA replication programmes in somatic and endocycling nuclei during plant development. Journal of Experimental Botany **65**, 2747–2756.

**Bennett MD, Smith JB.** 1976. Nuclear DNA amounts in angiosperms. Philosophical Transactions of the Royal Society B: Biological Sciences **274**, 227–274.

**Bonev B, Cavalli G.** 2016. Organization and function of the 3D genome. Nature Reviews. Genetics **17**, 661–678.

**Bouwman BA, de Laat W.** 2015. Getting the genome in shape: the formation of loops, domains and compartments. Genome Biology **16**, 154.

**Bryant JA, Aves SJ.** 2011. Initiation of DNA replication: functional and evolutionary aspects. Annals of Botany **107**, 1119–1126.

**Catalán P, Müller J, Hasterok R, Jenkins G, Mur LA, Langdon T, Betekhtin A, Siwinska D, Pimentel M, López-Alvarez D.** 2012. Evolution and taxonomic split of the model grass *Brachypodium distachyon*. Annals of Botany **109**, 385–405.

**Concia L, Brooks AM, Wheeler E, *et al*.** 2018. Genome-wide analysis of the Arabidopsis replication timing program. Plant Physiology **176**, 2166–2185.

**Concia L, Veluchamy A, Ramirez-Prado JS, *et al*.** 2020. Wheat chromatin architecture is organized in genome territories and transcription factories. Genome Biology **21**, 104.

**Cortes F, Gonzalez-Gil G, Lopez-Saez JF.** 1980. Differential staining of late replicating DNA-rich regions in *Allium cepa* chromosomes. Caryologia **33**, 193–202.

**Cremer T, Cremer C, Baumann H, Luedtke EK, Sperling K, Teuber V, Zorn C.** 1982. Rabl's model of the interphase chromosome arrangement tested in Chinese hamster cells by premature chromosome condensation and laser-UV-microbeam experiments. Human Genetics **60**, 46–56.

**Cremer T, Cremer M, Dietzel S, Müller S, Solovei I, Fakan S.** 2006. Chromosome territories—a functional nuclear landscape. Current Opinion in Cell Biology **18**, 307–316.

**Dekker J, Rippe K, Dekker M, Kleckner N.** 2002. Capturing chromosome conformation. Science **295**, 1306–1311.

**Dixon JR, Gorkin DU, Ren B.** 2016. Chromatin domains: the unit of chromosome organization. Molecular Cell **62**, 668–680.

**Doležel J, Binarová P, Lucretti S.** 1989. Analysis of nuclear DNA content in plant cells by flow cytometry. Biologia Plantarum **31**, 113–120.

**Doležel J, Sgorbati S, Lucretti S.** 1992. Comparison of three DNA fluorochromes for flow cytometric estimation of nuclear DNA content in plants. Physiologia Plantarum **85**, 625–631.

**Dong F, Jiang J.** 1998. Non-Rabl patterns of centromere and telomere distribution in the interphase nuclei of plant cells. Chromosome Research **6**, 551–558.

**Dong P, Tu X, Chu PY, Lü P, Zhu N, Grierson D, Du B, Li P, Zhong S.** 2017. 3D chromatin architecture of large plant genomes determined by local A/B compartments. Molecular Plant **10**, 1497–1509.

**Dong P, Tu X, Liang Z, Kang BH, Zhong S.** 2020. Plant and animal chromatin three-dimensional organization: similar structures but different functions. Journal of Experimental Botany doi.org/10.1093/jxb/eraa220

**Dong Q, Li N, Li X, *et al*.** 2018. Genome-wide Hi-C analysis reveals extensive hierarchical chromatin interactions in rice. The Plant Journal **94**, 1141–1156.

**Drinnenberg IA, Berger F, Elsässer SJ, *et al*.** 2019. EvoChromo: towards a synthesis of chromatin biology and evolution. Development **146**, dev178962.

**Dumur T, Duncan S, Graumann K, Desset S, Randall RS, Scheid OM, Prodanov D, Tatout C, Baroux C.** 2019. Probing the 3D architecture of the plant nucleus with microscopy approaches: challenges and solutions. Nucleus **10**, 181–212.

**Dvořáčková M, Raposo B, Matula P, Fuchs J, Schubert V, Peška V, Desvoyes B, Gutierrez C, Fajkus J.** 2018. Replication of ribosomal DNA in Arabidopsis occurs both inside and outside the nucleolus during S phase progression. Journal of Cell Science **131**.

**Evtushenko EV, Levitsky VG, Elisafenko EA, Gunbin KV, Belousov AI, Šafář J, Doležel J, Vershinin AV.** 2016. The expansion of heterochromatin blocks in rye reflects the co-amplification of tandem repeats and adjacent transposable elements. BMC Genomics **17**, 337.

**Feng S, Cokus SJ, Schubert V, Zhai J, Pellegrini M, Jacobsen SE.** 2014. Genome-wide Hi-C analyses in wild-type and mutants reveal high-resolution chromatin interactions in Arabidopsis. Molecular Cell **55**, 694–707.

**Finn EH, Misteli T.** 2019. Molecular basis and biological function of variability in spatial genome organization. Science **365**, eaaw9498.

**Fransz P, De Jong JH, Lysak M, Castiglione MR, Schubert I.** 2002. Interphase chromosomes in Arabidopsis are organized as well defined chromocenters from which euchromatin loops emanate. Proceedings of the National Academy of Sciences, USA **99**, 14584–14589.

**Fussell CP.** 1992. Rabl distribution of interphase and prophase telomeres in *Allium cepa* not altered by colchicine and/or ultracentrifugation. American Journal of Botany **79**, 771–777.

**Gilbert DM.** 2010. Evaluating genome-scale approaches to eukaryotic DNA replication. Nature Reviews. Genetics **11**, 673–684.

**Golicz AA, Bhalla PL, Edwards D, Singh MB.** 2020. Rice 3D chromatin structure correlates with sequence variation and meiotic recombination rate. Communications Biology **3**, 235.

**Grasser F, Neusser M, Fiegler H, Thormeyer T, Cremer M, Carter NP, Cremer T, Müller S.** 2008. Replication-timing-correlated spatial chromatin arrangements in cancer and in primate interphase nuclei. Journal of Cell Science **121**, 1876–1886.

**Harrison GE, Heslop-Harrison JS.** 1995. Centromeric repetitive DNA sequences in the genus Brassica. Theoretical and Applied Genetics **90**, 157–165.

**Hayashi K, Hasegawa J, Matsunaga S.** 2013. The boundary of the meristematic and elongation zones in roots: endoreduplication precedes rapid cell expansion. Scientific Reports **3**, 2723.

**Hiratani I, Ryba T, Itoh M, *et al*.** 2010. Genome-wide dynamics of replication timing revealed by in vitro models of mouse embryogenesis. Genome Research **20**, 155–169.

**Howe ES, Murphy SP, Bass HW.** 2013. Three-dimensional acrylamide fluorescence in situ hybridization for plant cells. Methods in Molecular Biology **990**, 53–66.

**Hřibová E, Holušová K, Trávníček P, *et al*.** 2016. The enigma of progressively partial endoreplication: new insights provided by flow cytometry and next-generation sequencing. Genome Biology and Evolution **8**, 1996–2005.

**Idziak D, Robaszkiewicz E, Hasterok R.** 2015. Spatial distribution of centromeres and telomeres at interphase varies among Brachypodium species. Journal of Experimental Botany **66**, 6623–6634.

**Jacob Y, Bergamin E, Donoghue MT, *et al*.** 2014. Selective methylation of histone H3 variant H3.1 regulates heterochromatin replication. Science **343**, 1249–1253.

**Jasencakova Z, Meister A, Schubert I.** 2001. Chromatin organization and its relation to replication and histone acetylation during the cell cycle in barley. Chromosoma **110**, 83–92.

**Kamm A, Galasso I, Schmidt T, Heslop-Harrison JS.** 1995. Analysis of a repetitive DNA family from *Arabidopsis arenosa* and relationships between *Arabidopsis* species. Plant Molecular Biology **27**, 853–862.

**Kempfer R, Pombo A.** 2019. Methods for mapping 3D chromosome architecture. Nature Reviews. Genetics **21**, 207–226.

**Koláčková V, Perničková K, Vrána J, *et al*.** 2019. Nuclear disposition of alien chromosome introgressions into wheat and rye using 3D-FISH. International Journal of Molecular Sciences **20**, 4143.

**Kotogány E, Dudits D, Horváth GV, Ayaydin F.** 2010. A rapid and robust assay for detection of S-phase cell cycle progression in plant cells and tissues by using ethynyl deoxyuridine. Plant Methods **6**, 5.

**Kwasniewska J, Zubrzycka K, Kus A.** 2018. Impact of mutagens on DNA replication in barley chromosomes. International Journal of Molecular Sciences **19**, 1070.

**Li F, Chen J, Izumi M, Butler MC, Keezer SM, Gilbert DM.** 2001. The replication timing program of the Chinese hamster beta-globin locus is established coincident with its repositioning near peripheral heterochromatin in early G1 phase. Journal of Cell Biology **154**, 283–292.

**Lieberman-Aiden E, van Berkum NL, Williams L, *et al*.** 2009. Comprehensive mapping of long-range interactions reveals folding principles of the human genome. Science **326**, 289–293.

**Lipps HJ, Postberg J, Jackson DA, Cremer T.** 2010. Evolutionary origin of the cell nucleus and its functional architecture. Essays in Biochemistry **48**, 1–24.

**Liu C, Cheng YJ, Wang JW, Weigel D.** 2017. Prominent topologically associated domains differentiate global chromatin packing in rice from Arabidopsis. Nature Plants **3**, 742–748.

**Liu C, Wang C, Wang G, Becker C, Zaidem M, Weigel D.** 2016. Genome-wide analysis of chromatin packing in *Arabidopsis thaliana* at single-gene resolution. Genome Research **26**, 1057–1068.

**Liu C, Weigel D.** 2015. Chromatin in 3D: progress and prospects for plants. Genome Biology **16**, 170.

**Manders EM, Stap J, Brakenhoff GJ, van Driel R, Aten JA.** 1992. Dynamics of three-dimensional replication patterns during the S-phase, analysed by double labelling of DNA and confocal microscopy. Journal of Cell Science **103**, 857–862.

**Mascher M, Gundlach H, Himmelbach A, *et al*.** 2017. A chromosome conformation capture ordered sequence of the barley genome. Nature **544**, 427–433.

**Nagaki K, Cheng Z, Ouyang S, Talbert PB, Kim M, Jones KM, Henikoff S, Buell CR, Jiang J.** 2004. Sequencing of a rice centromere uncovers active genes. Nature Genetics **36**, 138–145.

**Mickelson-Young L, Wear E, Mulvaney P, Lee TJ, Szymanski ES, Allen G, Hanley-Bowdoin L, Thompson W.** 2016. A flow cytometric method for estimating S-phase duration in plants. Journal of Experimental Botany **67**, 6077–6087.

**Pecinka A, Schubert V, Meister A, Kreth G, Klatte M, Lysak MA, Fuchs J, Schubert I.** 2004. Chromosome territory arrangement and homologous pairing in nuclei of *Arabidopsis thaliana* are predominantly random except for NOR-bearing chromosomes. Chromosoma **113**, 258–269.

**Pellicer J, Leitch IJ.** 2020. The Plant DNA C-values database (release 7.1): an updated online repository of plant genome size data for comparative studies. New Phytologist **226**, 301–305.

**Pope BD, Gilbert DM.** 2013. The replication domain model: regulating replicon firing in the context of large-scale chromosome architecture. Journal of Molecular Biology **425**, 4690–4695.

**Pope BD, Ryba T, Dileep V, *et al*.** 2014. Topologically associating domains are stable units of replication-timing regulation. Nature **515**, 402–405.

**Prieto P, Shaw P, Moore G.** 2004. Homologue recognition during meiosis is associated with a change in chromatin conformation. Nature Cell Biology **6**, 906–908.

**Rabl C.** 1885. Über Zelltheilung. Morphologisches Jahrbuch **10**, 214–330.

**Ramírez F, Bhardwaj V, Arrigoni L, Lam KC, Grüning BA, Villaveces J, Habermann B, Akhtar A, Manke T.** 2018. High-resolution TADs reveal DNA sequences underlying genome organization in flies. Nature Communications **9**, 189.

**Rawlins DJ, Highett MI, Shaw PJ.** 1991. Localization of telomeres in plant interphase nuclei by in situ hybridization and 3D confocal microscopy. Chromosoma **100**, 424–431.

**Robledillo LÁ, Koblížková A, Novák P, Böttinger K, Vrbová I, Neumann P, Schubert I, Macas J.** 2018. Satellite DNA in *Vicia faba* is characterized by remarkable diversity in its sequence composition, association with centromeres, and replication timing. Scientific Reports **8**, 1–11.

**Santos AP, Shaw P.** 2004. Interphase chromosomes and the Rabl configuration: does genome size matter? Journal of Microscopy **214**, 201–206.

**Schubert I, Shaw P.** 2011. Organization and dynamics of plant interphase chromosomes. Trends in Plant Science **16**, 273–281.

**Schubert V, Rudnik R, Schubert I.** 2014. Chromatin associations in Arabidopsis interphase nuclei. Frontiers in Genetics **5**, 389.

**Schwarzacher T, Heslop-Harrison JS.** 1991. In situ hybridization to plant telomeres using synthetic oligomers. Genome **34**, 317–323.

**Sexton T, Cavalli G.** 2015. The role of chromosome domains in shaping the functional genome. Cell **160**, 1049–1059.

**Sexton T, Yaffe E, Kenigsberg E, Bantignies F, Leblanc B, Hoichman M, Parrinello H, Tanay A, Cavalli G.** 2012. Three-dimensional folding and functional organization principles of the Drosophila genome. Cell **148**, 458–472.

**Sotelo-Silveira M, Chávez Montes RA, Sotelo-Silveira JR, Marsch-Martínez N, de Folter S.** 2018. Entering the next dimension: plant genomes in 3D. Trends in Plant Science **23**, 598–612.

**Szabo Q, Jost D, Chang JM, *et al*.** 2018. TADs are 3D structural units of higher-order chromosome organization in Drosophila. Science Advances **4**, eaar8082.

**Tiang CL, He Y, Pawlowski WP.** 2012. Chromosome organization and dynamics during interphase, mitosis, and meiosis in plants. Plant Physiology **158**, 26–34.

**Ulianov SV, Gavrilov AA, Razin SV.** 2015. Nuclear compartments, genome folding, and enhancer–promoter communication. International Review of Cell and Molecular Biology **315**, 183–244.

**Wang C, Liu C, Roqueiro D, Grimm D, Schwab R, Becker C, Lanz C, Weigel D.** 2015. Genome-wide analysis of local chromatin packing in *Arabidopsis thaliana*. Genome Research **25**, 246–256.

**Wear EE, Song J, Zynda GJ, *et al*.** 2017. Genomic analysis of the DNA replication timing program during mitotic S phase in maize (*Zea mays*) root tips. The Plant Cell **29**, 2126–2149.

**Weber CC, Pink CJ, Hurst LD.** 2012. Late-replicating domains have higher divergence and diversity in *Drosophila melanogaster*. Molecular Biology and Evolution **29**, 873–882.

**Werner JE, Kota RS, Gill BS, Endo TR.** 1992. Distribution of telomeric repeats and their role in the healing of broken chromosome ends in wheat. Genome **35**, 844–848.

**Zink D, Bornfleth H, Visser A, Cremer C, Cremer T.** 1999. Organization of early and late replicating DNA in human chromosome territories. Experimental Cell Research **247**, 176–188.

**Zynda GJ, Song J, Concia L, Wear EE, Hanley-Bowdoin L, Thompson WF, Vaughn MW.** 2017. Repliscan: a tool for classifying replication timing regions. BMC Bioinformatics **18**, 362.

# APPENDIX III

## Replication of DNA repeats in time and space

Němečková A., Vrána J., Doležel J., Hřibová E

In: Abstract of the: „Plant Genome Stability and Change“.

IPK Gatersleben, Germany 2018

# Replication of DNA repeats in time and space

Alžběta Němečková[1], Jan Vrána[1], Jaroslav Doležel[1], Eva Hřibová[1]

Institute of Experimental Botany, Slechtitelu 31, CZ-78371 Olomouc, Czech Republic

## Introduction

- Nuclear genome is replicated during S phase of cell cycle under strict control
- In contrast to numerous studies on DNA replication pattern in yeast, *Drosophila*, mouse and human, little is known about replication dynamics in plants
- In plants, experiments with fluorescently labelled analogues of thymidine incorporated into nascent DNA showed differences in replication patterns in S phase
- The use of EdU (5-ethenyl-2-deoxyuridin) opens a possibility to visualize and analyze replicating chromatin
- Analysis of closely related plant species differing in genome size and repetitive DNA sequences new insights into DNA replication program

## Aims of the study

- Comparison of DNA replication of DNA repeats in space and time in two closely related plant species with contrasting genome sizes – *Hordeum vulgare* (1C~5100 Mb, 2n=14) and *Brachypodium distachyon* (1C~355 Mb, 2n=10)
- Visualization of 3D organization of specific DNA sequences in the different phases of cell cycle S phase

## Experimental design

**1. Seeds preparation**

**2. Sample preparation**

- EdU incorporates under stable conditions
- Root fixation and suspension of intact nuclei
- Centrifugation and Click-iT reaction cocktail incubation
- Nuclei pelleting and resuspension in LB01 buffer containing DAPI

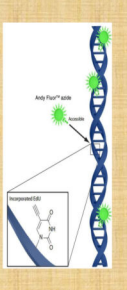

**3. Nuclei sorting**

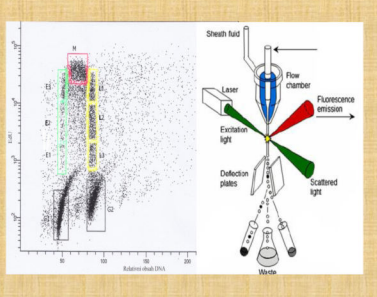


**4. 3D FISH**

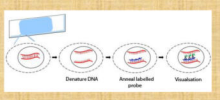

- Nuclei mounted in a PAA gel
- FISH procedure using (un)directly-labeled probes
- Probes specific for different repetitive DNA sequences as well as collinear genetic regions of *Brachypodium* and barley genomes

**5. Confocal scanning**

**6. Data analysis**

- Imaris software was used for 3D visualization
- Volume, distance and overlaps were determined

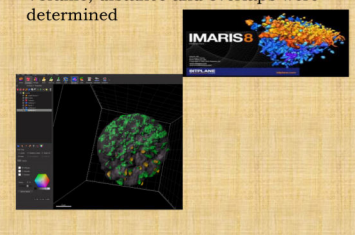


## Results

**Replication profile of centromere specific Ty3/Gypsy Cereba element during different stages of S phase (early = E, middle = M and late = L) in *Hordeum vulgare***

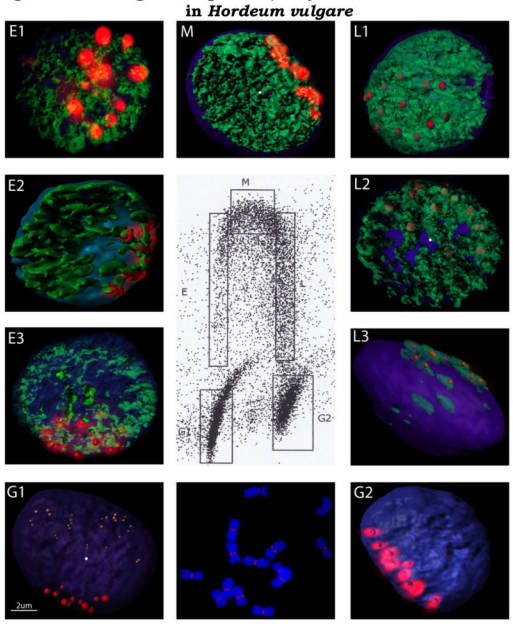


- Replicating chromatin labeled by EdU is characterized by specific pattern. In early S phase, EdU signals are localized to particular loci and separated from non-replicating chromatin labeled by DAPI while in late S phase, EdU signals overlapped with DAPI-stained heterochromatin. Highly heterochromatic regions seem to be replicated in late S phase
- 3D acrylamide FISH with probes specific to different DNA repeats revealed more complex mode of their replication
- While centromere specific Ty3/Gypsy Cereba repeat is replicated in all stages of late S phase, other highly repetitive DNA sequences are replicated in different mode
- While in *Brachypodium* EdU signals are located mostly in periphery of the nucleus in all stages of S phase and replication timing of homologous sequences (e.g. rRNA genes) differs

**Replication profile of 45 S rDNA during different stages of S phase (early = E, middle = M and late = L) in *Brachypodium distachyon***

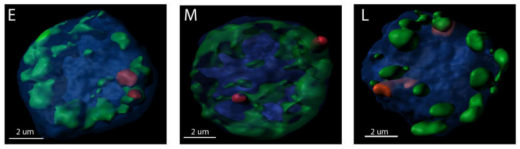


## Future work

- More detailed characterization of replicating DNA regions using high resolution microscopy
- Repli-seq analysis = sequencing library from E, M, L, G1 and G2 phase followed by illumina sequencing and analysis
- The information about replication time with methylation status

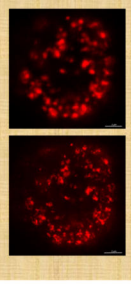

## Conclusion

- Dissimilar replication profile in nuclei of *Brachypodium* and *Hordeum* was observed
- Diferences in the replication pattern may related the organization and structure of their genome
- EdU analysis indicated that heterochromatin is replicated in late S phase
- 3D FISH revealed a more complex pattern of replication of highly-repetitive DNA

This research has been supported by Czech Science Foundation, grant „Spatial and temporal characterisation of DNA replication in phylogeneticaly related plant species with contrasting genome sizes “ (17-14048S). *We acknowledge the core facility CELLIM of CEITEC supported by the Czech-BioImaging large RI project (LM2015062 funded by MEYS CR) for their support with obtaining scientific data presented in this paper.*

## APPENDIX IV

# DNA replication timing program in barley (*Hordeum vulgare*)

Čížková J, Němečková A, Vrána J, Doležel J, Hřibová E.

In: International Conference on Polyploidy,

Ghent, Belgium 2019

# DNA replication timing program in barley (*Hordeum vulgare*)

Čížková J., Němečková A., Vrána J., Doležel J., Hřibová E.

Institute of Experimental Botany, Centre of the Region Haná for Biotechnological and Agricultural Research, Šlechtitelů 31, Olomouc, Czech Republic

## Introduction

- Nuclear genome is replicated during the S phase of the cell cycle under strict rules, which ensure accuracy and completeness of DNA duplication. The process is organized both temporally and spatially – replication initiates at multiple origins throughout the genome at different times during S phase. It was suggested, that early replicating chromatin is rich in genes and transcriptionally active, while late replicating chromatin is enriched for heterochromatin and repetitive elements.
- Replication timing programs have been described in yeasts and many animal species, but much less is known about the time course of DNA replication in plants. Up to now, only species with relatively small genomes, such as maize and Arabidopsis, have been studied in more detail.
- To provide more insights, we studied the replication machinery in barley (*Hordeum vulgare*), a representative of plants with large genome (1C ~ 5100 Mb) and high proportion of DNA repeats (more than 80%)

## Experimental design

EdU labeling of DNA in root meristem cells

↓

DNA fixation and nuclei isolation

↓

Alexa Fluor 488 click, DAPI staining

↓

Flow sorting of nuclei in early, middle and late S phase

↓

Immunoprecipitation of EdU labeled DNA

↓

DNA sequencing

3D acrylamide FISH with probes specific to different DNA repeats and rRNA genes

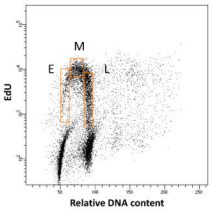


**Bivariate plot of relative DNA content and EdU incorporation.** Sub-populations of early (E), middle (M) and late (L) nuclei are indicated by orange rectangles.

## Repli-Seq

### A pilot study on late S phase nuclei

- Immunoprecipitation of DNA isolated from 500 000 late S phase nuclei resulted in gaining of 4.5 ng of EdU labeled DNA fragments
- Illumina libraries were prepared by NEBNext Ultra II DNA Library Prep Kit for Illumina and sequenced on MiSeq instrument
- After trimming to length and quality, 4.3 million high quality pair end reads were obtained and aligned to reference genome sequence of *H. vulgare* and specific repetitive DNA sequences and rRNA genes, which are missing in the reference genome sequence

**Mapping statistics of selected repetitive DNA sequences and rRNA genes**

| Reference | Reference Sequence Length | Mapped reads | Unmapped reads |
|---|---|---|---|
| 45S rDNA | 8418 | 78370 | 53 |
| 5S rDNA | 468 | 14 | 0 |
| Cereba | 14993 | 1531 | 2 |
| GAA microsatellite | 2853 | 289917 | 31 |
| CAA microsatellite | 380 | 6126 | 6 |

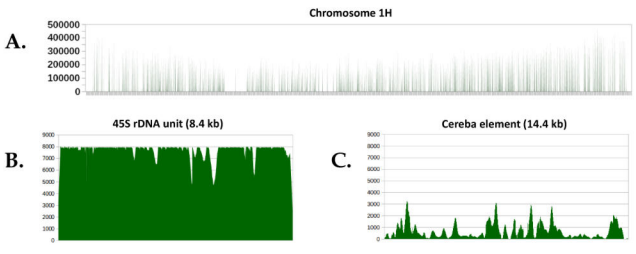


**Alignment of paired end reads isolated from late S phase.** (A) Chromosome 1H – coverage is depicted per 1 MB regions. (B) 45S rDNA unit. (C) Cereba element.

## 3D FISH

### A. Cereba + telomeric probe

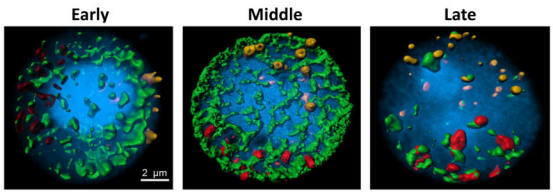


### B. Psc 119

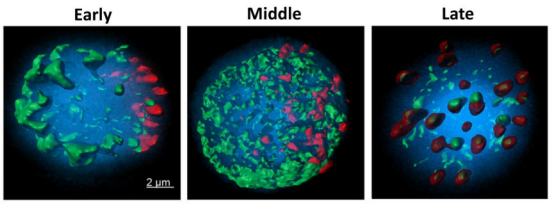


### C. 5S rDNA

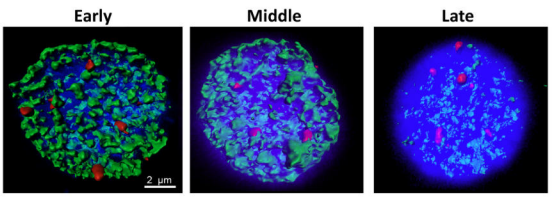


### D. 45S rDNA

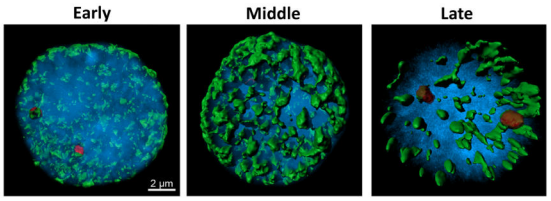


**Colocalization of EdU signals (green), corresponding to replicating DNA, and probes specific to different DNA repeats in early, middle and late S phase nuclei of barley.** (A) Centromeric retrotransposon Cereba (red) and probe for telomeres (yellow). (B) Sub-telomeric satellite repeat psc 119 (red). (C) 5S rDNA (red). (D) 45S rDNA (red). Models of nuclei were generated using Imaris image analysis software based on confocal laser scanning microscope images.

## Conclusions and future work

Our results provide the first picture of the complexity of DNA replication in time and nuclear space, reflecting different types of DNA sequences and their role in genome organization and function in barley. Replication of different DNA repeats varied in time, e.g. centromeric retrotransposon Cereba was replicated during all stages of S phase, sub-telomeric satellite repeats psc 119 was replicated during the late S phase. Difference in replication timing was observed also for rRNA genes, while 5S rRNA genes were replicated during early S phase, majority of 45S rRNA genes were replicated in very late S phase, probably reflecting the presence of large amounts of pseudogenic 45S rDNA units. Genome-wide replication timing program in barley will be further described based on Repli-Seq data from early, middle and late S phase nuclei in five biological replicates. Genomic regions that replicate predominantly in each of the stages will be identified.

This work has been supported by the Grant Agency of the Czech Republic (award No. 17-14048S) and the National Program of Sustainability I (award LO1204). The computing was supported by the National Grid Infrastructure MetaCentrum (grant No. LM2010005 under the program Projects of Large Infrastructure for Research, Development, and Innovations).

# APPENDIX V

## Chromatin arrangement across the whole cell cycle in the *Poaceae* family

Němečková A., Vrána J, Doležel J, Hřibová E

In: „MEETING OF THE GPZ GROUP, CYTOGENETICS 2019“.

Dresden, Germany 2019

# Cereals nuclear genome organization and replication of specific regions

Alžběta Němečková, Veronika Koláčková, Jaroslav Doležel, Eva Hřibová

Institute of Experimental Botany, The Czech Academy of Science, Šlechtitelů 31, CZ-78371 Olomouc, Czech Republic

## Introduction and Aims

- Rable orientation of interphase chromosomes is known in some cereal species that have nuclear genome >4,800 Mb while is absent in species with small genomes <1,000 Mb.
- There is also evidence that chromosome configuration is not preserved and should be tissue-specific or should change during the cell cycle.

- It inspired us to compare chromatin arrangement and replication time of specific DNA sequences in roots meristem during different stages of the cell cycle.
- We focus on 7 species of *Poaceae* family differing in genome sizes – Brachypodium, rice, maize, barley, rye, oat and wheat.

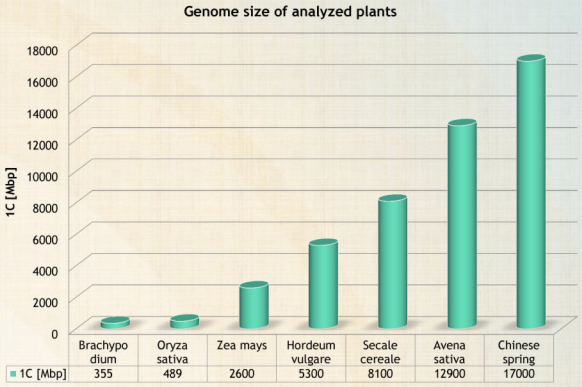


## Experimental background

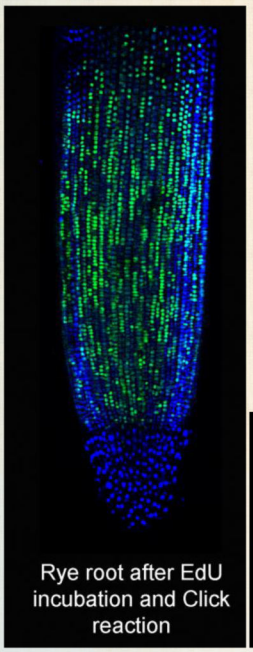

Rye root after EdU incubation and Click reaction

- Seedlings are incubated with EdU solution.
- EdU incorporates into newly synthesized strands of DNA during replication.
- Roots are fixed and suspension of intact nuclei is prepared.
- Newly synthesized DNA is visualized using fluorophore (Alexa 488).
- Nuclei are sorted based on DNA and EdU content.
- Sorted nuclei of the different stage are mounted in polyacrylamide gel.
- Embedded nuclei are used for IMUNO-FISH labeling.
- Confocal scanning is provided.
- Data are analyzed using Imaris software.

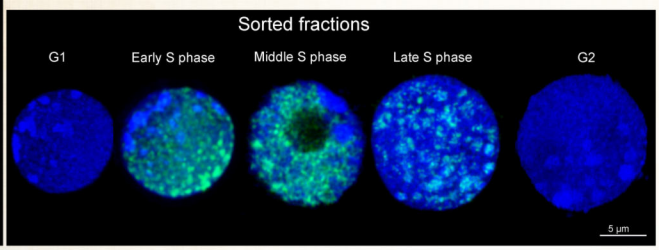


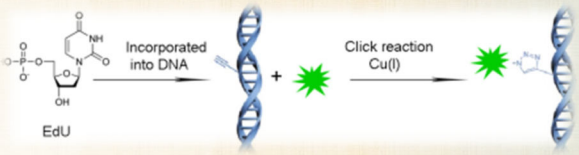


## Questions

- Is centromere - telomere orientation maintained during G1, S and G2 phase of the cell cycle?
- Is „RabI/Non-RabI" orientation connected to plant genome size?
- What is replication time of centromere and telomere sequences in related plant species?

## Results

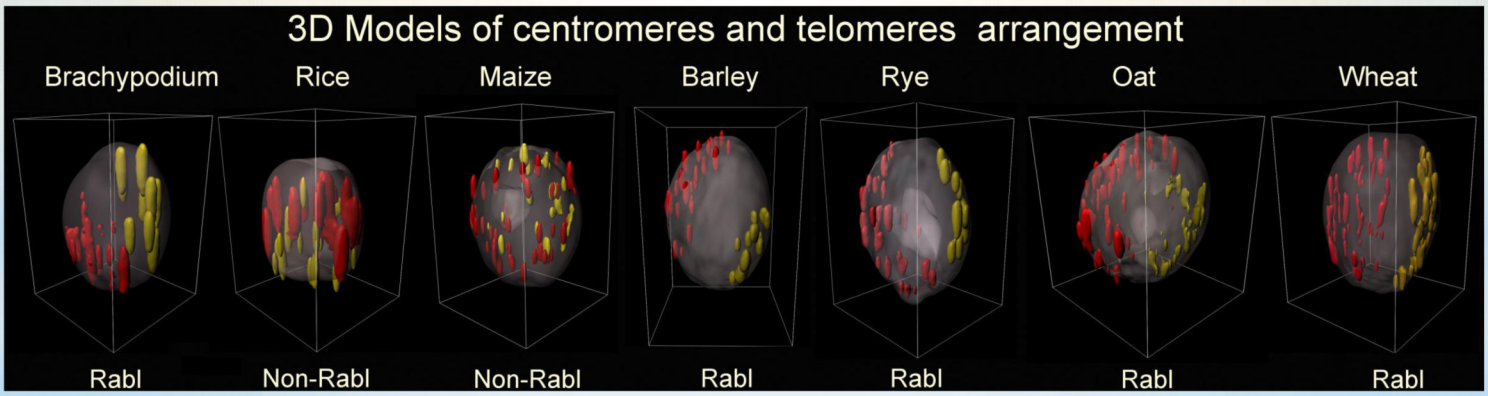


## Conclusions

- 3D visualization of telomeres and centromeres (CenH3) confirmed RabI orientation in all stages (G1, S, G2) in all species except maize and rice.
- EdU analysis indicated that centromeres are mostly replicated in early S phase while telomeres in late S phase in all tested species.
- In rye, there is nice evidence that replication is strongly connected to the structure of chromatin. Telomeres in heterochromatin regions are replicated in late S phase, while telomeres of euchromatin are replicated earlier (middle S phase).

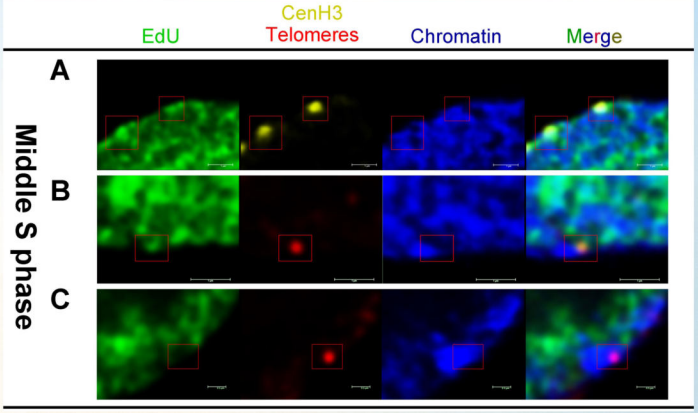


This research has been supported by Czech Science Foundation, grant „Spatial and temporal characterisation of DNA replication in phylogeneticaly related plant species with contrasting genome sizes " (17-14048S). *We acknowledge the core facility CELLIM of CEITEC supported by the Czech-BioImaging large RI project (LM2015062 funded by MEYS CR) for their support with obtaining scientific data presented in this paper.*